

**HEAT SHOCK PROTEIN GP96 DRIVES DICHOTOMOUS LYMPHOCYTE
RESPONSES VIA DNA METHYLOME REMODELING AND STAT1 SIGNALING IN
ANTIGEN PRESENTING CELLS**

by

Lauren Brooke Kinner-Bibeau

B.Sc. Microbiology, Colorado State University, 2012

Submitted to the Graduate Faculty of
the School of Medicine in partial fulfillment
of the requirements for the degree of
Doctor of Philosophy

University of Pittsburgh

UNIVERSITY OF PITTSBURGH

SCHOOL OF MEDICINE

This dissertation was presented

by

Lauren Brooke Kinner-Bibeau

It was defended on

June 9, 2017

and approved by

Christine Milcarek, Professor, Department of Immunology

Penelope Morel, Professor, Department of Immunology

Roderick O'Sullivan, Assistant Professor, Department of Pathology

Jon Piganelli, Associate Professor, Department of Surgery

Dissertation Advisor: Robert Binder, Associate Professor, Department of Immunology

Copyright © by Lauren Brooke Kinner-Bibeau

2017

HEAT SHOCK PROTEIN GP96 DRIVES DICHOTOMOUS LYMPHOCYTE RESPONSES VIA DNA METHYLOME REMODELING AND STAT1 SIGNALING IN ANTIGEN PRESENTING CELLS

Lauren B. Kinner-Bibeau, PhD

University of Pittsburgh, 2017

Immune responses primed by endogenous heat shock proteins (HSPs), specifically gp96, have been used for immunotherapy of cancer. Immunization with low doses of gp96 primes a response that is dominated by T helper type 1 (Th1) cells and cytotoxic T lymphocytes (CTLs), which allows for recognition and killing of tumor cells. However, increasing the dose of gp96 primes a response characterized by regulatory T (Treg) cells and immunosuppression. Although the T cell responses driving this dose dichotomy have been studied in multiple systems, innate mechanisms that control T cells in the context of gp96 immunization remains unknown. The antigen presenting cells (APCs) involved in this response are the main focus of Chapters 1 and 2 of this thesis. Here we show gp96 preferentially engages conventional and plasmacytoid dendritic cells (pDCs) under low and high doses respectively, through the HSP receptor CD91. We show that DNA methyltransferase 1 (DNMT1) is active in multiple APC population in response to gp96 stimulation, and that global DNA methylome and protein expression changes occur in these populations in response to *in vivo* immunization. Methylation-dependent upregulation of neuropilin-1 (Nrp1) on pDCs enables long term interactions with Treg cells that enhance their function in suppressing ongoing Th1 anti-tumor immunity. Our study defines a CD91-dependent mechanism through which gp96 controls dichotomous immune responses, relevant to the therapy of cancer and autoimmunity.

Additionally, we are interested in the signaling pathways initiated by gp96-CD91 interaction. Previous studies have shown that NF- κ B and p38 MAPK are activated in HSP-

responsive macrophages, but the consequences of p38 activation were not investigated. Chapter 3 will focus on the downstream mediators of p38, specifically the transcription factor STAT1, and the cytokine expression and secretion that follows. We show that gp96-treated macrophages upregulate STAT1-dependent cytokines as a result of STAT1 phosphorylation. This event requires intact CD91 and p38 MAPK. Importantly, STAT1 target CXCL10 is upregulated in response to gp96 and is critical for APC-NK cell crosstalk. Given that NK cells are required for anti-tumor immunity elicited by gp96 immunization, we hypothesize that STAT1 activation in responding APCs is necessary for tumor rejection.

TABLE OF CONTENTS

ACKNOWLEDGEMENTS	XIV
ABBREVIATIONS.....	XVI
1.0 PROJECT AIMS.....	1
1.1 AIM 1: IDENTIFY APC SUBSETS THAT INTERACT WITH GP96 AT HIGHER DOSES IN VIVO.....	2
1.2 AIM 2: DETERMINE EPIGENETIC AND TRANSCRIPTIONAL CHANGES IN APCs THAT CAN DRIVE SUPPRESSIVE TREG RESPONSES.....	2
1.3 AIM 3: EXAMINE STAT1 ACTIVATION IN GP96-TREATED MACROPHAGES	3
2.0 INTRODUCTION.....	5
2.1 HSPs AND ANTI-TUMOR IMMUNITY	6
2.1.1 Tumor antigens and generation of antigen-specific T cells.....	6
2.1.2 HSPs as tumor rejection antigens.....	7
2.1.3 Association of antigenic peptides with immunogenic HSPs.....	8
2.1.4 Clinical trials using HSPs.....	9
2.2 KNOWN MECHANISMS DRIVING HSP RESPONSES	11
2.2.1 Cross-presentation of peptides chaperoned by HSPs.....	11
2.2.2 CD91 as the receptor expressed on APCs.....	12
2.2.3 Signaling mediators activated by HSP-CD91 interaction	14
2.2.4 STAT1 as a potential mediator downstream of CD91.....	18
2.3 DOSE DICHOTOMY OF HSP-MEDIATED RESPONSES	20

2.3.1	Application of HSP immunization in autoimmune disease and solid organ transplantation	20
2.3.2	Mechanisms driving HD gp96-mediated suppression	22
2.3.3	HSPs in autoimmunity.....	25
2.4	DNA METHYLATION AS A MECHANISM FOR TRANSCRIPTIONAL REGULATION OF IMMUNE RESPONSES	26
2.4.1	DNA methylation is an epigenetic mark that regulates gene expression and histone modification	26
2.4.2	Regulation of DNA methyltransferases	29
2.4.3	DNA methylation in the immune system	30
2.5	INTRODUCTION SUMMARY	32
3.0	CHAPTER 1: CLASSIFICATION OF APCS ASSOCIATED WITH HIGH DOSE GP96 SUPPRESSION	34
3.1	RATIONALE	34
3.2	RESULTS	35
3.2.1	CD91 ⁺ DCs are required for gp96-mediated immune suppression.....	36
3.2.2	HD gp96 suppression cannot be overcome by IL-12	38
3.2.3	Dynamic cellular changes and alternative interactions of gp96 with DC populations at HD	40
3.2.4	pDCs express CD91 but do not mature when exposed to gp96	41
3.3	DISCUSSION.....	44
3.3.1	Effects of IL-12 on the tumor microenvironment.....	45
3.3.2	Implications of gp96 release by tumors and traumatic wounds.....	45

3.3.3	Tolerogenic pDCs in allograft transplantation and cancer.....	47
4.0	CHAPTER 2: GP96 DRIVES DICHOTOMOUS T CELL IMMUNE RESPONSES VIA DNA METHYLOME REMODELING IN APCs.....	50
4.1	RATIONALE	50
4.2	RESULTS	52
4.2.1	Gp96 treatment leads to formation of DNMT1 punctae in APCs	52
4.2.2	DNMT1 punctae formation is NF- κ B dependent.....	55
4.2.3	DNA methylome remodeling occurs in CD91 ⁺ cells in response to gp96 immunization	58
4.2.4	Increase in Nrp1 ⁺ pDCs following HD gp96 immunization	59
4.2.5	Gp96-mediated Nrp1 gene methylation regulates Nrp1 gene product expression in pDCs, but not cDCs	66
4.2.6	Gp96-stimulated pDCs stabilize and prolong interactions with Treg in a Nrp1-dependent manner	69
4.2.7	pDCs are required for gp96-mediated immune suppression by Tregs..	73
4.2.8	Nrp1 is essential for gp96-mediated Treg generation.....	75
4.3	DISCUSSION.....	77
4.3.1	Activation of DNMTs, transient methylation, and non-promoter methylation	78
4.3.2	Methylation of cell-cell adhesion genes: lessons from neurobiology	80
4.3.3	Regulation of pDC-Treg interaction	82
5.0	CHAPTER 3: STAT1 SIGNALING IN GP96-STIMULATED APCs.....	85
5.1	RATIONALE	85

5.2	RESULTS	87
5.2.1	DNA methylation is enriched at transcription factor binding sites	87
5.2.2	gp96 treatment preferentially targets pSTAT1-S727 in CD91⁺ APCs via a p38 MAPK-dependent pathway	89
5.2.3	Gp96-stimulated APCs increase transcription and secretion of CXCL10 and promote STAT1 binding to the <i>Cxcl10</i> promoter	93
5.2.4	NK cells require APCs and intact CXCR3 for maximal IFNγ production in response to gp96	94
5.3	DISCUSSION.....	95
5.3.1	Methylation of transcription factor binding sites	96
5.3.2	Activation of STAT1 and its specific gene signatures.....	97
5.3.3	APC-NK cell cross-talk and the role of NK cells in cancer.....	99
6.0	THESIS SUMMARY AND FUTURE DIRECTIONS	102
6.1	SUMMARY	102
6.2	FUTURE DIRECTIONS.....	104
6.2.1	Lymph node architecture and how gp96 engages pDCs versus cDCs .	104
6.2.2	Implications for clinical trials: Dosage and microneedle arrays	104
6.2.3	CD91 in cholesterol storage and metabolism	105
7.0	MATERIALS AND METHODS	108
7.1.1	WT mice.....	108
7.1.2	Generation of CD91^{f/f}CD11c^{cre} mice.....	108
7.1.3	Cell lines.....	108
7.1.4	Isolation of primary spleen cDCs, pDCs, NK cells, and T cells.....	109

7.1.5	Generation of primary murine BMDCs and PECs	110
7.1.6	Purification of HSPs	110
7.1.7	<i>In vivo</i> tumor growth assay	111
7.1.8	MBD methyl-sequencing and analysis	112
7.1.9	Bisulfite sequencing	113
7.1.10	Chromatin accessibility assay	113
7.1.11	Microscopy and analysis.....	114
7.1.12	Western blotting.....	114
7.1.13	Live cell imaging and analysis	115
7.1.14	Flow cytometry.....	116
7.1.15	<i>In vivo</i> T cell suppression assay	116
7.1.16	<i>In vivo</i> Nrp1 neutralization assay	117
7.1.17	Chromatin immunoprecipitation	118
7.1.18	ELISA and Luminex.....	119
7.1.19	Statistical analyses	119
BIBLIOGRAPHY		120

LIST OF TABLES

Table 1: Summary of clinical trials using autologous HSP	10
Table 2: CD91 expression in various APC subsets	15
Table 3. Cytokines produced by macrophages treated with immunogenic HSPs.	17
Table 4: Summary of suppressive responses to HSP	22
Table 5. List of methyl-seq DMRs (HD>LD, 29 targets).....	61
Table 6. List of methyl-seq DMRs (LD>HD, 26 targets).....	62
Table 7. List of GO analysis hits (HD>LD)	63
Table 8. List of GO analysis hits (LD>HD)	64

LIST OF FIGURES

Figure 1. HSP-CD91 interaction results in endocytosis and/or signaling.	16
Figure 2. Characterization of purified murine gp96.	36
Figure 3. HD gp96-mediated immune-regulatory response requires CD91+ DCs.....	37
Figure 4. IL-12 alone is not sufficient to overcome HD gp96-mediated immune-regulatory response.....	39
Figure 5. DC numbers following LD and HD gp96 immunization.	40
Figure 6. Preferential targeting of pDCs at HD gp96.	42
Figure 7. cDCs and pDCs express similar levels of CD91.....	43
Figure 8. cDCs undergo maturation in response to gp96, whereas pDCs remain immature.	44
Figure 9. DNMT1 forms punctae in DC nuclei following gp96 stimulation.....	53
Figure 10. DNMT3b forms punctae in macrophage nuclei following gp96 stimulation.....	54
Figure 11. DNMT1 punctae are not an artifact of increased protein or cell proliferation.	55
Figure 12. DNMT1 punctae formation in gp96-stimulated macrophages is NF- κ B dependent. 56	
Figure 13. Gp96 treatment does not result in phosphorylation of GSK3 β	57
Figure 14. Differential methylation of adhesion molecules in response to gp96.	60
Figure 15. DMRs are enriched on genes associated with adhesion.....	64
Figure 16. pDCs specifically increase expression of Nrp1 in response to HD gp96.	65
Figure 17. pDCs recapitulate in vivo HD phenotype in an in vitro culture system.....	66
Figure 18. Intronic methylation of Nrp1 enhances expression.	67
Figure 19. Nrp1 is in an euchromatin conformation, and thus poised for regulation, in naïve pDCs but not cDCs.	69

Figure 20. gp96-stimulated pDCs increase interaction with Treg in a Nrp1-dependent manner.	71
Figure 21. Duration of pDC-Treg interaction increases with increasing treatment dose of gp96.	72
Figure 22. pDCs are required for efficient suppression of CTL-mediated cytotoxicity by HD gp96.	73
Figure 23. HD gp96-mediated Treg induction is Nrp1-dependent.	75
Figure 24. HD gp96 immunization does not affect generation of antigen-specific CTLs.....	77
Figure 25. Chapter 2 summary.....	79
Figure 26. Potential NRSF binding motif identified in Nrp1 locus by MatInspector/Genomatix.	80
Figure 27. Activated p38 MAPK indirectly phosphorylates STAT1 at S727 site.....	86
Figure 28. DNA methylation is enriched at transcription factor binding sites.	87
Figure 29. STAT1 is phosphorylated in response to 20 min gp96 stimulation.	89
Figure 30. STAT1 phosphorylation is CD91 dependent and is not due to soluble factors produced by PECs.....	91
Figure 31. STAT1 phosphorylation is p38 MAPK-dependent.	92
Figure 32. gp96 upregulates CXCL10 expression.....	93
Figure 33. gp96 triggers STAT1 binding to the Cxcl10 promoter.	94
Figure 34. APC-NK cell cross-talk occurs in response to gp96 and is CXCR3-dependent.	95
Figure 35. 5-aza treatment alters STAT1 activity.....	97
Figure 36. CD91-deficient pDCs have less p-GSK3 β at baseline compared with wildtype.	106
Figure 37. Central memory CD4 ⁺ T cells express CD91 following immunization.	107
Figure 38. pDC depletion.....	117

ACKNOWLEDGEMENTS

First and foremost, I would like to thank my mentor Dr. Robert Binder for his thoughtful guidance through the years. Even through my wildest proposals and strangest ideas, you have supported me and have helped me become the scientist I am today. Perhaps the biggest lesson I have taken away from working with you is to always persevere even if it seems crazy, and to always maintain high expectations for myself. I would also like to thank each and every member of my amazing dissertation committee. I have often said that my committee is the best, and I still believe that. Many of your suggestions have vastly improved this project. For that and for your support, I am very appreciative. To Sarah Gaffen, thank you for answering all my emails and phone calls before I chose to go to Pitt. I don't know if you remember that, but I appreciated having someone to answer my questions. To Walt Storkus, Sarah Gaffen, Amanda Poholek, Dario Vignali, and many others, thank you for your insightful scientific discussions. I would also like to thank my undergraduate mentor Dr. Alan Schenkel who was the first to make me realize that immunology is my passion.

I am very grateful to those at the Pitt Center for Biological Imaging, specifically Dr. Simon Watkins and Callen Wallace, for their help with microscopy analysis and for setting up microscopes with too many buttons. I would like to thank Dewayne Falkner from the Flow Cytometry core for his help in sorting cells, and Alan Twaddle at the Bioinformatics Core for his help with the methyl-seq analysis.

I would also like to thank past and present members of the Binder lab who have provided technical help, scientific discussions, and assistance in experiments even when it meant getting to lab at 6 AM to pull out lymph nodes. Particularly, I would like to thank Abigail Sedlacek (i.e.

Floor Donut, i.e. Good Queen Ab, i.e. off-brand Lauren) for always being ready for conversation, whether it was about experiments, shopping, or Doctor Who. I'm so happy to have had someone I work so well with. I don't know how I will function in another lab without you! Special thanks also to my fellow graduate students in the Department of Immunology and IBGP program who make coming to lab enjoyable and often way too entertaining.

To my dear friends, you bring light and inspiration to my life. I thank all the citizens of Heidiland (you know who you are) for making each day more magical than the last. To Becca Eels, thank you for always letting me pet your cats and watch bad TV with you, because that was always the best way to wind down after a hard Monday. To David Ricks and Austen Burke, thank you for being my first friends in Pittsburgh when I knew nobody. To all our Deely Street apartment neighbors, I don't know how we lucked out every single time but all of you have made coming home truly a treat. A big thank you to all my friends in Colorado who encouraged me to be who I am, and who continue to remind me why I am here.

I am very blessed to have had such a supporting family. Thank you to my loving parents for making me who I am today and for always being excited to visit Pittsburgh. To my very strange but wonderful sister, thank you for being there to chat on the phone about literally anything and for letting me just get all my weirdness out.

Finally, to my fiancé and better half Matt Bibeau, you are my world. Thank you for making me grilled cheese when life is too stressful, or going on random adventures to Lawrenceville, or playing board games at breweries, or watching Spongebob in the dark with me. The day you told me you would come with me to grad school I was in Pittsburgh, and I think that is part of why I chose to move here. Your endless support gave me the confidence to get to where I am, and for that I am appreciative.

ABBREVIATIONS

5-azaC: 5-azacytidine

5hmC: 5-hydroxymethylcytosine

APC: antigen presenting cell

BMDC: bone marrow derived dendritic cell

cDC: conventional dendritic cell

CTL: cytotoxic T lymphocyte

CTLA-4: cytotoxic T-lymphocyte-associated protein 4

DAMP: damage-associated molecular pattern

DMR: differentially methylated region

DNMT: DNA methyltransferase

EAE: experimental autoimmune encephalomyelitis

ELISA: enzyme-linked immunosorbent assay

EZH2: enhancer of zeste homolog 2

FACS: fluorescence-activated cell sorting

FBS: fetal bovine serum

GAS: gamma-activated sequence

GSK3: glycogen synthase kinase 3

HD: high dose

HDAC: histone deacetylase

HMGB1: high mobility group box 1

HPV: human papillomavirus

hr: hour(s)

HSP: heat shock protein

i.d.: intradermal

i.p.: intraperitoneal

IDO: indoleamine 2,3 dioxygenase

IFN: interferon

IRSE: IFN-stimulated response elements

iTreg: induced T regulatory cell

KLF4: Kruppel-like factor 4

LCMV: lymphocytic choriomeningitis virus

LD: low dose

LDL: low-density lipoprotein

LPS: lipopolysaccharide

Lrp1: low density lipoprotein receptor related protein-1

MACS: magnetic-activated cell sorting

MBD: methyl-binding domain protein

MDSC: myeloid-derived suppressor cell

MHC: major histocompatibility complex

min: minutes(s)

MSA: mouse serum albumin

MTB: *Mycobacterium tuberculosis*

ncRNA: non-coding RNA

NOD: non-obese diabetes

Nrp1: neuropilin-1

Nse: nuclease

nTreg: natural T regulatory cell

OVA: ovalbumin

pDC: plasmacytoid dendritic cell

PEC: peritoneal exudate cell

PLC: protein loading complex

PRC2: Polycomb repressive complex 2

RA: rheumatoid arthritis

s.c.: subcutaneous

SAM: S-adenosyl methionine

TAP: transporter associated with antigen processing

Tconv: T conventional cell

TCR: T cell receptor

TDE: tumor-derived exosome

TFBS: transcription factor binding site

Th: T helper

TL-dMNA: Tip-loaded dissolvable microneedle array

TLR: toll-like receptor

Treg: T regulatory cell

TSS: transcription start site

wk: week

1.0 PROJECT AIMS

Immunogenic HSPs such as gp96 have been used for clinical treatment of cancer, however current vaccination strategies require improvement. Specifically, it is unknown why some patients do not respond to therapy using gp96. Though it is clear that gp96 drives dichotomous T cell responses following *in vivo* immunization, it is unknown what events must occur upstream in order to obtain fully activated Treg. A further understanding of how Treg can expand in response to higher doses of gp96 is required not only for improvement of gp96 as a cancer immunotherapy, but also for potential development of HD gp96 for treatment of autoimmune disease and solid organ transplantation. In this thesis, I aim to identify the APC subset responsible for driving Treg responses to gp96, the key mediators that are produced, and how expression of these mediators is regulated. Using fluorescent gp96 immunization, we have identified a subset of pDCs which increases uptake of gp96 at higher doses. Using whole genome methyl-sequencing, we have identified neuropilin-1 (Nrp1) as a key mediator in this response. Expression of Nrp1 by pDCs increases both *in vivo* and *in vitro* by qPCR and flow cytometry, and is required for pDC-Treg stabilization as measured by live cell imaging in the presence of Nrp1 neutralizing antibody. We have also confirmed that pDCs and Nrp1 are both required for *in vivo* HD gp96 responses, measured by cytotoxicity levels and Treg expansion. Finally, we have begun to understand STAT1 signaling pathways that are activated in response to gp96 treatment. Together, these studies

improve our understanding of how APCs can respond to gp96 in different settings, and may provide insight to improve upon future immunotherapy.

1.1 AIM 1: IDENTIFY APC SUBSETS THAT INTERACT WITH GP96 AT HIGHER DOSES IN VIVO

We have established a model of HD gp96 immunization that results in establishment of tumor even when mice are immunized with irradiated tumor cells. Using CD91^{f/f}CD11c^{cre} mice, we will determine whether the gp96 receptor CD91 is required for HD gp96 immunity. We will also test whether Th1-skewing cytokine IL-12 can overcome suppressive immunity. Using fluorescently labeled gp96, we will also determine specifically which APC subsets in the draining lymph nodes interact with gp96 at different doses. CD91 expression in different APCs identified in this experiment will also be compared by flow cytometry. Finally, we will analyze the maturation profiles of various APC populations treated with gp96. The findings from this Aim reveal that CD91-expressing APCs are required for HD gp96 responses, and that pDCs may play a role in driving this response.

1.2 AIM 2: DETERMINE EPIGENETIC AND TRANSCRIPTIONAL CHANGES IN APCs THAT CAN DRIVE SUPPRESSIVE TREG RESPONSES

We will first test whether DNMTs, the enzymes responsible for the maintaining DNA methylation status in cells, are activated in APCs treated with gp96. To do this, APCs will be observed by

immunofluorescence and confocal microscopy for any changes in DNMT localization, and by western blot of nuclear proteins for any changes in DNMT expression. NF- κ B inhibitor cardamonin will be included to test whether these events are NF- κ B dependent. We will correlate these data with whole genome methyl-sequencing of gp96-responsive cells in LD and HD gp96 immunized animals. Using the data generated by this study, we will then determine the role(s) of specific target genes that may contribute to suppressive immunity. One gene of interest that we have identified from this screen is *Nrp1*, which controls the interaction between Treg and APCs. *Nrp1* expression on pDCs was confirmed *in vitro* and in LD and HD gp96 immunized animals. The ability of pDCs to interact with T cells (including Treg) will be verified by live cell microscopy, and *Nrp1* dependence will be tested by addition of *Nrp1* neutralizing antibody. Finally, the *in vivo* significance of both pDCs and *Nrp1* will be tested using modified versions of our HD gp96 model, in which suppression is measured using an *in vivo* cytotoxicity assay and Treg expansion. This Aim demonstrates that although epigenetic modifications occur in gp96-responsive APCs, there may be differences between individual subsets. Furthermore, it establishes a role for *Nrp1*⁺ pDCs in driving suppressive responses to gp96.

1.3 AIM 3: EXAMINE STAT1 ACTIVATION IN GP96-TREATED MACROPHAGES

Peritoneal macrophages will be treated with gp96 and phosphorylation of STAT1 at different sites will be observed by western blot. This will also be tested for dependence on p38 MAPK by pretreating macrophages with p38 inhibitor SB203580, and for CD91 dependence using CD91-deficient macrophages. We will also test whether STAT1 phosphorylation requires soluble factors made in response to gp96 treatment by culturing CD91 deficient macrophages in supernatants from

treated wildtype cells. CXCL10 mRNA and protein levels will be examined by qPCR and Luminex. Binding of STAT1 to the CXCL10 promoter will be observed using chromatin immunoprecipitation. Finally, we will test whether CXCL10 is required for NK cell activation following co-culture with macrophages by incubated cells in the presence of blocking antibody against the receptor for CXCL10, CXCR3. This Aim demonstrates that CXCL10 is a main driver of APC-NK cell in response to gp96 stimulation.

2.0 INTRODUCTION

HSPs are constitutively expressed intracellular chaperones present in all cell types, from prokaryotes to eukaryotes. Within host cells, HSPs can bind to endogenous peptides, lipids, and myriad other molecules. HSP-bound peptides can be of self, tumor, or pathogen origin, all of which can be synthesized by mammalian host cells under steady state, tumorigenesis, or infection, respectively. One of their main functions is to ensure the proper folding and assembly of proteins. Interestingly, certain members of the HSP family can elicit protective immunity when they interact with immune cells. These are broadly referred to as the immunogenic HSPs and are classified as danger-associated molecular patterns (DAMPs). Because of their unique antigen-binding and adjuvant properties, immunogenic HSPs have been used for cancer immunotherapy. Tumor-derived HSP vaccines are promising, but treatment in human patients requires improvement. Whether lack of efficacy is due to some inherent property of HSPs or suppressive factors in the tumor microenvironment is not known. HSPs are able to suppress immune responses when given at higher doses or when they interact with suppressive APC subsets including pDCs and myeloid derived suppressor cells (MDSCs)(1, 2). Both of these suppressive APC subsets are highly prevalent in tumor-bearing hosts (3, 4). The suppressive response to HSPs is dominated by Treg which ultimately overcome the CTLs which are necessary for protective anti-tumor immunity (5, 6). My thesis work has been to elucidate the mechanisms used by HSPs on a cellular, genomic, and immunologic level to better understand the dose dichotomy of HSP vaccination. Data generated by these studies may offer potential improvements upon current clinical trials and motivate interest in HSPs as a putative therapy for autoimmune disease. In this introduction, I will

review several key facets of HSPs, their receptor CD91, and prospective avenues by which HSPs may regulate immune responses.

2.1 HSPS AND ANTI-TUMOR IMMUNITY

2.1.1 Tumor antigens and generation of antigen-specific T cells

Prior to the 1940's, it was debated whether immunity was generated against tumors. Yet in 1943, it was demonstrated that mice immunized with tumor cells are immune to subsequent challenge with the same cells used for immunization (7). These and other studies revealed that tumors possess specific antigens which alert the immune system, resulting in killing of tumor cells. Tumor antigens may take the form of peptides or other molecules that are distinct from “normal” tissue due to the accumulation of genetic mutations or post-translational modifications. These antigens may be shared between tumors of the same histology, or truly unique to a specific tumor. Shared antigens tend to originate from molecules that are critical for tumor cell proliferation and survival, such as mutated B-RAF and MART-1 (8, 9). Unique tumor antigens are more difficult to identify, since in many cases they are specific to the patient from which the tumor was isolated (10).

One goal of tumor immunotherapy is to immunize against tumor antigen mainly through generation of specific T cells (11). Briefly, antigen-specific CTLs require 3 signals in order to become activated: 1) antigen must be presented in the context of the major histocompatibility complex (MHC) on APCs, 2) co-stimulatory markers (i.e., CD40, CD80, CD86) on APCs must engage cognate receptors (i.e., CD28) on CTLs, and 3) activating cytokines such as IL-2 must be present to enhance CTL activation and survival. Successful immunization against tumors must

employ all three signals for full stimulation of CTLs. Additionally, elicitation of antigen-specific CTLs may require some degree of cognate CD4⁺ Th cell licensing of the APC via the CD40-CD40 ligand (CD40L) axis and cytokines such as IFN γ (12, 13).

2.1.2 HSPs as tumor rejection antigens

Once it was discovered that tumors indeed elicit specific immunity, the question of how this immunity is generated was of key importance. There are several approaches to answer this question. Identification of tumor-specific antigens recognized by T cells is one such approach. However, the tools necessary for identifying such molecules were not readily available until recently. Another approach to this question involves biochemical/chromatographical fractionation of tumor cell homogenates to identify the immunogenic fraction. Using this method, Srivastava *et al.* immunized mice with different tumor cell fractions and challenged mice with live tumor cells to test for change in tumor growth (14). Fractions capable of eliciting protective immunity were then refractionated on additional chromatographical properties until homogenous fractions were obtained and identified. Through this work it was revealed that gp96 (and later, other immunogenic HSPs) was the protein responsible for tumor rejection. Specificity of the immune response elicited by gp96 was identical to irradiated tumor cells, in that gp96 preparations are protective only against the tumor cells from which they are derived (i.e., HSPs are not cross-protective). This is due to the tumor-specific peptides which are bound by gp96.

2.1.3 Association of antigenic peptides with immunogenic HSPs

To date, six immunogenic HSPs have been characterized: gp96, hsp70, hsp90, calreticulin, hsp110, and grp170. Data presented in this section will focus on the first four HSPs listed since these are the most well studied. These immunogenic HSPs shuttle peptides from the proteasome to MHC during peptide processing in APCs. The peptides bound by HSPs thereby comprise the entire antigen repertoire of their host cell (15, 16). This is consistent with the absence of free peptides in cells due to the instability of free short peptides within the cytosol (16, 17). However, generation of endogenous peptides and presentation of these antigens on MHC I to T cells constantly occurs in cells. How then do these peptides circulate from the proteasome to MHC? Cytosolic hsp70 and hsp90 shuttle peptides from the proteasome to the transporter associated with antigen processing (TAP)(18-20). Once antigenic peptides pass through TAP, they are chaperoned by gp96 to the peptide loading complex (PLC)(16, 21). In the PLC, MHC is bound by calreticulin to retain it in its partially folded state (22, 23). Consistent with this, gp96 and calreticulin can be co-immunoprecipitated with MHC (24). Work from our lab shows that treating cells with calreticulin-specific siRNA results in accumulation of gp96-associated peptides and a reduction in MHC-bound peptides, confirming that gp96 and calreticulin work together to relay peptides to MHC (16). Similarly, cells treated with hsp90 inhibitors generate “empty” MHC that is immediately internalized (20). Work using a TAP-deficient cell line (RMA/S) has shown that most, but not all, peptides that are bound to gp96 are required to first go through TAP (25).

2.1.4 Clinical trials using HSPs

The immunostimulatory properties of HSPs thus provide an attractive therapy for cancer, since this circumvents the need for identification of specific tumor antigens and adjuvants. HSP vaccination has been shown to work both prophylactically and therapeutically in mouse models of cancer. Prophylactic treatment with tumor-derived HSPs usually involves isolation of tumor-derived HSPs, injection of HSP, and challenge using the same tumor from which the HSP was derived. In mice, this has been done using numerous tumor models that vary across cell type and immunogenicity, including fibrosarcoma (14, 26, 27), B cell leukemia (28), colon carcinoma (29), and lung carcinoma (30). Therapeutic efficacy has also been demonstrated in animal models. This has been shown using two different approaches: 1) HSPs are derived from established tumors and injected into the tumor-bearing host, or 2) mice are injected with tumor-derived HSP 1-2 weeks following tumor challenge. Kovalchin *et al.* have shown that surgical removal of Meth A tumor and subsequent immunization with Meth A-derived gp96 provides a greater survival advantage over surgery alone (31). In the same study, it was shown that up to 31 days following tumor challenge, treatment with tumor-derived HSP resulted in decreased metastasis. Similar results have been shown using a B16 melanoma model (32).

Similar to mouse models, human responses to HSP immunization have also been documented. In the case of humans, autologous HSPs are derived from the patient's established tumor following resection of primary or metastatic tumor. Thus, in the setting of human cancer, HSPs are used as a therapeutic vaccine to resolve existing tumor and preclude malignancy. A summary of completed and ongoing clinical trials is provided below (Table 1; adapted from (33)). There have been no reports of severe side effects following HSP vaccination. As aforementioned, although the results from clinical trials using HSPs have been promising, some patients do not

respond to HSP immunotherapy. This may be due to a variety of factors, including disease stage and the level of suppression within the tumor microenvironment. Clearly, a better understanding of how HSPs generate immunity is required to improve upon current treatments.

Table 1: Summary of clinical trials using autologous HSP

Tumor type	Trial	Year	Outcome	Reference
Varied	I	2000	6/12 T cell, 8/12 NK cell expansion (FC, ELISPOT)	(34)
Colorectal	II	2003	CD8 ⁺ T cell response (IFN γ ELISPOT); 79% OS, 33% DFS	(35)
Melanoma	II	2002	2/28 CR, 3/28 SD, 11/28 CTL activation, 3/28 DFS	(36)
Melanoma	II	2006	11/18 SD, 5/18 T cell, 12/18 NK cell response	(37)
Melanoma	III	2008	No difference in OS	(38)
Melanoma	I/II	2010	5/26 CTL response; 45% PFS	(39)
Non-Hodgkins lymphoma	II	2003		(40)
Non-Hodgkins lymphoma	II	2007	8/20 SD	(41)
Pancreatic adeno-carcinoma	I	2007	1/5 T cell response, 3/10 SD	(42)
Renal cell carcinoma	II	2008	2/60 CR, 2/60 PR, 7/60 SD, 33/60 progressed, 16/60 USD	(43)
Renal cell carcinoma	III	2008	No difference in OS, recurrence in 37.7% treated with gp96, 39.8% in untreated	(44)
Glioblastoma	I/II	2012	11/12 T cell response	(45)
Glioblastoma	II	2014	Ongoing	(46)
Glioblastoma	II	2017	Ongoing	(47)

Abbreviations: FC, flow cytometry; OS, overall survival; DFS, disease-free survival; CR, complete response; SD, stable disease; PFS, progression-free survival; PR, partial response; USD, unconfirmed stable disease

2.2 KNOWN MECHANISMS DRIVING HSP RESPONSES

2.2.1 Cross-presentation of peptides chaperoned by HSPs

Unlike presentation of endogenous peptides, cross-presentation is an activity that is restricted only to professional APCs, specifically dendritic cells (DCs). Extracellular antigen is taken up, processed, and presented on MHC I by APCs to CTLs. Naïve T cells can then be activated in response to foreign antigen, and this event called cross-priming. In general, cross-priming is measured by stimulating APCs with antigen or immunogenic cell lysates, co-culturing APCs with T cells, and measuring T cell activity by target cell lysis and/or cytokine production. Cross-priming activity can also be assayed *in vivo* by these methods and by detection of tetramer-positive CTLs. Substantial evidence exists for HSP-mediated cross-presentation and priming events (48-53). We have shown that depletion of major HSPs, but not antigenic proteins, from tumor cell lysates diminishes cross-priming (49). Similarly, using FITC-labeled ovalbumin (OVA) peptide, uptake and presentation by APCs was enhanced when OVA was bound to HSP (48). This study utilized HSPs bound to an extended 18-mer OVA peptide (EQLESIINFEKLLVLLKK) to demonstrate that the peptides require additional processing by the APC and do not merely associate with extracellular MHC. To show that gp96 can efficiently cross prime T cells, Staib *et al.* complexed gp96 to melanoma antigen MART-1 and co-incubated APCs primed with gp96/MART-1 with MART-1 specific CTL clone 2/9 (50). Interferon (IFN) γ production by CTLs was measured by ELISA. The authors found that pre-incubation of APCs with gp96/MART-1 complexes resulted in maximal IFN γ secretion by CTLs. Finally, antigen-specific CTLs can be detected *in vivo* following immunization with gp96. In one such study, gp96 was purified from a tumor cell line which expresses *Escherichia coli* (*E. coli*)-derived β -gal (51). Thus, if gp96 can cross-prime CTLs,

immunization with these gp96 preparations should result in β -gal specific T cells. Mice were injected with an intraperitoneal (i.p.) dose of gp96, and after 5 days their splenocytes were treated twice with β -gal peptide. Specific lysis of target cells by CTLs was significantly higher in gp96-immunized mice compared with vehicle controls. The ability of HSPs to induce maturation in APCs will be discussed in the next section. Taken together, the ability of HSPs to bind antigenic peptides, induce cross-priming of T cells, and allow for efficient uptake explains how HSPs act as their own adjuvant to promote anti-tumor immunity.

Importantly, HSP-bound peptides can also be presented on MHC II for activation of CD4⁺ T cells (52, 54, 55). Similar to CTL activity assays, CD4⁺ T cell activity against tumor cells can be measured *in vitro* by proliferation and IL-5 secretion. In one such study, CD4⁺ T cell clones (24D3 and 12D1) were obtained from mice immunized with Meth A tumor cells. Specific anti-tumor activity was increased in 24D3 and 12D1 T cells when they were co-cultured with APCs pulsed with Meth A gp96 (52). Activated CD4⁺ T cells were also detected *in vivo* in gp96 immunized hosts. Thus, HSP immunization can result in activation of both CD8⁺ and CD4⁺ T cells.

2.2.2 CD91 as the receptor expressed on APCs

APCs can take up extracellular matter via several pathways, including pinocytosis and receptor-mediated endocytosis. By the mid-1990's it was known that phagocytic cells were responsible for uptake and presentation of HSP-bound peptides, but the mechanism through which HSPs were being internalized was unknown. When compared with free peptide, HSP-bound peptides were re-presented ~100-fold more efficiently (56). Given the efficient association of HSP-bound peptides with MHC (57), it was proposed that professional APCs express HSP-specific receptor(s) (58). To determine which, if any, receptor could bind HSP, membrane extracts derived from a detergent-

treated macrophage-like cell line (RAW264.7) were applied to gp96-immobilized agarose columns (59). Through mass spectrometry, low density lipoprotein receptor related protein-1 (Lrp1; herein called CD91) was identified as the specific receptor for gp96. Following CD91-dependent internalization in macrophages, gp96 is trafficked to an endocytic compartment that is negative for transferrin, Rab5a, and CD1 (21). This compartment stained positive for Fc receptor and MHC I, which is consistent with gp96-associated peptide presentation on MHC. It was later confirmed that hsp70, hsp90, and calreticulin share CD91 as their receptor as well (60).

In agreement with *in vitro* studies, our lab has demonstrated that gp96 binding *in vivo* is strictly dependent on CD91 expression by DCs (61). In this study, gp96 was fluorescently labeled and tracked following *in vivo* immunization. CD11b⁺CD11c⁺ conventional DCs (cDCs) were the main cell type associated with gp96. This population also expressed the highest level of CD91 compared with other DC subsets observed in this study, suggesting that CD91 expression is correlated with HSP uptake. Following release from damaged cells *in situ* or through administration via vaccination, CD91 has been demonstrated to be essential for endocytosis of HSP-peptide complexes and cross-presentation of the chaperoned peptide (48, 52, 53, 59, 60, 62). Selective deletion of CD91 in cDCs renders mice incapable of priming Th1/CTL immune responses against tumors when immunized with gp96 (26). Therefore, in addition to binding antigenic peptides, HSPs provide an efficient means by which APCs can take up antigenic peptides via receptor-mediated endocytosis.

Other endocytic receptors for HSPs have been proposed, including LOX-1 (63), SRA (64), and SREC-1 (65). Toll-like receptor 2 (TLR2) and TLR4 have also been proposed to bind HSPs to activate various signaling pathways (66, 67), however binding to TLRs is not sufficient for internalization of HSP-peptide complexes as these receptors are not endocytic.

Presentation of peptide alone is not sufficient to generate anti-tumor immunity; co-stimulatory molecules and cytokines are additionally required for full activation of T cells. In addition to its activity as an endocytic receptor, studies have shown that signaling pathways are activated downstream of HSP-CD91 interaction (62). This is not surprising since other CD91 ligands can mediate proliferation, migration, maturation and differentiation in various cell types through this receptor using diverse signaling pathways (62, 68, 69). CD91 is expressed on multiple professional APCs, including macrophages, cDCs, and pDCs (Table 2). When gp96 binds to CD91 on DCs, intracellular signaling pathways are activated to drive their phenotype (62, 70), as discussed in the next section. With the exception of pDCs, all APCs that have been tested increase maturation markers MHC II and CD86, but not CD80 or CD40. To our knowledge, there have been no reports comparing cytokine expression in response to gp96 using APCs with comparable levels of CD91.

2.2.3 Signaling mediators activated by HSP-CD91 interaction

The size, intricate secondary structure, and ligand repertoire of CD91 contribute to the complexity of signaling pathways initiated by this receptor. It is widely expressed on immune cells (particularly APCs), neurons, hepatocytes, adipocytes, and fibroblasts (60, 71-74). Due to its ability to bind a large array of ligands, many biological functions have been ascribed to CD91. It is indispensable for prenatal development, axonal regeneration, cholesterol metabolism, and uptake of apoptotic cells (68, 75-78). For the purpose of this thesis, its signaling activity and role in the immune response will be the main focus.

Table 2: CD91 expression in various APC subsets

APC type	HSP tested	CD91 expression	Specific binding tested?	Mediators/outcome	Ref
RAW264.7 mac, PECs	gp96	MS	Yes (<i>in vitro</i>); gp96-FITC uptake (IF, FC), blocked by α 2M	Re-presentation (MHC I)	(59)
BMDCs, PECs	gp96, hsp90, hsp70, CRT	IF	Yes (<i>in vitro</i>); gp96-FITC uptake (FC), blocked by anti-CD91 antibody	Re-presentation (MHC I)	(60)
BMDCs, BMMs	hsp70		Yes (<i>in vitro</i>); blocked by anti-CD91 antibody	Re-presentation (MHC II)	(48)
spleen DCs, BMDCs	gp96		Yes (<i>in vitro</i>); blocked by anti-CD91 antibody	Re-presentation (MHC I,II)	(52)
RAW264.7 mac, PECs	gp96, hsp70, CRT	WB, FC	Yes (<i>in vitro</i>); blocked by anti-CD91 antibody	p38 MAPK, NF- κ B, TNF, IL-6, IL1 β , maturation	(62)
CD11b ⁺ CD11c ⁺ DCs	gp96	WB, FC, IF	Yes (<i>in vivo</i>); gp96 _{A488} uptake (IF, FC)	Re-presentation (MHC I)	(61)
Adherent PECs	gp96	FC		CXCL10, RANTES, maturation	(30)
BMDCs, CD11c ⁺ DCs	gp96	WB, FC	Yes (<i>in vivo</i>); blocked by CD91 inhibitor RAP	IL-1 β , maturation	(26)
pDCs, CD11b ⁺ CD11c ⁺ DCs, BMDCs	gp96	FC	Yes (<i>in vivo</i>); gp96 _{A488} uptake (FC)	Maturation (BMDCs), Nrp1 (pDCs), DNMT1	(79)
monocytes (human)	hsp70	FC		Maturation	(80)
pDCs (human)	gp96	FC	Yes (<i>in vitro</i>); gp96 _{A488} uptake, blocked by α 2M	IL-8, NF- κ B	(1)
monocytic DCs (human)	hsp70	WB, FC		Re-presentation (MHC II), IL-5, IL-10, IFN γ	(81)

All APCs are murine derived unless otherwise stated. Abbreviations: BMDC, bone marrow-derived DC; BMM, bone marrow-derived macrophage; PEC, peritoneal exudate cells; mac, macrophage; CRT, calreticulin; MS, mass spectrometry; WB, western blot; FC, flow cytometry; IF, immunofluorescence; RAP, receptor-associated protein

CD91 is a member of the low density lipoprotein (LDL) receptor family and is a type I transmembrane receptor. It is synthesized as a 600 kDa protein containing a furin cleavage site. Upon transport to the cell surface, CD91 is processed into two domains, the 515 kDa α -chain and the 85 kDa β -chain. The two domains are then non-covalently re-associated to form a functional receptor. The α -chain contains four potential ligand-binding domains, with most ligands binding

domains II and IV (68). The specific domain utilized by the various immunogenic HSPs is an area of active research. The β -chain is comprised of a short extracellular portion, a transmembrane domain, and an intracellular domain. This intracellular domain contains two NPXY motifs that become phosphorylated upon ligand binding and are responsible for binding pTyr-binding domains of signaling proteins (82). This event regulates association with adaptor molecules including Disabled-1 (DAB-1), FE65, JNK-interacting protein 1 (JIP1), postsynaptic density protein 95 (PSD-95), Src homology 2 domain containing protein (SHC), sorting nexin 17 (Snx17), and CED-6/GULP (83). Association of adaptor molecules seems to be ligand-specific, therefore HSP-CD91 binding may involve some but not all of the molecules listed above.

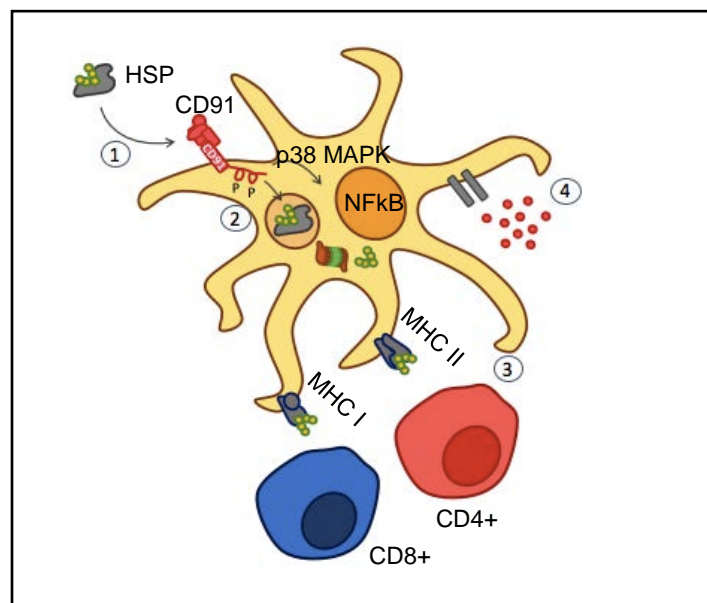


Figure 1. HSP-CD91 interaction results in endocytosis and/or signaling.
 (1) HSP-CD91 interaction; (2) Endocytosis and processing; (3) Presentation of peptide and T cell activation; (4) Increased maturation markers and cytokines.

In addition to acting as an endocytic receptor, CD91 also acts as a signaling receptor in response to HSP binding (Figure 1). Previous studies from our lab have revealed that gp96 and calreticulin require the membrane distal but not proximal NPXY motif for NF- κ B activation,

whereas hsp70 utilizes both motifs (62). This suggests that different HSPs may employ different signaling pathways downstream of binding to CD91. Differential cytokine profiles in response to gp96, calreticulin, and hsp70 provide additional evidence for this idea (Table 3). All three HSPs can activate NF- κ B and result in upregulation of co-stimulatory molecules including CD86 and MHC II. As a result, cDCs stimulated by extracellular gp96 undergo maturation. This satisfies all three criteria for generation of T cell immunity, making these DCs highly proficient at priming Th1/CTL responses.

Table 3. Cytokines produced by macrophages treated with immunogenic HSPs.

	gp96	calreticulin	hsp70	Regulation
IL-1ra	++++	++	-	NF- κ B/STAT1
G-CSF	+	+	-	MAPK
IL-6	+++	+++	+	NF- κ B/MAPK
CXCL10	+	+	+	NF- κ B/STAT1
CCL17	+	+	+	NF- κ B
IL-12p70	++	++	++	NF- κ B
CXCL11	-	+	-	NF- κ B/STAT1
TREM1	++++	++	-	STAT1
IL-1β	+++	+++	+++	NF- κ B
TNF-α	+	++++	-	NF- κ B

Modified from Pawaria and Binder (62).

Our lab has also shown that activation of p38 MAPK occurs for all HSPs tested (62). We have observed no evidence for activation of Akt, ERK1/2, JNK 1/2/3, MKK 3/6, or MAK2. p38 MAPK is an ubiquitously expressed and evolutionarily conserved signaling molecule that is activated via phosphorylation. Immunological stress and cytokines activate the p38 pathway which contributes to expression of immune mediators (84-86). Along with PI3K, p38 is crucial for IL-12 expression in DCs (87). Given this, it is not surprising that HSPs activate the p38 pathway in APCs since Th1 activation is a hallmark of gp96-mediated anti-tumor immunity. p38 MAPK can also

lead to activation of various transcription factors, including STAT1, ATF-2, MEF-2, CREB and Elk-1 (88).

2.2.4 STAT1 as a potential mediator downstream of CD91

Outside of its potential role as an intermediary of Th1 responses, it is currently unknown what the downstream consequences of p38 MAPK activation are for HSP-mediated immunity. MAPKs are activators of STAT1, a cytokine-activated transcription factor well known for its role in cellular responses to IFN stimulation. Expression of STAT1 target genes can lead to many outcomes including cell growth, antiviral activity, and inflammation (89). STAT1 phosphorylation in response to bacterial lipopolysaccharide (LPS) and cell stress is p38 MAPK-dependent (90). Our lab has previously shown that several STAT1-regulated cytokines are expressed in response to HSP stimulation *in vitro* (30, 62)(Table 3), suggesting that STAT1 may be activated in response to HSPs.

Under basal conditions, STAT1 exists in an inactive state. It contains two potential phosphorylation sites, one tyrosine (Y701) and one serine (S727), both of which can trigger activation. Phosphorylation of Y701 induces SH2 domain-mediated dimerization and nuclear translocation of STAT1 in response to type I and II IFNs (91), whereas S727 phosphorylation increases transcription factor activity downstream of IFN γ (92). Upon phosphorylation, STAT1 can form either a homodimeric or heterotrimeric complex. IFN γ induces formation of the STAT1/STAT1 homodimer which binds to palindromic gamma-activated sequences (GAS). Stimulation by type I IFN produces a STAT1/STAT2 heterodimer which subsequently forms a trimeric complex with IFN regulatory factor 9 (IRF9). The full trimeric complex has an affinity

for IFN-stimulated response elements (IRSE). Binding of STAT1 to GAS versus IRSE in part explains the specific gene signatures that arise in response to different IFNs.

IFN-independent STAT1 activation is less well understood. Phosphorylation of STAT1 at S727 (pSTAT1-S727) is mediated by p38 MAPKs in response to cell stress in macrophages (90, 93). Although phosphorylation at both Y701 and S727 is required for IFN-dependent nuclear translocation and gene expression, p38-mediated S727 phosphorylation alone is sufficient for activation of a distinct STAT1 signature in response to viral infection. pSTAT1-S727 induced by viral infection can upregulate cytokines IL-1 β , IL-8, and ISG54 (93). Interestingly, rapid phosphorylation of S727, but not Y701, occurs in response to LPS, ultraviolet radiation, and IL-1 β (90, 94-96). Luu and colleagues have shown that stimulation of TLRs 2, 3, 4, 7, or 9 triggers S727 phosphorylation within 10-30 minutes, whereas only TLRs 3 and 4 can activate Y701 by 2 hrs post stimulation (97). Rapid phosphorylation of S727 was directly associated with the TLR pathway via TRAF6. LPS-treated macrophages exhibited nuclear translocation of STAT1 and enhancement of NF- κ B signaling upon S727 phosphorylation. Late phosphorylation of Y701 seemingly occurs indirectly through autocrine signaling in response to factors produced in response to TLR stimulation. In all cases, activation of STAT1 was IFN-independent. We propose that immunogenic HSPs utilize a similar signaling pathway to upregulate STAT1 target cytokine expression. This hypothesis is tested in Chapter 3 of this thesis.

2.3 DOSE DICHOTOMY OF HSP-MEDIATED RESPONSES

2.3.1 Application of HSP immunization in autoimmune disease and solid organ transplantation

Vaccination with tumor-derived gp96 elicits a potent anti-tumor T cell response in mice and humans characterized by Th1 responses. However, priming of Th1 responses is precisely dependent on the dose of gp96 and immunization with a microgram (herein called low dose, LD) of gp96 elicits Th1/anti-tumor immunity. Intriguingly, a ten-fold higher dose of gp96 (high dose, HD) elicits a suppressive immune phenotype characterized by the preferential expansion of CD4⁺ Treg. Whereas CTLs are known for their ability to lyse infected and tumor cells, Treg shut down pro-inflammatory responses and are essential for preventing autoimmunity.

The existence of a suppressive response driven by gp96 has been recognized since the initial identification of HSPs as tumor rejection antigens. Srivastava and colleagues appreciated that increased “units” of immunization no longer resulted in tumor protection (14). In fact, increased dose led to accelerated tumor growth in some experiments. Few attempts were made to further understand this phenomenon until over a decade later, demonstrated by Chandawarkar and colleagues. In agreement with previous findings, intradermal (i.d.) injection of 1 µg Meth A gp96 elicited tumor-protective immunity, whereas injection of 10 µg Meth A gp96 did not (98). Furthermore, immunization with the higher dose of gp96 generated a suppressive response that could be transferred through the CD4⁺ T cell compartment. The same group later showed that suppression does not require source specificity per se, but an ongoing T cell response is necessary for full HD gp96-mediated suppression (99). A non-obese diabetes (NOD) mouse model was used in this study to show that timing of HD gp96 immunization was crucial for its outcome. The

autoimmune process of insulinitis begins around 6 wk of age in NOD mice (100). Treatment of NOD mice at the onset of insulinitis (6-8 wk) resulted in complete protection against disease. All NOD experiments were performed using liver- or pancreas-derived gp96 preparations, suggesting that the response is independent of antigen.

The HD gp96 response has also been used for the prevention of autoimmune disease in mouse models of experimental autoimmune encephalomyelitis (EAE)(99) and rheumatoid arthritis (RA)(101), for the extension of allograft survival in mice and rats (102, 103), and for suppression of other Th1-mediated immune responses (104, 105). Kovalchin and colleagues found that treatment of mice with HD gp96 significantly improved survival of skin grafts in mice by about 5-fold, even with major antigenic disparity (102). Similar findings from Slack *et al.* showed that donor-derived, but not recipient-derived, HD gp96 could prolong transplant survival (103). In this study, Lewis rats were immunized with HD gp96 derived from either Wistar or Lewis rats. Hearts from Wistar rats were then transplanted into Lewis rat recipients. Heart grafts in the group that received Wistar (donor) gp96 showed prolonged survival over those treated with Lewis (recipient) gp96. This suggests that gp96-bound alloantigenic peptides may be important in the context of transplant survival and is one of only a few studies which have shown any degree of specificity in the gp96 used to generate HD suppression. In the future, additional experiments should be performed using an antigen-specific model to confirm these findings. Finally, Li *et al.* have shown that HD liver-derived gp96 can limit immune hyperactivation in the liver using a model of ConA- and anti-CD137-induced liver injury (104). In addition to mammalian HSPs, a suppressive response hallmarked by Treg and IL-10 production can be achieved using microbial hsp70 (101). However, the mechanisms driving responses to microbial and mammalian HSPs may differ. Taken

together, HD gp96 suppression can be used to treat a wide range of conditions and is a viable option for the treatment of autoimmunity and transplantation.

2.3.2 Mechanisms driving HD gp96-mediated suppression

The apparent *volte-face* immune response elicited with LD versus HD gp96 immunization has until 2012 lacked a mechanistic explanation, despite the application of the phenomenon to ameliorate multiple pathological conditions in mice and humans. Table 4 provides a representative list of studies that have elucidated the regulatory responses elicited by immunogenic HSPs.

Table 4: Summary of suppressive responses to HSP

HSP type	Targeted cells	Mediators	Outcome	Reference
mouse gp96	Treg (<i>in vivo</i> HD)	IL-10, Ki67	increased Foxp3 ⁺ Treg; decreased liver inflammation	(104)
mouse gp96	Treg (<i>in vivo</i> HD)	IL-10	decreased CTL activation	(105)
mouse gp96	<i>in vivo</i> HD	-	decreased EAE, diabetes	(99)
mouse, rat gp96	<i>in vivo</i> HD	-	increased allograft survival	(102, 103)
mouse gp96	mouse Treg (<i>in vitro</i>)	NF-κB, IL-10, TGF-B, Foxp3	-	(104)
tumor gp96	<i>in vivo</i> HD	-	decreased tumor immunity	(98)
tumor hsp70	MDSC (<i>in vitro</i>)	STAT3	decreased T cell proliferation, IFNγ production	(2)
MTB-hsp70	<i>in vivo</i>	IL-10	decreased RA	(101)
MTB-hsp70	Treg (<i>in vivo</i>)	IL-10	decreased <i>L. monocytogenes</i> killing	(106)
human gp96	human pDCs (<i>in vitro</i>)	IL-8, NF-κB	decreased monocyte maturation	(1)

As previously mentioned, HD gp96 immunization involves CD4⁺ T cells including Treg. Treg can drive suppressive immunity through many mechanisms, including: 1) production of suppressive cytokines such as IL-10, 2) sequestration of survival signal IL-2, 3) conversion of ATP to adenosine, and 4) inhibition of APCs via cytotoxic T-lymphocyte-associated protein-4 (CTLA-

4) (107). Similar to CTLs, Treg are activated via MHC-T cell receptor (TCR) engagement and IL-2 (108, 109), although in some cases this appears to be dispensable (110). In the same study demonstrating the efficacy of HD gp96 in treating liver inflammation, it was also revealed that suppression was specifically generated through Treg (104). HD gp96 immunization resulted in 29 and 78% higher numbers of Treg in spleen and liver, respectively. These Treg were more highly active by Ki67 staining and expressed more Foxp3 and IL-10 compared with vehicle treated controls. In a similar study, mice were immunized with LD or HD gp96 conjugated to specific peptide (K^d restricted epitope)(105). Using tetramer to detect antigen-specific CTLs following 2 rounds of immunization, Liu and colleagues detected fewer tetramer-positive CTLs and more Treg in HD versus LD immunized mice. Treg specificity was not measured, so whether these Treg are antigen specific or if they utilize a bystander suppression mechanism is unknown. Treg depletion by cyclophosphamide resulted in restoration of CTLs in this system. Thus there exists a balance between Treg and CTLs that is dependent on gp96 dose. Although gp96 immunization simultaneously activates both CTLs and Treg, CTL activation outpaces that of Treg following LD immunization, whereas the opposite is true in the context of HD gp96. Because a low level of Treg may be generated in response to LD gp96, it is also important to consider their role in suppressing tumor immunity. It is entirely possible that this low level of Treg activation in response to gp96 is critical for contraction of the pro-inflammatory phase, similar to situations of infection and pregnancy. Yan *et al.* showed that depletion of Treg following LD gp96 treatment greatly enhanced tumor rejection compared with either treatment alone (111). It was concluded from this study that the efficacy of gp96 immunization in clinical trials could be improved by blocking Treg. Taken together, it is clear that CD4⁺ T cells, particularly Foxp3⁺ Treg, are the driving force behind HD gp96 suppression.

Comparatively little is known about the effects of HD gp96 on the phenotype of APCs. Increasing the concentration of gp96 *in vitro* from 50 µg/ml to 250 µg/ml enhances NF-κB signaling in APCs (62), yet the functional outcome of this was not tested. It is possible that targeting an alternate APC type may result in activation of suppressive immunity. pDCs are a subset of DCs with diverse functions, and are mainly involved in anti-viral responses and induction of Treg under certain contexts including cancer (112, 113). These cells are highly prevalent in tumors and tumor draining lymph nodes and may contribute to the suppressive tumor microenvironment (4). Human pDCs bind gp96 and activate the NF-κB pathway in a CD91-dependent manner (1). Moreover, gp96-stimulated pDCs can limit the maturation of monocytic macrophages and their production of pro-inflammatory cytokines IL-6, IL-8, and TNF. Whether pDCs play any role in activating Treg in response to gp96 was not tested in this study. pDCs do not, however, increase expression of immunosuppressive enzyme indoleamine 2,3 dioxygenase (IDO) in response to gp96 (104).

There is also a potential role for MDSCs in generating a suppressive response to hsp70. MDSCs are a heterogeneous population of cells from the myeloid lineage that robustly expand under chronic inflammatory conditions such as cancer and infection. MDSCs are distinct from other myeloid cells in that they possess strong immunosuppressive properties (114). Hsp70-positive tumor-derived exosomes (TDEs) harvested from the supernatants of tumor cells can bind to MDSCs *in vitro* and promote suppressive activity via STAT3 (2). When TDE-stimulated MDSCs were co-cultured with OVA-specific CTLs, T cell proliferation and IFN γ production were blunted. This activity was determined to be hsp70-specific, since TDEs derived from hsp70-deficient tumor cells did not activate this pathway. Treatment of MDSCs with recombinant hsp70 alone was sufficient to trigger this suppressive phenotype as well.

Clearly, APC responses to HSPs are dependent upon the type of APC which is engaged. The fact that both pDCs and MDSCs can bind to HSPs, initiate suppressor functions, and are prevalent in tumor-bearing hosts is a concern for use of HSPs cancer immunotherapy. A further understanding of how these APCs respond to HSPs is therefore required to improve upon clinical trials using HSPs.

2.3.3 HSPs in autoimmunity

Because of the immunogenic properties of HSPs, it was hypothesized that local and continuous stimulation by extracellular HSPs could result in chronic immune activation and inflammation. Humans with RA have elevated gp96 and hsp70 in the synovial fluid of inflamed joints (115-117). Furthermore, treatment of fibroblasts with synovial fluid from RA patients resulted in increased surface hsp70. Surface expression of hsp70 is known to occur on stressed cells to make them more vulnerable uptake by CD91 (78, 118). It is possible that elevated hsp70 in the synovial fluid and surface expression of hsp70 by fibroblasts contributes to the local inflammatory response by binding its receptor and triggering cytokine release.

Whether vaccination with self- or even bacteria-derived HSPs can elicit an autoimmune response in the host was a primary concern when HSP immunotherapy was first introduced. Yet in both rodents and humans, autoimmunity following HSP treatment has never been recorded (119). Treatment of rats with *Mycobacterium tuberculosis* (MTB)-derived hsp70 (MTB-hsp70) prior to adjuvant-induced arthritis actually prevents autoimmune sequelae (119, 120). Pre-treatment of mice with MTB-hsp70 can also suppress T cell responses to *Listeria monocytogenes* via IL-10 production (106). In both cases, these suppressive responses seem to be directed toward the HSP molecule itself rather than peptides bound by it. Whereas RA patients have a persistence

of hsp70 in the synovial fluid, immunization provides a fixed bolus of HSP that is taken up within a 48-hour period (61). The level of HSP persistence and availability to APCs may explain the apparent discrepancy between these studies.

2.4 DNA METHYLATION AS A MECHANISM FOR TRANSCRIPTIONAL REGULATION OF IMMUNE RESPONSES

With the development of the Human Genome Project and next generation sequencing, interest in genomic regulation has exploded over the last decade. Yet genomic sequences are only a minute part of the picture. We can now appreciate that many other factors are involved in transcriptional regulation, particularly epigenetic modifications. Epigenetic marks include but are not limited to: post-translational modification of histone tails, chromatin packaging, non-coding RNAs (ncRNAs), and DNA methylation. This section will focus on DNA methylation, since in certain cells DNMT1 can work in tandem with active NF- κ B (121), an important moderator of immune responses. Thus DNA methylation may be a viable mechanism through which HSP responses are arbitrated.

2.4.1 DNA methylation is an epigenetic mark that regulates gene expression and histone modification

DNA methylation is the only epigenetic mark known to directly modify DNA via covalent attachment of a methyl group to the C5 position of cytosine residues. It preferentially occurs on CpG dinucleotide sequences, although methylation has been detected on non-CpG in embryonic

stem cells, adult mammalian neurons, MTB-infected macrophages, and human CD4⁺ T cells (122-125). Presumably, non-CpG methylation has been detected only recently due to advances in our ability to measure methylation at single base resolution by bisulfite PCR. Overexpression of DNMT3a, one enzyme responsible for catalyzing DNA methylation, can result in higher frequency of non-CpG methylation of the *Ifng* promoter in HEK 293 cells (122). Many roles have been classically attributed to DNA methylation, including imprinting and X-chromosome activation, silencing of transposons and repeat elements, and repression of tissue-specific genes (126). All are examples of established epigenetic marks that persist even through cell division. This is partially due to an abundance of methylated cytosines (hypermethylation) flanking CpG islands (127). It was therefore assumed that DNA methylation provided a stable and often permanent mechanism of repression that was not amenable to environmental cues. Recent data has challenged this notion, and a dynamic role for DNA methylation in translating environmental signals into a functional outcome in cells has been appreciated (128, 129). One such example was demonstrated by Meaney and Szyf, who observed structural and methylation changes at the *Gabra1* promoter of rat pups was dependent on the amount of maternal care received by the pups, as measured by licking (128). *Gabra1* encodes for the γ -aminobutyric acid receptor (GABA_AR). GABA_AR is widely expressed in the central nervous system and upon binding of its ligand, results in an inhibitory effect on neurotransmission. Additionally, Guo *et al* performed genome-wide DNA methylation studies in forebrain cells from mice given electroconvulsive stimulation (to activate neurons) and compared them to mice that did not receive treatment. At 0 hr, 4 hr, and 24 hr following treatment, mouse neurons were harvested for analysis. In as little as 4 hr, ~1.4% of all CpGs were either demethylated or *de novo* methylated (130). Many of these changes were stable over at least a 24 hr period. Specific examples in the context of the immune system, including responses to infection

and cellular activation, are discussed in Section 1.4.3 of this thesis. Changes to the DNA methylome in these studies occurred in as little as 20 minutes to several hours following treatment, suggesting that methylation of certain genes may occur on a shorter time scale than previously proposed.

Methylation of promoters results in suppression via several mechanisms: 1) blocking of transcription factor binding by the methyl group itself, 2) recruitment of methyl-binding domain (MBD)-containing proteins that physically block transcription factors (131), and/or 3) recruitment of histone deacetylases (HDACs) which promote chromatin condensation (132-134). Whether the relationship between DNA methylation and gene expression is causal or associative has been debated. In some cases, it may be that methylation is simply a mark used in daughter cells to instruct them to shut down expression using so-called “epigenetic memory” (135). It seems that these events are dependent upon context and genomic location.

A growing body of literature supports the notion that DNA methylation is intricately tied to histone modifications. Histones are proteins that package DNA into structures called nucleosomes, which wind DNA into either an open (euchromatin) or closed (heterochromatin) conformation. Post-translational modification of histone tails can impact the status of chromatin accessibility at nucleosomes. In general, acetylation of lysines on histones H3 and H4 is associated with transcription, whereas the transcriptional outcome of lysine methylation may vary depending on the site (136). MBD proteins have been shown to bind HDACs and form a repressor complex within promoter regions (134, 137, 138). In fungi and cancer cells, preexisting H3K9 methylation or the histone methyltransferases themselves can interact with DNMT3a and promote methylation of target genes (139, 140). These findings were confirmed in a mammalian system using mice deficient in *Suv39h*, a histone methyltransferase that catalyzes H3K9 methylation. In this study,

Suv39h was required for DNA methylation at pericentric, but not centromeric, repeats (141). EZH2, a functional component of the PRC2, is known to catalyze methylation at H3K27 (142) and can also interact with DNMT (143). Its methylation activity is associated with transcriptional repression through formation of heterochromatin. Methylated H3K27 acts as a docking point for a group of proteins responsible for repressing gene transcription, including Polycomb proteins (142). In fact, Polycomb-mediated H3K27 methylation was found to predict methylation of genes in tumor cells (144). It is thought that this allows for formation of “epigenetic memory” in dividing cells. Clearly there exists intricate communication between epigenetic machinery to regulate transcriptional activity.

2.4.2 Regulation of DNA methyltransferases

DNA methylation is catalyzed and maintained by a family of enzymes called DNMTs. In almost all known cases, S-adenosyl methionine (SAM) is used as the methyl donor and involves DNMT-associated factors. SAM is produced in mitochondria of cells and thus may be impacted by the metabolic state of the cell. In fact, when rats were fed a diet enriched in folate, a vitamin that acts as a methyl donor, they were found to have increased levels of DNA methylation in their colon and liver compared with rats given a folate-free diet (145). Similar studies performed in mice showed that folate-deficient diet led to impaired vessel function and changes in methylation in the brain (146). It is also possible that the nutrient-poor tumor microenvironment can have an impact on DNA methylation changes associated with cancer (147).

DNMTs are ubiquitously expressed and their expression is upregulated upon entering the cell cycle. Its location at the replication fork of DNA and its preference for hemimethylated DNA is in agreement with its role as a maintenance methyltransferase. The mammalian DNMT family

includes four members: DNMT1, DNMT3a, DNMT3b, and DNMT3L. All mammalian DNMTs have some capacity to maintain methylation, although DNMT1 is predominantly responsible for maintenance during cell replication and is the most abundant DNMT in adult mammalian cells (148). During embryogenesis and in response to certain stimuli, DNMT3a and 3b are the dominant *de novo* methyltransferases. They can methylate hemimethylated and non-hemimethylated DNA equally well (149). A fourth protein, DNMT3L, is structurally similar to DNMT3 and is required for proper methylation but is inactive on its own (150). Some studies have indicated that DNMT1 associates with DNMT3 to initiate *de novo* methylation and that DNMT3 contributes to maintenance despite its lack of preference for hemimethylated DNA (151, 152). Thus, cooperation between all DNMTs is required for proper methylation.

2.4.3 DNA methylation in the immune system

In contrast to histone modification, how immune cells utilize DNA methylation to process environmental cues is not well studied. A growing body of evidence suggests that the DNA methylome of cells is highly susceptible to manipulation following signal transduction (129) and infection with bacteria (125, 153), viruses (154), or protozoa (155). Two independent groups have shown that infection of human primary DCs or a monocytic cell line with MTB leads to dynamic remodeling of the methylome (125, 153). Pacis *et al.* showed that differential methylation was associated with changes in activating histone marks (measured by ChIP-seq) and transcription (measured by RNA-seq)(153). However, a paired time-course analysis of DNA methylation and gene expression did not suggest that demethylation preceded expression. The authors did not measure whether 5-hydroxymethylcytosine (5hmC), the rate-limiting step of demethylation, preceded expression. Interestingly, Sharma and colleagues observed non-canonical genome-wide

methylation changes at non-CpG residues in MTB-infected macrophages (125). Considering many of the detected regions were found in ncRNA genes, including lncRNA, miRNA, piRNA, and snoRNA, it is thought that MTB infection specifically targets regulatory regions of the genome. Pathogens may also seize control of host epigenetic machinery to deter pathogen recognition. Langerhans cells use E-cadherin to navigate stratified epithelium and allow for detection of cancer-associated viruses, including human papillomavirus (HPV). It appears that HPV E7 protein directly associates with DNMT1 to drive repression of E-cadherin and contribute to HPV persistence (154). Finally, methylome remodeling in *Leishmania donovani*-infected macrophages leads to repression of host responses (155).

Manipulation of the T and B cell methylome has also been reported, particularly in naïve versus effector populations. Early work in this field showed that treatment of primary mouse CD8⁺ T cells with DNMT inhibitor 5-azacytidine (5-azaC) resulted in a 25-fold increase in IFN γ expression and a 14-fold increase in IL-3 expression (156). Activation of T cells using anti-CD3/28 stimulation resulted in site-specific demethylation of *Ifng* and *Il3* promoters. It was later shown by the same group that demethylation of *Ifng* is heritable in CD44^{high} memory CD8⁺ T cell clones (157). Using a P14-transgenic mouse model with a knock-in TCR specific for lymphocytic choriomeningitis virus (LCMV) epitope GP33-41, Scharer *et al.* observed dynamic methylome alteration of CD8⁺ T cells after *in vivo* LCMV infection (158). Biologically relevant gene promoters such as *Gzmb* and *Zbtb32* were demethylated in effector T cells compared with naïve controls. Demethylation of key genes appears to poise the activated T cells for rapid expression of effector molecules. This is not unlike memory CD4⁺ T cells, which demethylate *Il13*, *Il17a*, and *Ccl3*, all of which can be promptly expressed upon reencountering antigen (159). Several groups have reported that the *IL2* promoter is demethylated in memory T cells for the same reason (160,

161). Engagement of the TCR by ligands that induce strong signaling favors DNMT1 activation via a glycogen synthase kinase (GSK3)-dependent pathway (162). This results in methylation and repression of Foxp3 in conventional T cells (Tcon). Finally, plasma cell and germinal center B cell differentiation is also dependent on DNA methylation (163, 164). Taken together, it is quite clear that DNA methylation plays an emerging role in the immune system as a translator of environmental cues to control responses to infection, cytokine stimulation, and cellular activation.

2.5 INTRODUCTION SUMMARY

The central hypothesis of this thesis is that specific subsets of APCs may respond to gp96 in fundamentally different ways, which influences their ability to activate T cells. I propose that this is a result of epigenetic differences in these populations. In this thesis, Chapter 1 will focus on the expression of CD91 on various DC subsets and determine which interact with gp96 following LD or HD gp96 immunization. Uptake of gp96 at LD has previously been characterized by our lab, demonstrating that CD11b⁺CD11c⁺ cDCs are required for cross-priming of T cells (61). However, it is possible that a different APC subset is targeted at HD, given that stimulation of various DC types *in vitro* may lead to either a pro- or anti-inflammatory phenotype. There may exist an active mechanism driving accessibility of gp96 for different APC subsets. Thus, experiments in Chapter 2 will further dissect the mechanisms used by regulatory DCs identified in Chapter 1 to understand the HD suppressive response. To this effect, we have observed that DNMT activation in gp96-stimulated cells leads to methylome remodeling in responsive APCs. In pDCs, remodeling occurs on the gene body of *Nrp1*. This event triggers expression of *Nrp1* and facilitates

pDC-Treg stabilization. Finally, Chapter 3 will focus on signaling mediators downstream of CD91 and how signaling events in APCs drive cross-talk with NK cells in response to gp96.

3.0 CHAPTER 1: CLASSIFICATION OF APCs ASSOCIATED WITH HIGH DOSE GP96 SUPPRESSION

PREFACE

Most of the data in this chapter has been published in *Nature Communications*, of which I am first author (79). Figures 4A-C, 5, and 7-10 are copyright (2017) Nature Publishing and is distributed under a Creative Commons CC-BY license. This information is presented here and expanded upon by the author.

3.1 RATIONALE

It is known that cDCs are required to take up HSP at LD to elicit immunity (61). Additionally, the response generated by these APCs has been widely studied *in vitro* using bone marrow-derived DCs (BMDCs), peritoneal exudate cells (PECs), and various DC- and macrophage-like cell lines. Whether these APCs are responsible for generating the response observed with HD gp96 has not been considered.

There are two possibilities to explain the innate response to HD gp96: 1) an alternate APC subset gains access to gp96 at HD, or 2) saturation of the receptor results in a phenotype switch in responding APCs. The latter is less likely, given that mediators of the LD response including maturation markers and NF- κ B continue to elevate in DCs given increased concentrations of gp96.

It is known that human pDCs, when given gp96 *in vitro*, can bind gp96 with similar efficiency as monocytes (1). Human pDCs do not undergo maturation in response to treatment and instead inhibit activation of monocytes. This suggests that variant responses can be achieved depending on the APC subset that is targeted; however, whether pDCs are targeted following HD gp96 immunization was not tested in these studies.

We have followed up on these studies and have observed increased uptake of fluorescently labeled gp96 by pDCs following HD gp96 immunization *in vivo*. We have also found that CD91 is indispensable for this response, similar to LD immunization. Intriguingly, the HD response is potent enough that it is not overcome with the addition of IL-12 into the system. The work presented herein is essential not only for developing potential immunotherapy for autoimmunity, but will also improve our understanding of how suppressive responses to HSPs are elicited in general. In turn, this knowledge can help improve upon current clinical trials using HSPs for tumor immunotherapy, since pDCs are prevalent within tumor-bearing hosts.

3.2 RESULTS

For the experiments presented in this thesis, homogenous preparations of gp96 were isolated from murine liver. Gp96 purity (Figure 2A,B) and biochemical activity (Figure 2C) were tested to ensure that the properties of gp96 were preserved. For *in vivo* gp96 tracking experiments, gp96 preparations were fluorescently labeled with Alexafluor 488 (gp96_{A488}). Uptake of gp96_{A488} can be detected by flow cytometry and confocal microscopy (61).

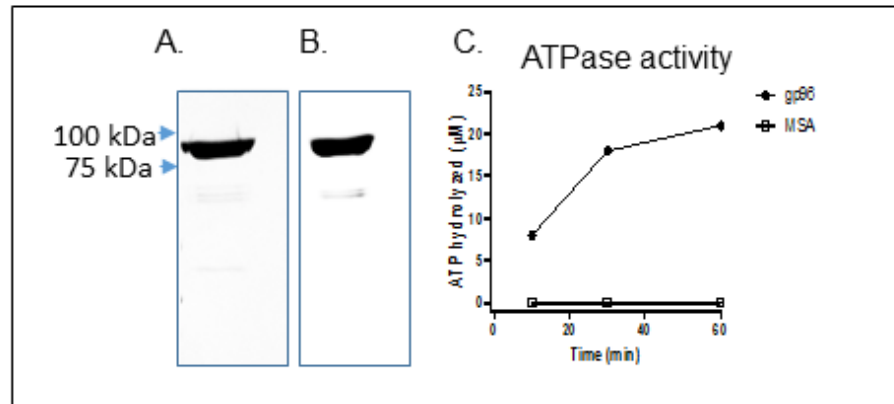


Figure 2. Characterization of purified murine gp96.

Characterization of purified murine gp96. Gp96 preparations were tested for purity and biochemical activity to ensure quality of protein. A-B. gp96 was analyzed by 10% SDS-PAGE following staining with Coomassie blue (A), and by immunoblotting with a gp96 specific monoclonal antibody (B). C. ATP hydrolysis by gp96 was assessed. Gp96 was incubated at 37°C for indicated time period with ATP. Following addition of malachite green, µM ATP hydrolyzed was calculated from a standard curve. MSA was used as a negative control.

3.2.1 CD91⁺ DCs are required for gp96-mediated immune suppression

We tested whether CD91 was required to generate immune suppression in a murine model of cancer when mice were immunized with HD gp96. Towards this goal, we have generated mice that are selectively deficient in CD91 expression on CD11c⁺ cells (CD91^{f/f}CD11c^{cre}) and characterized their phenotype. These mice have normal numbers of APCs (including cDCs and pDCs), T cells, and B cells at steady state (26) and were used in a gp96-mediated suppression assay (Figure 3A). CD91^{f/f}CD11c^{cre} or wild type littermates (CD91^{f/f}) were immunized with

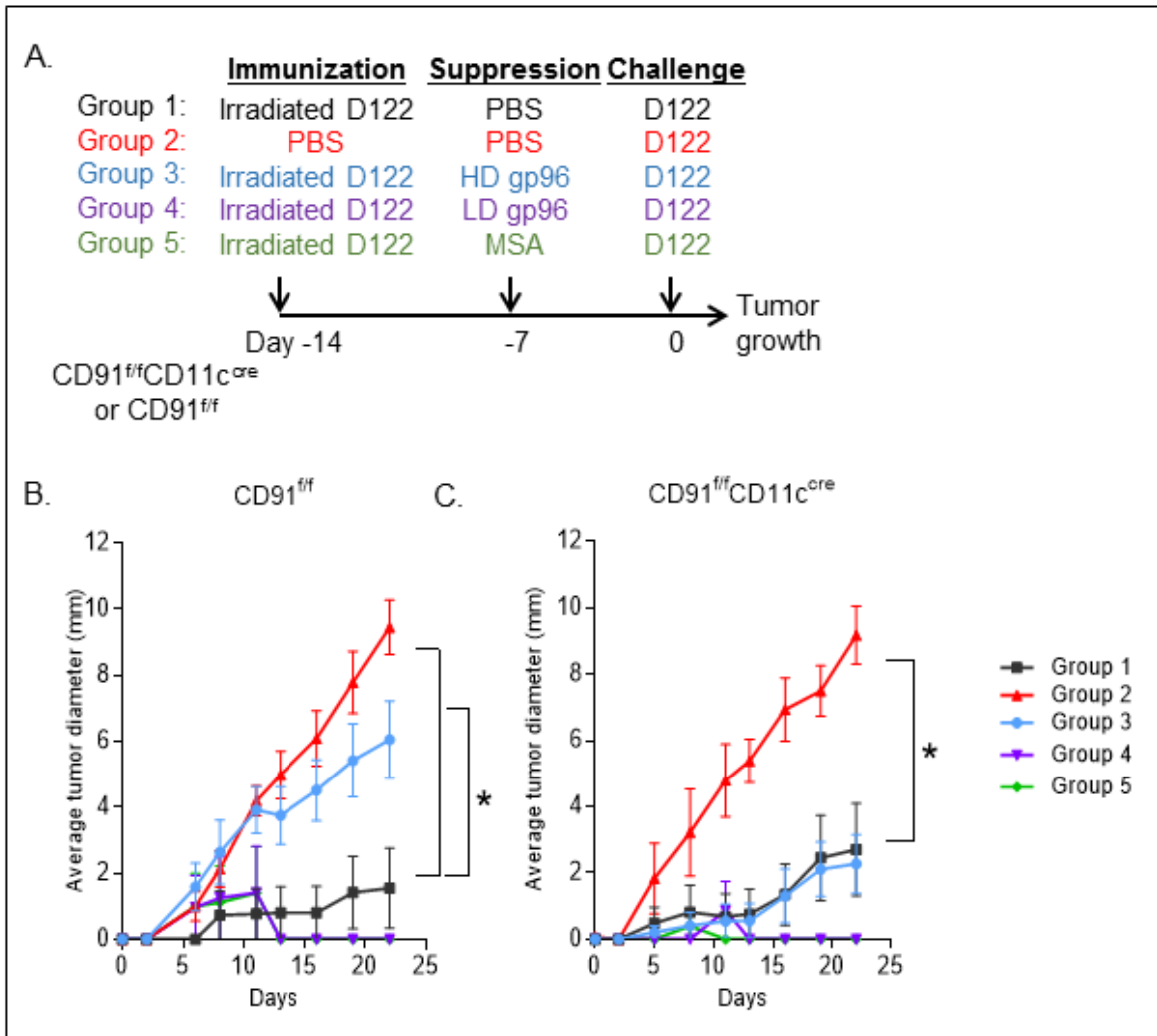


Figure 3. HD gp96-mediated immune-regulatory response requires CD91+ DCs.

A. The experimental set up to test the role of CD91⁺ DCs in HSP-mediated immune-regulatory response. Immunization was carried out using irradiated D122 (Groups 1,3,4,5) or control PBS (Group 2). Suppression of anti-tumor immunity, elicited by irradiated D122, was mediated by HD gp96 treatment (Group 3) or control PBS (Groups 1&2). LD gp96 and MSA treated mice were included as negative controls. All mice were challenged with D122 and tumor growth was monitored. B. Tumor growth in wild type littermates (CD91^{f/f}). C. Tumor growth in mice lacking expression of CD91 in CD11c⁺ cells (CD91^{f/f}CD11^{cre}). Shown is the average tumor diameter \pm SEM. n=3-5/group, data are from 1 representative experiment of 3 independent experiments. [The value of SEM in Group 3 is too small to be seen in the graph].

irradiated tumor cells. Mice were treated with HD gp96 followed by tumor challenge. Groups that received LD gp96 or mouse serum albumin (MSA) instead of HD gp96 were included as negative controls. Tumor growth was monitored in all mice by measurement of tumor in two perpendicular axes. Regardless of CD91 expression, mice immunized with irradiated tumor cells only (Group 1)

were able to reject a subsequent challenge with that tumor (Figure 3B,C), while unimmunized mice developed progressive tumors (Group 2). In a separate cohort (Group 3), immunized mice were administered HD gp96 7 days prior to tumor challenge. Vaccinated CD91^{f/f} mice were unable to limit tumor growth following HD gp96 administration (Figure 3B). However, similarly treated CD91^{f/f}CD11c^{cre} mice remain protected against challenge (Figure 3C). These results indicate that CD91⁺CD11c⁺ APCs were necessary for HD gp96-mediated suppression of protective anti-tumor immunity in vaccinated hosts. This observation was also dependent upon the dose of gp96 since mice treated with LD gp96 failed to suppress anti-tumor immunity, consistent with previous reports.

3.2.2 HD gp96 suppression cannot be overcome by IL-12

In all models of LD and HD gp96 immunization that have been tested, T cells are indispensable for immunity. IL-12 production by APCs is important for differentiation of naïve T cells into Th1 cells and stimulates IFN γ production by lymphocytes (165-167). IL-12 is also known to be released upon HSP immunization and co-administration of HSP + IL-12 enhances anti-tumor immunity (60, 130). Given the important role for this cytokine, we tested whether exogenous administration of IL-12 could counteract the effects of HD gp96. For these experiments we utilized the same model described in Section 2.2.1 and Figure 3A, with an additional group that was given IL-12 via the i.p. route every day for 6 days (Figure 4A). All mice used in this experiment were CD91^{f/f}, mimicking wildtype. Intriguingly, this did not seem

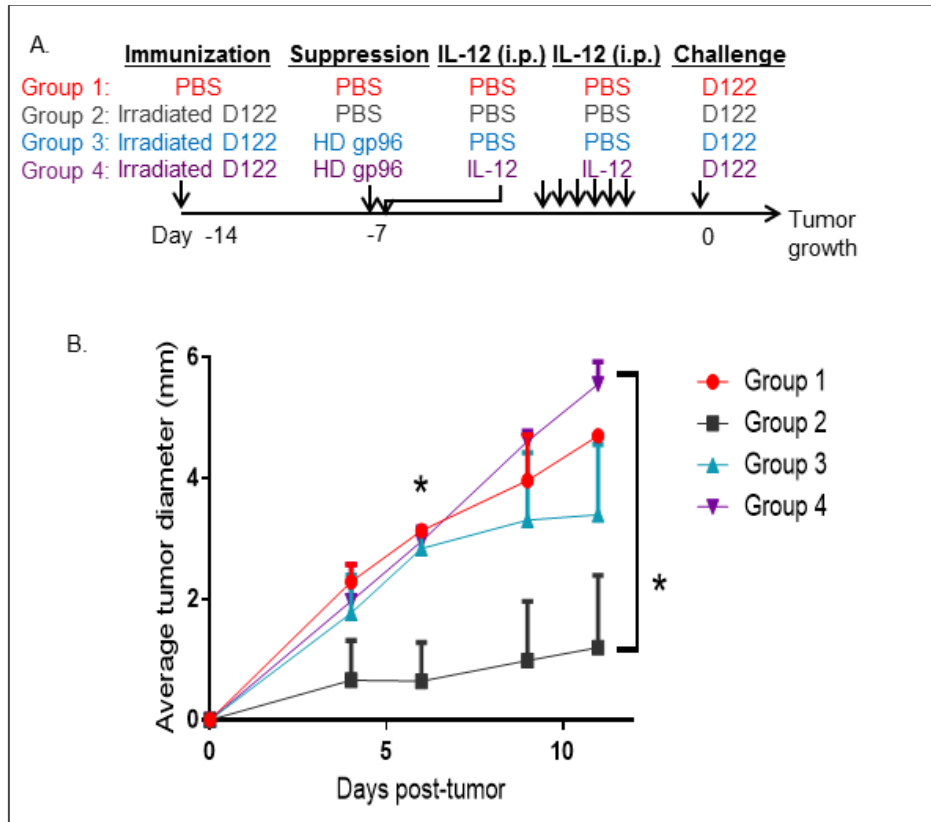


Figure 4. IL-12 alone is not sufficient to overcome HD gp96-mediated immune-regulatory response.

A. The experimental set up to test the role of IL-12 in HD immunity. Immunization was carried out using irradiated D122 (Groups 2-4) or control PBS (Group 1). Suppression of anti-tumor immunity, elicited by irradiated D122, was mediated by HD gp96 treatment (Groups 3&4) or control PBS (Groups 1&2). Group 4 mice were given daily treatments of IL-12 i.p. for 7 days prior to challenge. All mice were challenged with D122 and tumor growth was monitored. B. Tumor growth in mice given IL-12 was equivalent to growth in Group 3. Shown is the average tumor diameter \pm SEM. $n=3-5$ /group, data are from 1 representative experiment.

to have an effect on overall tumor growth (Figure 4B). Tumors grew with HD gp96 treatment regardless of IL-12, suggesting that the HD gp96 response is not overcome by IL-12. This may be due to a variety of factors, including lack of antigen specificity in our model or the need for a combination of cytokines in addition to IL-12. It is also possible that the level of Treg-driving cytokines and other signals may be high enough to signal the contraction phase of the immune response, regardless of IL-12 levels.

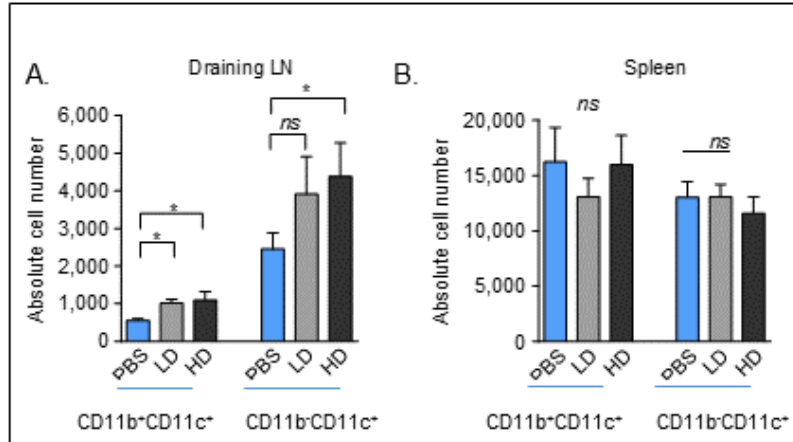


Figure 5. DC numbers following LD and HD gp96 immunization.

A,B. Mice were immunized intradermally with LD or HD gp96 or given PBS. After 18 hr, draining lymph node (A) and spleens (B) were harvested and absolute numbers of CD11b⁺ and CD11c⁺ populations were analyzed. n=5/group, data are from 1 representative experiment of 3 independent experiments performed.

3.2.3 Dynamic cellular changes and alternative interactions of gp96 with DC populations at HD

We have previously shown that immunization with LD gp96 leads to priming of anti-tumor immune responses. This is in stark contrast to responses elicited by HD gp96 shown here. To understand this operational dichotomy in greater detail, we investigated the CD91⁺CD11c⁺ cells necessary for gp96-mediated immune responses. We first analyzed the two major APC types within this population, both of which express CD91 (61). Mice were immunized with LD or HD gp96 or administered PBS. Lymph nodes or spleens were isolated after 18 hr and cells were analyzed by flow cytometry. The total number of CD11c⁺CD11b⁺ cells and CD11c⁺CD11b⁻ cells in the lymph nodes of immunized mice were increased 2-3 fold over samples from unimmunized mice regardless of whether mice were immunized with LD or HD gp96 (Figure 5A). Such increases were not observed in spleen samples (Figure 5B). Thus, comparative differences in the

number of cells in these two populations in lymph nodes by themselves could not account for altered immune responses observed after immunization with LD vs HD gp96.

We next examined the APCs that engage gp96 following immunization at either dose. Gp96 was labeled with A488 and LD or HD gp96_{A488} was administered to mice. Draining lymph nodes were examined by flow cytometry after 8 hr and analyzed for A488 fluorescence (Figure 6A). CD11c⁺CD11b⁺ and CD11c⁻CD11b⁺ cells were preferentially engaged by gp96 at both doses. For CD11c⁺CD11b⁺ cells this appeared unrelated to the dose of gp96 used for immunization (Figure 6B). Interestingly, CD11c⁻CD11b⁺ cells made up a smaller percentage of gp96_{A488}⁺ cells at HD compared to LD (Figure 6B). Of the APCs that were detected in this study, pDCs (CD11c^{low/+}CD11b⁻B220⁺PDCA⁺) were the only subset that made up a larger percentage of gp96_{A488}⁺ cells at HD (Figure 6B). We thus focused on pDCs for two reasons; first, this cell population incorporated more gp96 at HD versus LD, and second, pDCs are known for their immunosuppressive properties in certain contexts. Upon further analysis the number of pDCs that were gp96_{A488}⁺ increased ~5-fold between LD and HD (Figure 6C,D).

3.2.4 pDCs express CD91 but do not mature when exposed to gp96

We next wanted to confirm CD91 expression in pDCs from CD91^{fl/fl}CD11c^{cre} mice, given the low CD11c expression in these cells. Lymph nodes were first isolated from CD91^{fl/fl}CD11c^{cre} or CD91^{fl/fl} mice and analyzed for cDCs and pDCs. We show for the first time that CD91 expression was undetectable on pDCs isolated from CD91^{fl/fl}CD11c^{cre} mice and its deletion was as complete as that for cDCs (Figure 7A). Interaction of gp96 with different populations of DCs is strictly correlated with, and dependent on, the levels of CD91 that they express. This correlation is also

true when the gp96-mediated phenotype is measured in DCs. pDCs expressed CD91 to similar levels seen in cDCs (Figure 7A). CD91 levels did not significantly change on either population following immunization of mice with any dose of gp96 (Figure 7B).

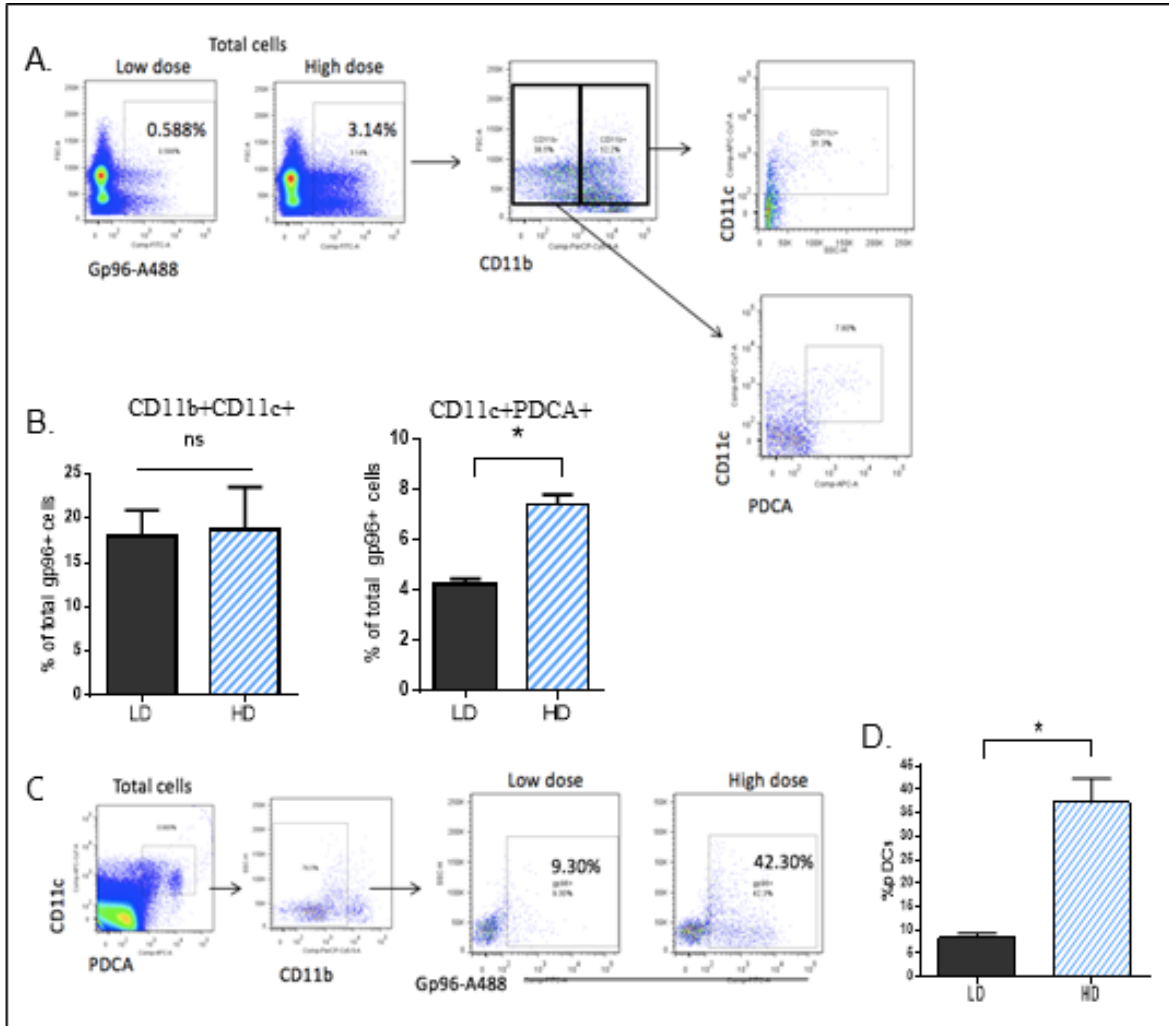


Figure 6. Preferential targeting of pDCs at HD gp96.

Mice were immunized with LD or HD gp96_{A488}. Lymph nodes were harvested 8 hr later. Lymph node cells were analyzed for A488 positivity by flow cytometry using CD11b, CD11c, B220, and PDCA cell surface markers. A-B. Total A488⁺ were gated and the makeup of this population was analyzed using DC markers. C-D. The percent of pDCs that are A488⁺ is shown. Data are from 1 representative experiment of 3 independent experiments.

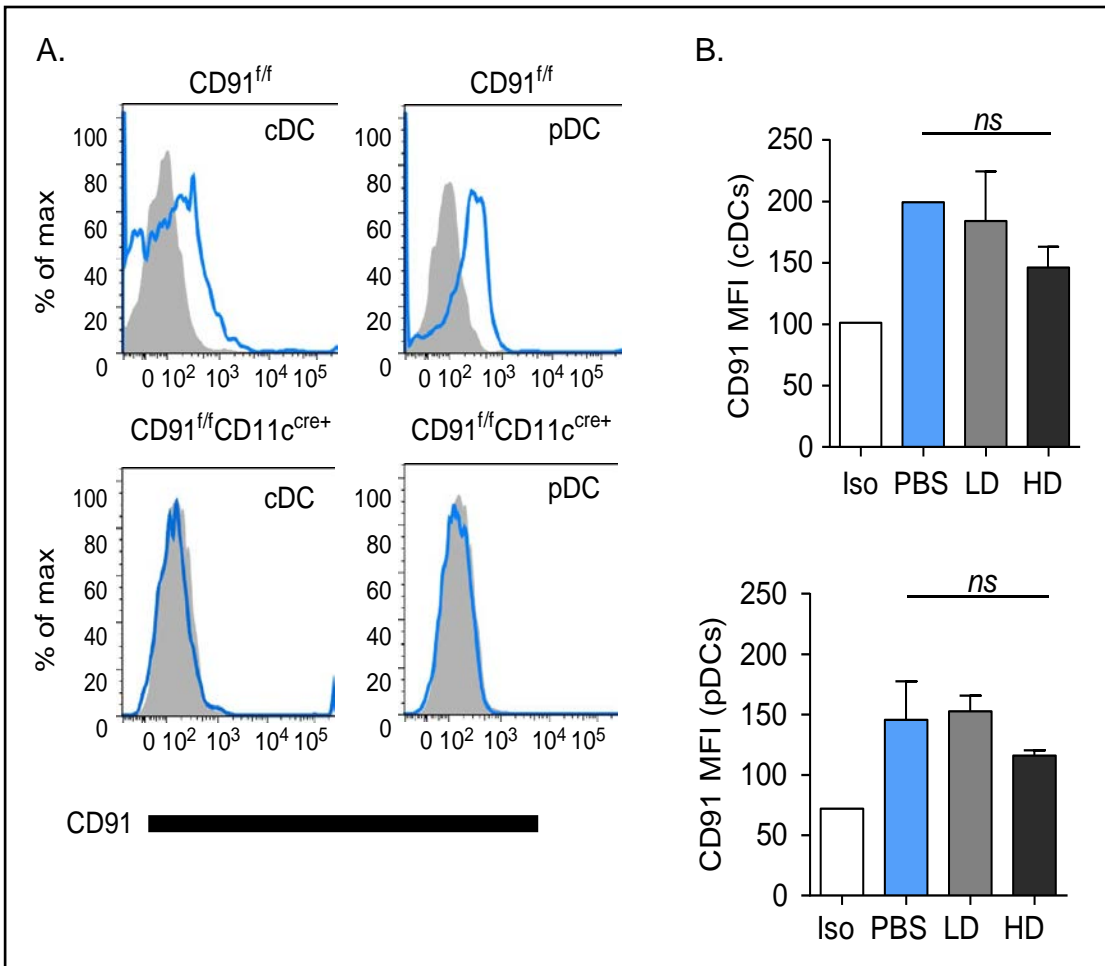


Figure 7. cDCs and pDCs express similar levels of CD91.

A. Histograms depict CD91 staining within representative lymph node cDC (CD11b⁺CD11c⁺) or pDC (CD11c^{low/+}CD11b⁻B220⁺PDCA1⁺) populations from naïve CD91^{f/f} or CD91^{f/f}CD11c^{cre} mice. B. Mice were immunized with LD or HD gp96 or given PBS. At 18 hr post-immunization, lymph nodes were harvested and stained for CD91 in pDCs and cDCs. Shown are CD91 MFI values for each population. n=5/group, data are from 1 representative experiment of 3 independent experiments.

Maturation is a hallmark of the cDC response to gp96 and other HSPs. This is mainly driven by NF-κB activation following HSP-CD91 binding. It has been previously shown, however, that although NF-κB translocation to the nucleus occurs in human pDCs in response to gp96, they do not upregulate expression of maturation markers known to be expressed by cDCs including CD86 and MHC (1). To test whether murine pDCs exhibit a similar phenotype, we isolated BMDCs (representing cDCs) and spleen pDCs and stimulated them with gp96 *in vitro*. pDCs were given CpG as a positive control. After 24 hrs, cells were harvested and analyzed by flow cytometry

for expression of costimulatory and maturation markers. Similar to previous studies, in response to gp96 BMDCs upregulated CD86 and MHC class II, but not CD80 (Figure 8A). In contrast, these markers did not increase on gp96-stimulated pDCs (Figure 8B).

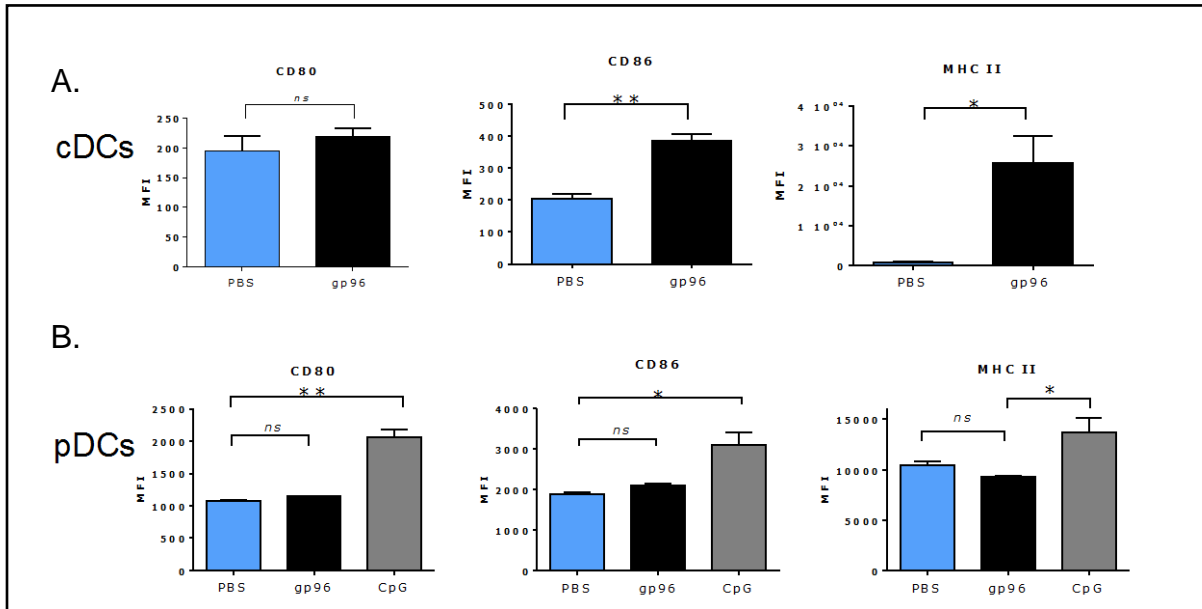


Figure 8. cDCs undergo maturation in response to gp96, whereas pDCs remain immature.

cDCs (A) or pDCs (B) were stimulated with HD gp96 for 24 hours *in vitro* and then analyzed for maturation markers CD80, CD86, and MHC II by flow cytometry. CpG-stimulated pDCs were included as a control for pDC maturation. Average MFI is shown for each marker.

3.3 DISCUSSION

To briefly summarize the findings of this section, CD91 is required for generation of suppressive HSP responses and addition of exogenous IL-12 into the system is not sufficient to overcome the HD response. CD91 is expressed by multiple APC types including both cDCs and pDCs, making each population a potential target at both LD and HD gp96. However, pDCs are the only APC subset whose gp96 uptake is greatly increased following HD immunization. Unlike cDCs, pDCs do not undergo maturation in response to gp96, further supporting their putative role in suppressive responses. Chapter 2 will further discuss the pDC phenotype elicited by HD gp96.

3.3.1 Effects of IL-12 on the tumor microenvironment

Our lab has shown that CD91 is necessary and sufficient for HSP-mediated cross-priming of CTLs both *in vitro* and *in vivo*. HD suppression also appears to be CD91-dependent in our models. It is rather surprising that daily treatment of mice with IL-12 was not adequate to overcome HD suppression. It is entirely possible that there are other cytokines in addition to or instead of IL-12 that drive this response. The RAW264.7 macrophage cell line and peritoneal macrophages express modest levels of IL-12p70 when treated with gp96, hsp70, and calreticulin (62, 70). Other pro-inflammatory cytokines known to enhance effector lymphocyte function that are released in response to HSPs include IL-6, CXCL10, IL-1 β , and TNF- α . It may be that some combination of these must be present to overcome suppression.

IL-12 in the tumor microenvironment leads to augmented production of IFN γ by CTLs and NK cells and can enhance their cytotoxic capabilities (168). Immunotherapy using tumor antigen-loaded DC in combination with recombinant IL-12, or antigen-loaded DCs which overexpress IL-12, was shown to greatly improve MCA205 tumor rejection (169). Treatment with IL-12 alone or with spleen peptide-pulsed DC with IL-12 did not significantly increase tumor killing. It is possible that in our HD model, lack of antigen-specific peptides does not provide any additional efficacy of IL-12 treatment. To address this, these experiments should be repeated using OVA-expressing tumor cells and OVA-bound gp96 to create a defined, antigen-specific system.

3.3.2 Implications of gp96 release by tumors and traumatic wounds

Under certain physiologically relevant conditions, cells may release HSPs into the extracellular space. This occurs even at steady state, as soluble hsp70 can be detected in the serum of healthy

humans (170). This may allow for some cross-recognition of HSPs in the peripheral circulation. Extracellular HSPs have been detected at higher levels in some disease states, such as in bronchoalveolar lavages of humans with lung inflammation (171), synovial fluid of RA patients (115, 116), and tumors (172, 173). The immune outcome of local HSP release depends on the microenvironment, the local APCs, and presumably the amount of HSP that is being released.

Active secretion of hsp70 has been detected in human prostate tumor cell line PC-3 and human colorectal tumor line HRT-18 (172). Low levels of extracellular hsp70 can also be detected in untreated solid tumor stroma formed after *in vivo* challenge with these cell lines. Induction of tumor necrosis by cryo-thermal therapy significantly increases hsp70 within the tumor microenvironment and serum of tumor-bearing mice (173). When DCs were treated with serum from cryo-thermal treated mice, expression of maturation markers CD86 and MHC II was significantly increased. DC maturation was hsp70-dependent since depletion of hsp70 from serum did not induce expression of these molecules. Additionally, Kottke *et al.* showed that intraprostatic injection of hsp70-overexpressing adenovirus followed by damage of prostate cells results in release of hsp70, uptake by immune cells, and increased IL-6 and TGF- β production (174). Subsequently, auto-reactive Th17 cells are activated and are cross-reactive against prostate cancer cells. Thus, mice treated in this way are better protected against challenge with prostate tumor cells. Although not an example of natural release by tumors, this is in agreement with studies from our lab showing activation of Th17 cells following gp96 immunization (62).

There are also examples of higher doses of local HSP release following a large volume of cell death. The microenvironment of a trauma wound is one such example. Due to vascular disruption, wounded tissue tends to be oxygen and nutrient deficient. Jayaprakash *et al.* have shown that hsp90 is a key mediator of wound healing in the hypoxic wound microenvironment

(175). Hypoxia induced high intracellular expression of the hsp90 β isoform which stabilizes CD91 at the cell surface. Concomitantly, hsp90 α was secreted in large amounts, which then bound to CD91 and promoted wound healing. Renal tubule cells subjected to hypoxic environments have also been shown to increase expression of gp96 (176), although temporal expression was not tested. CD91 can promote skin cell migration in response to extracellular hsp90, and thus may be important for responses to hypoxia and wound healing (177). Furthermore, CD91 is known to be highly expressed by trophoblasts, placental decidua, and decidual DCs, and its expression is altered by the presence of progesterone during pregnancy (178). It is possible that the suppressive response to HSPs was evolved to protect the host against cytokine storm in response to traumatic wounds, to promote wound healing, or possibly to protect the developing fetus during pregnancy. Taken one step further, we hypothesize that within the microenvironment of large tumors, increased local release of HSPs may contribute to immune suppression.

3.3.3 Tolerogenic pDCs in allograft transplantation and cancer

I present evidence in this section that pDCs increase interaction with gp96 from LD to HD by ~5-fold. Gp96⁺ cells are mainly comprised of CD11b and CD11c expressing cells, as shown in previous work (61) and the data presented here. Comparison between gp96⁺ populations revealed that pDCs are the only APC population we tested that make up a higher percentage of gp96⁺ cells at HD compared with LD (Figure 6B). This is in agreement with our finding that a CD11b⁻CD11c⁺ DC population is preferentially targeted with HD gp96 immunization.

pDCs are classically associated with anti-viral responses, because they produce 200-1000 times more type I IFNs than any other cell type in response to microbial challenge (179). In

response to inflammation, pDCs are recruited from their steady state locations (blood, thymus, and secondary lymphoid organs) to the site of inflammation and associated draining lymph nodes. Mounting evidence suggests that pDCs can act as professional APCs, particularly after TLRs or endocytic receptors are engaged. Interestingly, ligation of certain endocytic receptors on pDCs such as BDCA-2 and DCIR actually impairs IFN production while increasing their ability to present antigen (180-182). The maturation status of pDCs does not seem to dictate their interaction with T cells as reliably as mature cDCs do. While steady state immature pDCs almost exclusively promote tolerance, mature pDCs may promote either pro- or anti-inflammatory responses depending on the local environment.

For the purposes of this Discussion, I will focus on the suppressive properties of pDCs and their role in promoting tolerance to allografts and tumors, as these are two situations in which HD gp96 is relevant. Using a specific antibody (called YAe) to recognize donor-derived MHC I-E^d peptide presented by recipient MHC I-A^b, Ochando and colleagues observed that a population of CD11c⁺B220⁺PDCA⁺Gr1⁺CD19⁻ pDCs are a main source of alloantigen presentation within a cardiac allograft (183). YAe⁺ pDCs migrate to lymph nodes in tolerized mice, yet in mice that rejected the transplants YAe⁺ pDCs were largely detected in the spleen. This was mainly due to the fact that YAe⁺ pDCs colocalized with T cells in the lymph node where they facilitated the development of Treg. In another study, pDCs were shown to express high levels of gut-homing chemokine receptor CCR9 (184). These pDCs are immature (low levels of CD40, CD80, CD86 and intermediate levels of MHC II), and upon maturation they lose expression of CCR9. Adoptive transfer of OVA-loaded CCR9⁺ pDCs into recipient mice was correlated with a loss in OVA⁺ CTL proliferation and a strong induction of Foxp3⁺ Treg. CCR9⁺ pDCs were also sufficient to protect

mice from lethal graft versus host disease. pDCs capable of inducing IL-10 producing Treg have also been identified in humans (185).

pDCs are found in abundance within the tumor microenvironment and tumor draining lymph nodes of some cancers. Whether pDCs contribute to tumor rejection or persistence is an area of debate and may depend on the type of tumor. In human melanoma, pDCs within the primary tumor and draining lymph nodes have defects in maturation and contribute to insufficient T cell priming (186). In a murine model of melanoma, pDCs in the tumor-draining lymph nodes produce large amounts of IDO (187). Production of the tryptophan-catabolizing enzyme IDO by pDCs is known to enhance Treg activation, such that Tregs isolated from tumor draining lymph nodes efficiently shut down CTL proliferation (188). Tumor cell necrosis results in release of many DAMPs including HSPs, self-DNA, and high motility group box 1 (HMGB1). Treatment of pDCs with DAMPs such as HMGB1 inhibits maturation and adhesion molecule expression, and inhibits Th1-skewing responses in CpG-stimulated pDCs (189). We hypothesize that a similar pathway is being induced in pDCs that bind gp96.

4.0 CHAPTER 2: GP96 DRIVES DICHOTOMOUS T CELL IMMUNE RESPONSES VIA DNA METHYLOME REMODELING IN APCS

PREFACE

Most of the data in this chapter has been published in *Nature Communications*, of which I am first author (79). Figures 12, 14, 15, 17-26, and 28, and Tables 5-8 are copyright (2017) Nature Publishing and is distributed under a Creative Commons CC-BY license. This information is presented here and expanded upon by the author.

4.1 RATIONALE

Given the findings that pDCs are actively targeted following HD gp96 immunization, it is possible that signaling and expression events are elicited in these DCs that are distinct from their cDC counterparts. The fact that pDCs do not undergo maturation in response to gp96 stimulation suggests that either 1) pDCs utilize a different HSP receptor, resulting in differential activation of downstream signaling events, or 2) pDCs activate a genetic profile that is distinct from cDCs. Similar to cDCs, pDCs bind gp96 in a CD91-dependent manner, such that addition of CD91 neutralizing antibodies or CD91 ligand $\alpha 2M$ to the culture medium abrogates binding of labeled gp96 (1). Observation of gp96-treated pDCs by microscopy also revealed that NF- κ B is translocated to the nucleus following gp96 stimulation. Therefore, it is unlikely that an ancillary receptor and/or signaling pathway is promoted by gp96 binding in pDCs. I instead propose that

HSP-CD91 binding activates distinct gene signatures in pDCs that are absent in cDCs, and that this signature is a product of epigenetic regulation.

For many years, DNA methylation was regarded as a stable and often permanent epigenetic mark that invariably leads to gene silencing. Consequently, its role in controlling transcription and driving immune cellular responses has been neglected. Emerging studies show that in T cells and APCs, active modification of the methylome may occur in response to external stimuli, controlling IL-2 production and proteome modifications in response to pathogens. Interestingly, NF- κ B can reportedly interact with DNMT1 and guide it to target genes (121). In this study, both NF- κ B and DNMT1 were required for full methylation and repression of target gene *BRMS1*. Breast cancer metastasis suppressor 1 (*BRMS1*) is a tumor metastasis suppressor that is downregulated in many cancers, thus understanding the mechanisms through which its expression is repressed is critical. Because NF- κ B is intricately involved in APC responses to gp96 and other immunogenic HSPs, it is possible that it plays a role in modifying the epigenetic landscape of HSP-responsive cells. Secreted hsp90 can bind prostate cancer cells and promote expression of the methyltransferase enhancer of Zeste homolog 2 (*EZH2*), a catalytic component of the Polycomb complex 2 (*PRC2*)(190). Binding of hsp90 induced ERK signaling, which in turn stabilized *PRC2* and enhanced recruitment of *EZH2* to the E-cadherin promoter. This work is among the first to show that signaling events initiated by HSPs have the potential to drive downstream epigenetic events.

In this section, I present data to support that gp96 influences activation of epigenetic machinery to regulate the DNA methylome of responding cells. In particular, dynamic changes to the methylation status of genes involved in cell-cell adhesion, signaling, and angiogenesis occur following gp96 immunization. Through these assays I have identified *Nrp1*, an adhesion molecule expressed by pDCs and Treg, as a promising candidate for driving the HD gp96 response.

4.2 RESULTS

4.2.1 Gp96 treatment leads to formation of DNMT1 punctae in APCs

DNA methylation is catalyzed by the enzymes DNMT1, DNMT3a, and DNMT3b. We tested whether cDCs and pDCs cultured in the presence of gp96 modify nuclear organization of DNMTs by confocal microscopy. Splenic pDCs and a range of cDCs including BMDCs, primary isolated splenic CD11c⁺ DCs, and PECs, were separately cultured in the presence of gp96 for 6 hr on glass coverslips. The cells were then probed by immunocytochemistry for formation of punctate DNMT structures within the nucleus, an established indicator of binding of DNMT to target genes (162). Using the analysis tools described in Methods, the average number of DNMT punctae per cell was calculated. We observed a significant and similar increase in DNMT1 punctae in gp96-stimulated cDCs and pDCs after 6 hr (Figure 9A,B,C) compared to the diffuse with little to no punctae in PBS-treated cells. Conversely, DNMT3b punctae was detected only in PECs (Figure 10). Thus, DNMT1 is universally activated in response to gp96, whereas DNMT3b may only be activated in select cell populations. This is consistent with previous reports which show that DNMT1 and DNMT3b can form complexes independent of DNMT3a (191). Gp96-mediated DNMT1 punctate enrichment was accompanied by elevated, but not significantly increased, DNMT1 protein in nuclear extracts purified from BMDCs (Figure 11A,B). Therefore, changes to DNMT1 nuclear architecture, *rather than* overall increased DNMT1 expression, were initiated by gp96 in responding cells. DNMT1 punctae formation was not a result of proliferation as treated cells did not significantly proliferate throughout the duration of the experiment and lacked co-localization of DNMT with Ki67 (Figure 11C,D) which is expressed at the S-phase during cell proliferation and DNA replication.

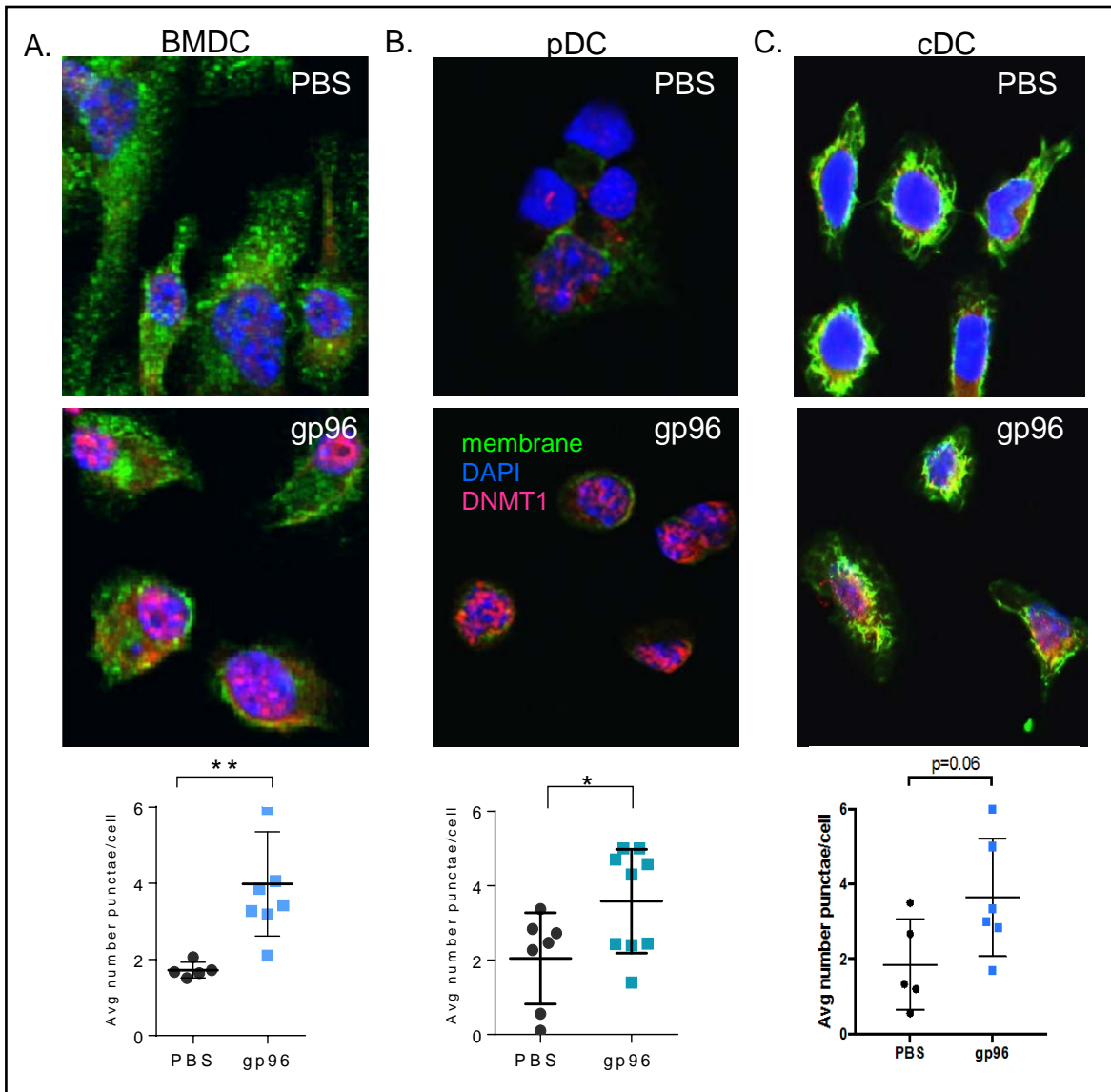


Figure 9. DNMT1 forms punctae in DC nuclei following gp96 stimulation.

A. Indicated DCs were stimulated with gp96 or treated with PBS *in vitro* on coverslips for 6 hr. Cells were stained and analyzed by confocal microscopy. B. DNMT1 punctae were quantified using NIS Elements software and in-house algorithms as described in Methods. Each point represents the average punctae per cell from one field of view. Data are from 1 representative experiment of 3 independent experiments.

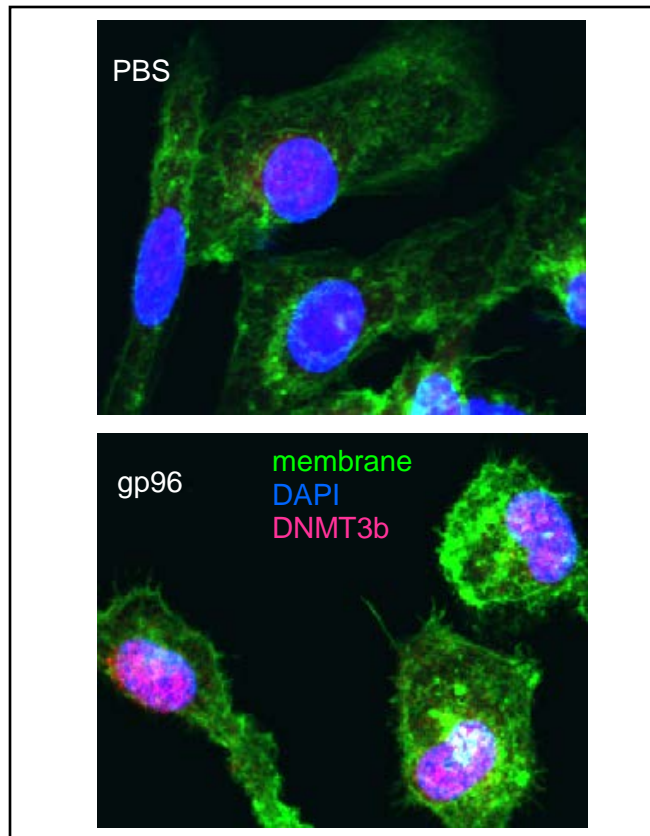


Figure 10. DNMT3b forms punctae in macrophage nuclei following gp96 stimulation.

PECs were stimulated with gp96 or treated with PBS *in vitro* on coverslips for 6 hr. Cells were stained and analyzed by confocal microscopy.

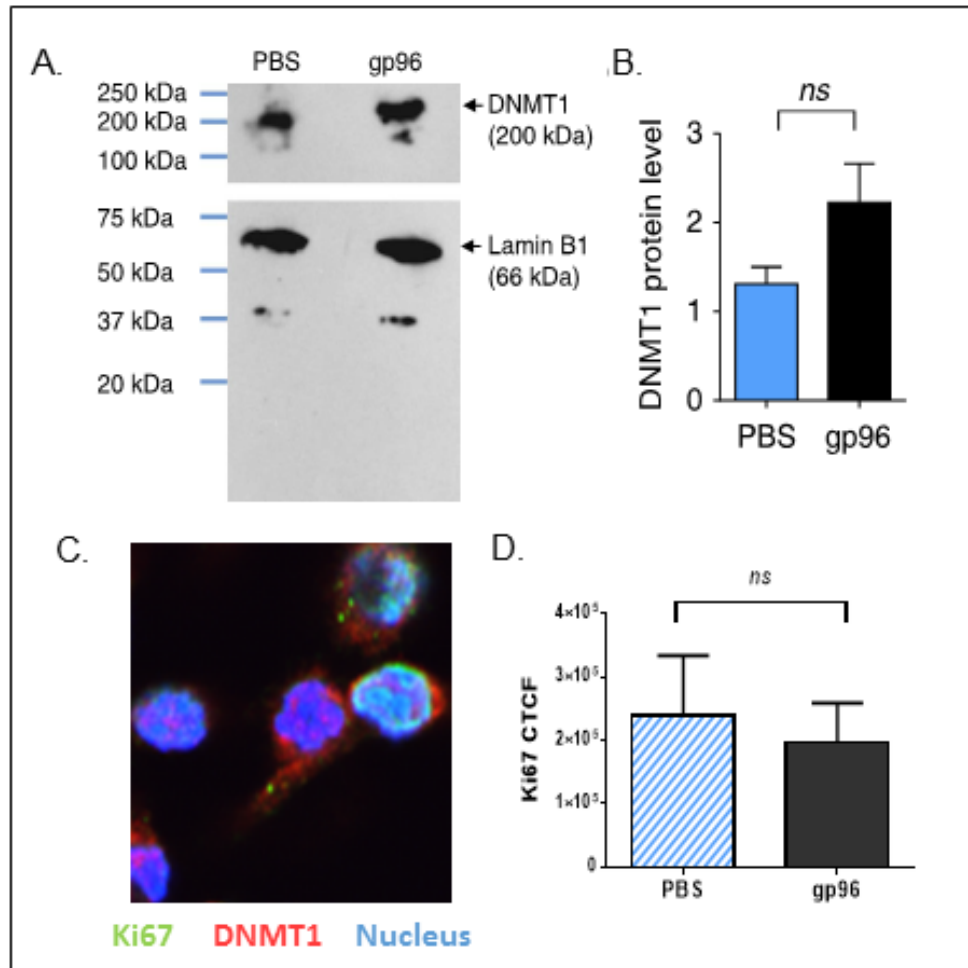


Figure 11. DNMT1 punctae are not an artifact of increased protein or cell proliferation.

A-B. Nuclear extracts from cDCs after 18 hr gp96 stimulation were harvested for western blot analysis. Lamin B1 was used as a loading control. Data are from 1 representative experiment of 3 independent experiments. C-D. BMDCs were treated with gp96 for 6 hr then stained for Ki67 and observed by confocal microscopy. CTCF was calculated in Image J using the calculation: Integrated Density – (Area of selected cell X Mean fluorescence of background readings)

4.2.2 DNMT1 punctae formation is NF- κ B dependent

We next sought to determine the signaling mechanism(s) responsible for this DNMT activity. It has been shown in tumor cells that DNMT1 can complex with the phosphorylated p65 subunit of NF- κ B (121). Because NF- κ B is critical for the gp96 response in all APC types that have been tested, we hypothesized that this is a mechanism utilized by gp96. PECs were given gp96 *in vitro* in the presence or absence of NF- κ B inhibitor cardamomin. This inhibitor prevents degradation of

I κ B α and thus prevents its activation and nuclear translocation. We treated PECs with 10 μ M cardamonin, consistent without previously published studies on NF- κ B activation in HSP-treated PECs and RAW macrophages (62). DMSO-treated cells were included as a control. After 6 hr incubation, cells were stained and observed by microscopy for changes in DNMT architecture. Addition of cardamonin to the media was sufficient to prevent DNMT1 punctae (Figure 12A,B). Thus, NF- κ B seems to play a role in DNMT activation, similar to previously published findings.

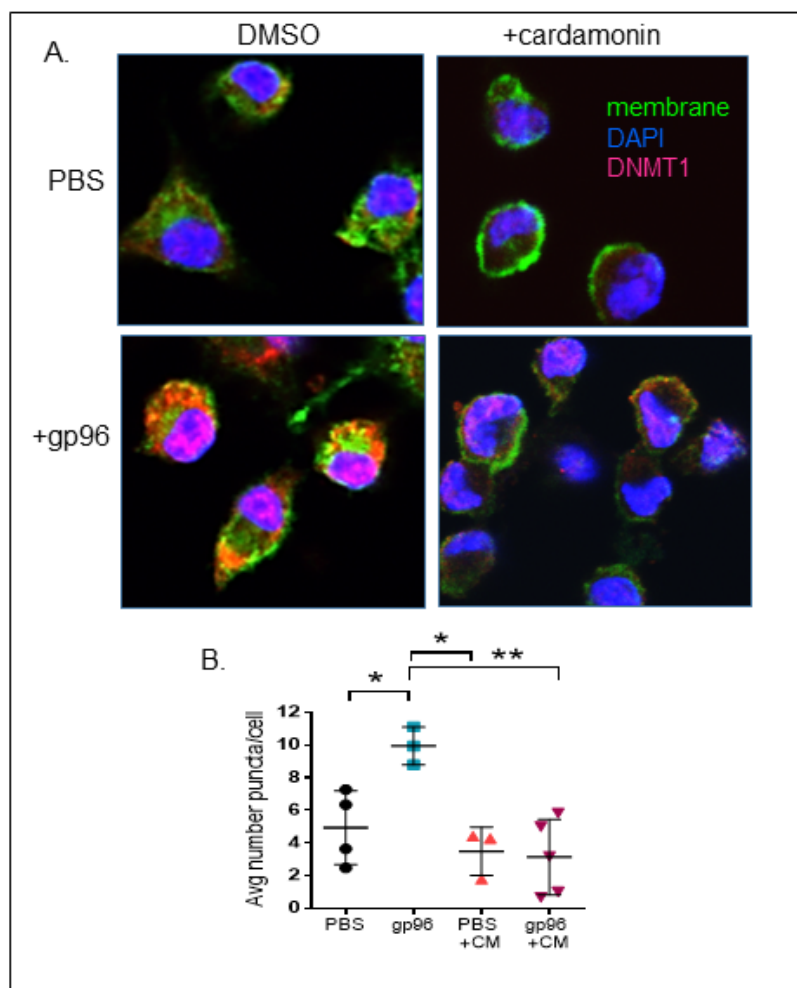


Figure 12. DNMT1 punctae formation in gp96-stimulated macrophages is NF- κ B dependent.

A-B. PECs were treated with HD gp96, in the presence of 10 μ M NF- κ B inhibitor cardamonin (DMSO as negative control). DNMT1 punctae analysis was performed by confocal microscopy after 6 hr. CM, cardamonin.

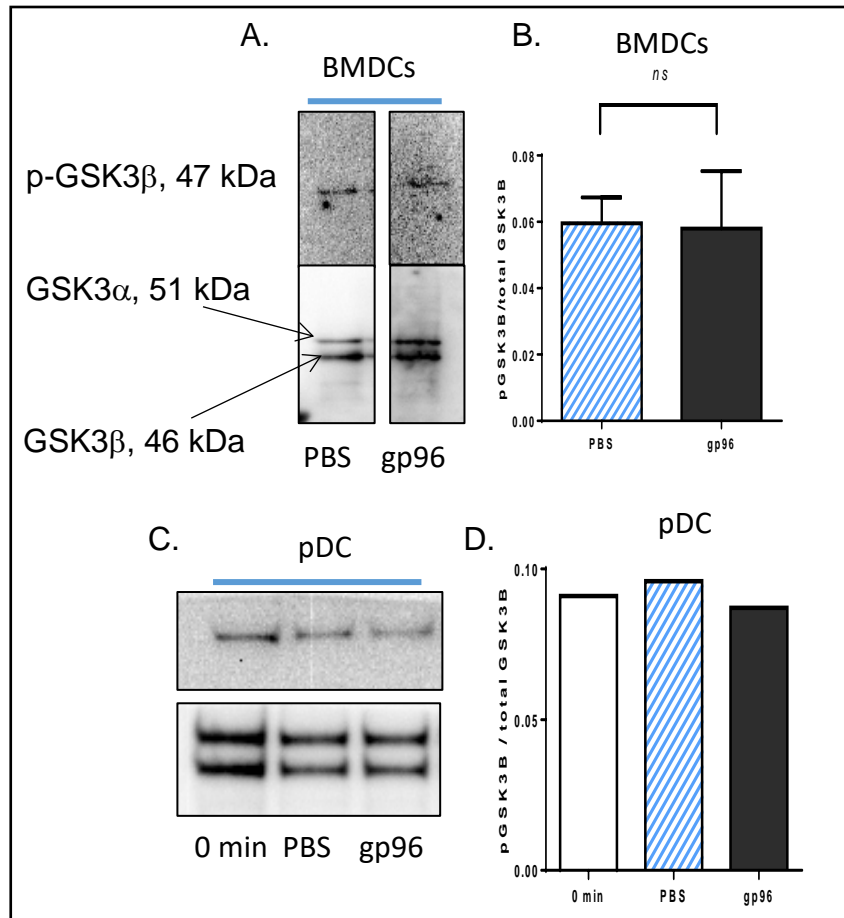


Figure 13. Gp96 treatment does not result in phosphorylation of GSK3 β . BMDCs (A-B) or pDCs (C-D) were treated with 200 ug/ml gp96. After 15 min, cell lysates were harvested for western blot analysis.

Another signaling pathway involved in DNMT1 activation and expression is via phosphorylation of GSK3 β (192). Inhibition of GSK3 β , which occurs via phosphorylation, is associated with stabilization of DNMT by preventing its degradation. This phenomenon has been observed in both T cells and cancer cells (162, 192). CD91 is known to control GSK3 signaling to regulate lipolysis (77) and response to apolipoprotein E (193, 194), but whether this pathway is utilized downstream of HSP-CD91 interaction has not been reported. We tested whether phosphorylation of GSK3 β occurs in cDCs and pDCs stimulated with gp96. All samples were normalized to total GSK3 β . We did not observe any increase in p-GSK3 β signal in response to

gp96 compared to PBS controls in either cell type (Figure 13A-D), suggesting that this pathway is not involved in gp96 responses or gp96-mediated regulation of DNMT.

4.2.3 DNA methylome remodeling occurs in CD91⁺ cells in response to gp96 immunization

DNA methylation is a critical modification responsible for transcriptional regulation of cytokines, growth factors, molecules involved in synapse formation and other aspects of immunologic responses. Given that APCs activate DNMTs via an NF- κ B dependent pathway (Figure 12), we hypothesized that APCs undergo methylome remodeling in response to gp96 immunization. We examined DNA methylation first in total CD91⁺ cells following immunization of mice with LD or HD gp96 to determine if changes in methylation was a mechanism for controlling the divergent T cell immune response. A whole genome methyl-seq approach was taken using MBD protein-based purification of methylated DNA. Mice were immunized with LD or HD gp96 or given PBS. Eighteen hr post-immunization, mice were sacrificed and CD91⁺ cells were isolated by FACS from draining lymph nodes. The target cell population and time point were chosen in accordance with the outcomes in Figure 4 and previously published results (61). We generated 36-55 million filtered and aligned single-end reads per sample. Methylated DNA was sequenced to ~11-fold coverage and analyzed for differential methylation. In this manuscript, intergenic regions are defined as any sequence >2,000 bp distal from annotated genes including alternate promoter and cis-acting regulatory sequences. Intragenic regions include sequences <2,000 bp up or downstream from an annotated gene or within the gene body. Consistent with previous reports, the majority of detected differentially methylated regions (DMRs) occurred in intergenic regions, and those which occurred in intragenic regions were largely located within introns (Figure 14A,B). Only a small

percentage of DMRs were detected on promoter regions. Methylation was largely not present at transcription start sites (TSS) and CpG islands (Figure 14C), although methylation signal did increase immediately flanking these sites. This patterning is consistent with what others have reported for DNA methylation sequencing (153).

From this dataset, 184 intergenic and 55 intragenic DMRs were identified exhibiting variance between LD and HD gp96 immunized cohorts (Tables 5 and 6). Of the 55 intragenic DMRs, 29 were hypermethylated in HD and 26 were hypermethylated in LD. Methylation scores for all detected peaks were plotted, with DMRs highlighted to show divergence between samples (Figure 14D). Using parameters described in Methods, Gene Ontology (GO) analysis was performed on intragenic DMR genes and showed that the bulk of intragenic DMRs occur within pathways which primarily regulate cell-cell contact and adhesion, intracellular signaling and angiogenesis (Figure 15A; Table 7,8). A representative list of genes, most of which are expressed by APCs (Tables 7 and 8), enriched for cell-cell interaction are shown (Figure 15B).

4.2.4 Increase in Nrp1⁺ pDCs following HD gp96 immunization

We then focused on differential methylation and expression of target adhesion molecules in CD91-expressing APCs since APC-T cell contact is critical for proper T cell activation. One of the identified adhesion molecules, Nrp1, known to control Treg responses when expressed in pDCs, was notable. Nrp1 has the most well-established role in controlling DC-Treg interaction at steady state and regulating Treg activation in the tumor microenvironment (195-197). *Nrp1* showed intragenic methylation in samples from HD gp96 immunized mice but not from LD immunized mice (Figure 15B). To determine the effect of gene methylation on Nrp1 protein expression, mice

were immunized with gp96 and 18 hr later draining lymph nodes were stained for markers of cDCs and pDCs and analyzed for Nrp1 expression by flow cytometry. The percentage of Nrp1⁺ pDCs was significantly increased when mice were immunized with HD but not LD gp96 (Figure 16A). Interestingly, cDCs showed no increase in Nrp1 expression following gp96 immunization at either dose. No changes in Nrp1 expression were detected in B cells, T cells, NK cells and other CD11c⁺ DCs (Figure 16B) at any dose of gp96 tested.

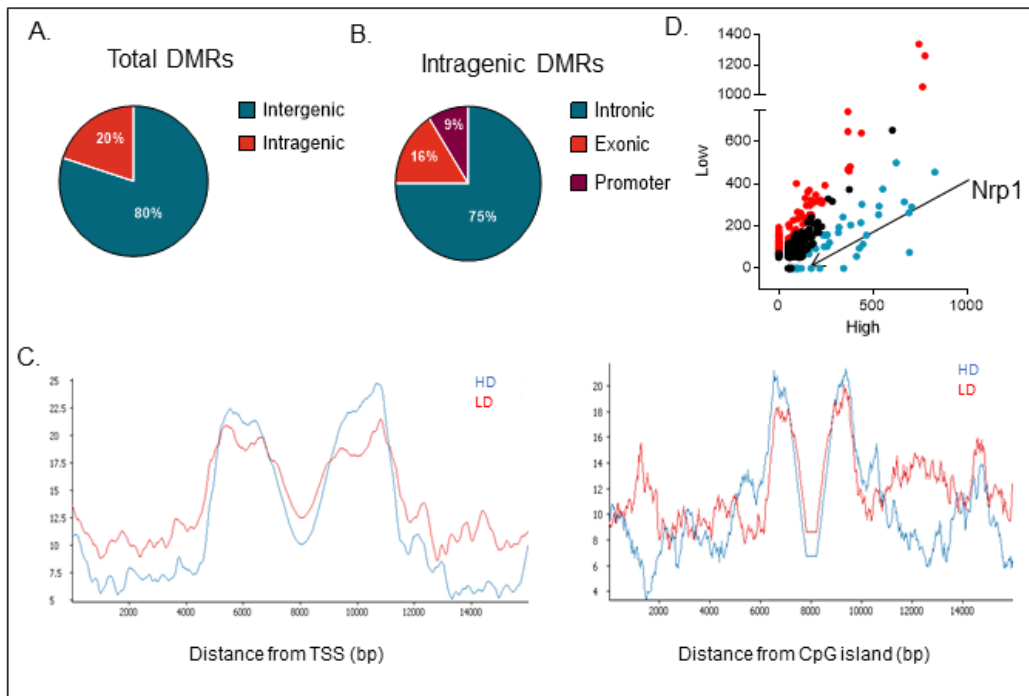


Figure 14. Differential methylation of adhesion molecules in response to gp96.

Mice were immunized with LD or HD gp96 or treated with PBS. DNA was purified from isolated CD91⁺ lymph node cells, fragmented and methylated sequences were enriched using methyl-binding domain protein (MBD). Methylated DNA was sequenced. A. Pie chart shows distribution of total DMRs on intergenic versus intragenic regions. Here, intergenic is defined as any sequence >2000 bp away from any annotated gene, and intragenic is defined as any sequence within 2000 bp of an annotated gene. B. Intragenic DMRs were analyzed for distribution on gene elements (promoters, introns, and exons). C. Average signal profile for methylation enrichment across transcription start sites (TSS) and CpG islands. D. Scatter plot of coverage scores for all methylated genes in LD and HD samples. Any genes defined as DMRs are highlighted.

Table 5. List of methyl-seq DMRs (HD>LD, 29 targets)

Gene name	RefSeq accession	Chr #	Peak start	Peak end	HD cov	LD cov	Delta (HD-LD)	APC expression	DC-T cell interaction
Magi2	NM_001170746	chr5	18985287	18985930	706.93	290.78	416.15	-	
Anks1b	NM_001128086	chr10	89716364	89717299	829.69	456.22	373.47	-	
Cep128	NM_181815	chr12	92462122	92462553	413.38	56.47	356.91	cDC, pDC, mo	-
Apool	NM_026565	chrX	109482705	109483140	428.42	94.6	333.82	cDC, pDC, mac	
Adamts13	NM_001190374	chr7	89618915	89619291	467.33	157.3	310.03	-	
Smo	NM_176996	chr6	29697352	29699387	534.21	295.08	239.13	mo, LC, mac	-
Nlgn1	NM_001163387	chr3	25820638	25821459	437.08	216.12	220.96	cDC, mo, LC, mac	-
Pisd-ps2	NR_003519	chr17	3081229	3083292	552.73	375.78	176.95	cDC, pDC, mo, LC, mac	-
Maoa	NM_173740	chrX	16247784	16248261	242.09	103.15	138.94	LC, mac	-
Unc13c	NM_001081153	chr9	73675204	73675598	320.61	195.01	125.6	-	
Gsted	NM_026231	chr3	132728372	132728926	196.14	93.23	102.91	cDC, mac	-
Bmper	NM_028472	chr9	23094351	23094641	101.46	0	101.46	cDC, pDC	-
Olfr593	NM_146380	chr7	110358292	110358906	255.6	156.56	99.04	-	
Gphn	NM_145965	chr12	79375574	79376162	256.73	160.44	96.29	cDC, pDC, mo LC, mac	-
Gtf2h2	NM_022011	chr13	101241094	101241462	161.11	68.55	92.56	cDC, pDC, mo LC, mac	-
Ston2	NM_175367	chr12	92981055	92982529	86.76	0	86.76	cDC, mac	-
Meis1	NM_010789	chr11	18852461	18852694	81.39	0	81.39	cDC, pDC, mo LC, mac	-
Gpr98	NM_054053	chr13	81551933	81552441	77.93	0	77.93	-	
Myo3b	NM_177376	chr2	69875218	69875746	76.25	0	76.25	-	
Cpxm2	NM_018867	chr7	139307057	139307716	76.23	0	76.23	LC	-
Wdte1	NM_199306	chr4	132873894	132874522	75.33	0	75.33	cDC, pDC, mo LC, mac	-
Gabbr2	NM_001081141	chr4	46807144	46807883	74.68	0	74.68	cDC, pDC, mo LC, mac	-
Cdhr3	NM_001024478	chr12	33760550	33761112	73.54	0	73.54	cDC	-
Nrp1	NM_008737	chr8	130909774	130910078	72.41	0	72.41	cDC (low), pDC (high), mo	(182-184)
Cell11	NM_011330	chr11	81877343	81877624	72.41	0	72.41	cDC, pDC, mo LC, mac	-
Shroom3	NM_015756	chr5	93190064	93190518	72.13	0	72.13	cDC, pDC, mo LC, mac	-
Nell1	NM_001037906	chr7	57580690	57580936	61.26	0	61.26	-	
Kctd16	NM_026135	chr18	40538033	40538370	61.26	0	61.26	-	
Kcnh1	NM_001038607	chr1	194023294	194023710	173.55	113.32	60.23	LC	-

APC expression was determined using publicly available RNA seq data from The Immunological Genome Project (Immgen). Coverage for LD and HD samples is reflective of the average number of peaks found at that location and was calculated using BEDtools. Abbreviations: chr, chromosome; cov, coverage; cDC, conventional DC; pDC, plasmacytoid DC; LC, Langerhans cell; mo, monocyte; mac, macrophage

Table 6. List of methyl-seq DMRs (LD>HD, 26 targets)

Gene name	RefSeq accession	Chr #	Peak start	Peak end	HD cov	LD cov	Delta (HD-LD)	APC expression	DC-T cell interaction
Fam172a	NM_138312	chr13	77919765	77920290	367.91	742.72	-374.81	cDC, pDC, mo L.C, mac	-
Tbc1d9	NM_001111304	chr8	85752214	85755805	94.18	401.81	-307.63	cDC, mo, L.C, mac	-
Hpse2	NM_001081257	chr19	43313714	43314089	764.69	1053.75	-289.06	-	-
Sgez	NM_145841	chr8	38696342	38696718	367.91	648.16	-280.25	-	-
Tmem232	NM_001008973	chr17	65629264	65629806	154.26	362.48	-208.22	-	-
Stam2	NM_019667	chr2	52551744	52558220	0	163.43	-163.43	cDC, pDC, mo L.C, mac	-
Dach2	NM_001142570	chrX	110665377	110665793	53.44	207.81	-154.37	-	-
Tmem132c	NM_175432	chr5	127752052	127752513	171.25	323.82	-152.57	cDC	-
Coll19a1	NM_007733	chr1	24452000	24452373	146.76	297.98	-151.22	-	-
Pik3c2g	NM_207683	chr6	139870145	139870612	77.18	228.28	-151.1	-	-
Itgbl1	NM_145467	chr14	124343810	124344457	197.85	347.7	-149.85	-	-
Nbea	NM_030595	chr3	55924530	55925050	246.34	393.42	-147.08	cDC, pDC, mo, mac	-
Unc80	NM_175510	chr1	66728690	66729004	56.57	196.22	-139.65	-	-
Klra2	NM_001170851	chr6	131177385	131177785	101.61	234.86	-133.25	mo, mac	-
Sntg1	NM_027671	chr1	8708056	8708514	166.38	297.98	-131.6	-	-
Cntn5	NM_001033359	chr9	10173900	10174397	131.91	242.32	-110.41	-	-
Pip5k1a	NM_008847	chr3	94896304	94896722	0	109.78	-109.78	cDC, pDC, mo L.C, mac	-
Lama2	NM_008481	chr10	27302267	27302697	0	108.28	-108.28	-	-
Inpp5a	NM_001127363	chr7	146703630	146703951	0	107.37	-107.37	cDC, pDC, mo L.C, mac	-
Gabrg3	NM_008074	chr7	64227382	64227879	380.3	482.22	-101.92	cDC, mac	-
Kir3dl1	NM_177749	chrX	133051381	133052112	367.63	468.62	-100.99	-	-
Ube2e2	NM_144839	chr14	19535822	19536247	374.14	461.11	-86.97	cDC, L.C, mac	-
Ncam1	NM_001113204	chr9	49463833	49464363	0	86.52	-86.52	mac	-
Cadps2	NM_001252105	chr6	23410121	23410681	0	73.7	-73.7	mac	-
Ctnd2	NM_008729	chr15	30589483	30589996	0	67.3	-67.3	cDC, pDC, L.C	-
Rbfox1	NM_021477	chr16	7242782	7243199	0	64.83	-64.83	cDC, pDC, mo L.C, mac	-

APC expression was determined using publicly available RNA seq data from The Immunological Genome Project (Immgen). Coverage for LD and HD samples is reflective of the average number of peaks found at that location and was calculated using BEDtools. Abbreviations: chr, chromosome; cov, coverage; cDC, conventional DC; pDC, plasmacytoid DC; LC, Langerhans cell; mo, monocyte; mac, macrophage

Table 7. List of GO analysis hits (HD>LD)

Subcategory name	pval	neg log pval	# genes	GeneIDs
Cell adhesion	0.00012	3.919514213	6	Nlgn1, Gpr98, Cpxm2, Cdhr3, Nell1, Nrp1
Cell junction	0.000136725	3.864152068	7	Nlgn1, Gphn, Anks1b, Unc13c, Dennd1a, Gabbr2, Shroom3
Synapse	0.000286469	3.542922368	6	Nlgn1, Gphn, Anks1b, Unc13c, Dennd1a, Gabbr2
Cell projection	0.00258205	2.588035352	5	Smo, Anks1b, Dennd1a, Gabbr2, Nrp1
Cell-cell adhesion	0.0077048	2.11323863	3	Nlgn1, Gpr98, Cdhr3
Protein binding	0.00280261	2.552437333	20	Magi2, Kctd16, Nlgn1, Gpr98, Gsted, Gphn, Bmper, Ston2, Meis1, Myo3b, Dennd1a, Wdtd1, Nell1, Gabbr2, Nrp1
Postsynaptic membrane	0.000966876	3.01462922	4	Nlgn1, Gphn, Anks1b, Gabbr2
Cell communication	0.00914359	2.038883256	6	Smo, Nlgn1, Gpr98, Maoa, Unc13c, Bmper
Cell-cell signaling	0.00918952	2.036707173	4	Smo, Nlgn1, Maoa, Unc13c
Synaptic transmission	0.0351746	1.453770833	3	Nlgn1, Maoa, Unc13c
Signaling	0.0486346	1.313054652	10	Smo, Magi2, Nlgn1, Gpr98, Maoa, Olf593, Unc13c, Bmper, Gabbr2, Nrp1
Regulation of developmental process	0.0015	2.823952173	7	Smo, Nlgn1, Meis1, Nell1, Nrp1, Ccl11, Shroom3
Anatomical structure development	0.0077048	2.11323863	10	Smo, Nlgn1, Gpr98, Gphn, Bmper, Meis1, Nell1, Nrp1, Ccl11, Shroom3
Growth	0.0297471	1.526555367	4	Smo, Wdtd1, Nrp1, Ccl11
Vasculature development	0.0332004	1.478856684	4	Smo, Meis1, Nrp1, Ccl11
Angiogenesis	0.0494972	1.305419368	3	Meis1, Nrp1, Ccl11

Table 8. List of GO analysis hits (LD>HD)

Subcategory name	pval	neg log pval	# genes	GeneIDs
Inositol phosphate metabolism	0.0188722	1.72417747	3	Pip5k1a, Inpp5a, Pik3c2g
Phosphatidylinositol signaing	0.0245305	1.6102936	3	Pip5k1a, Inpp5a, Pik3c2g
Phosphatidylinositol phosphate kinase	0.0439244	1.357294162	2	Pip5k1a, Pik3c2g
Cell adhesion	0.05073	1.294735138	5	Ncam1, Ptpm, Lama2, Cntn5, Krla2, Col19a1, Ctnnd2
Biological adhesion	0.05073	1.294735138	7	Ptpm, Lama2, Negr1, Cntn5, Krla2, Col19a1, Ctnnd2

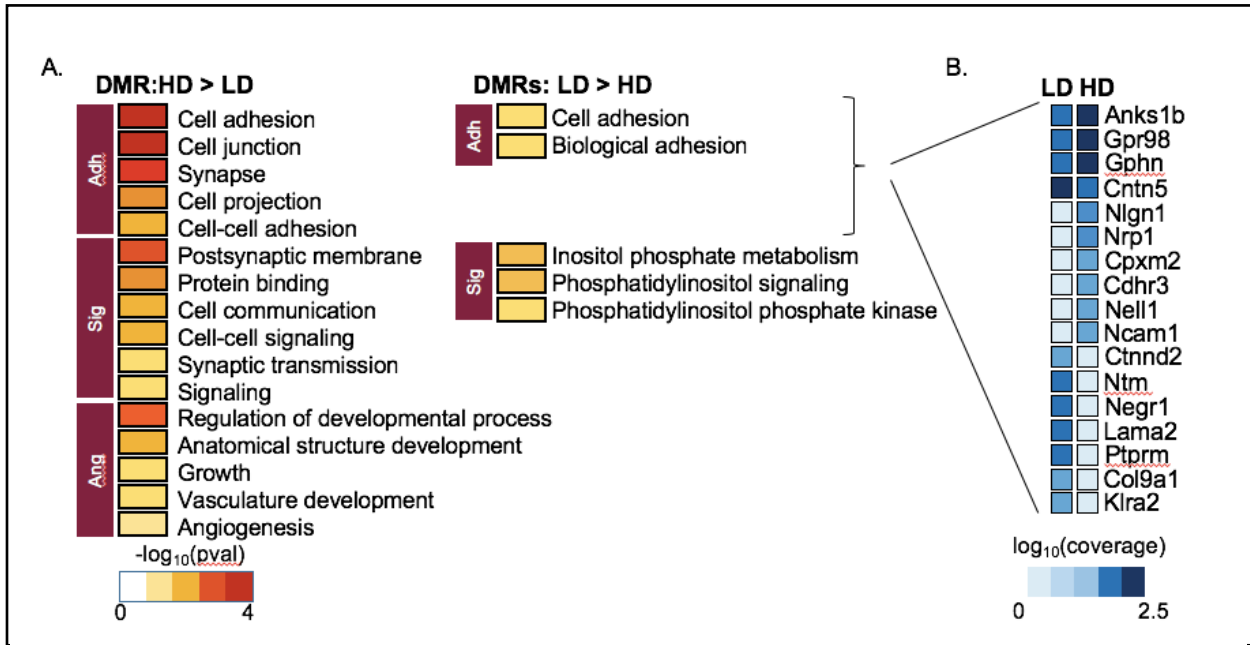


Figure 15. DMRs are enriched on genes associated with adhesion.

A. Gene Ontology analysis of all DMRs identified in LD and HD. Adh = adhesion; Sig = signaling; Ang = angiogenesis. B. Sample genes within the adhesion gene family set, with log(coverage) shown.

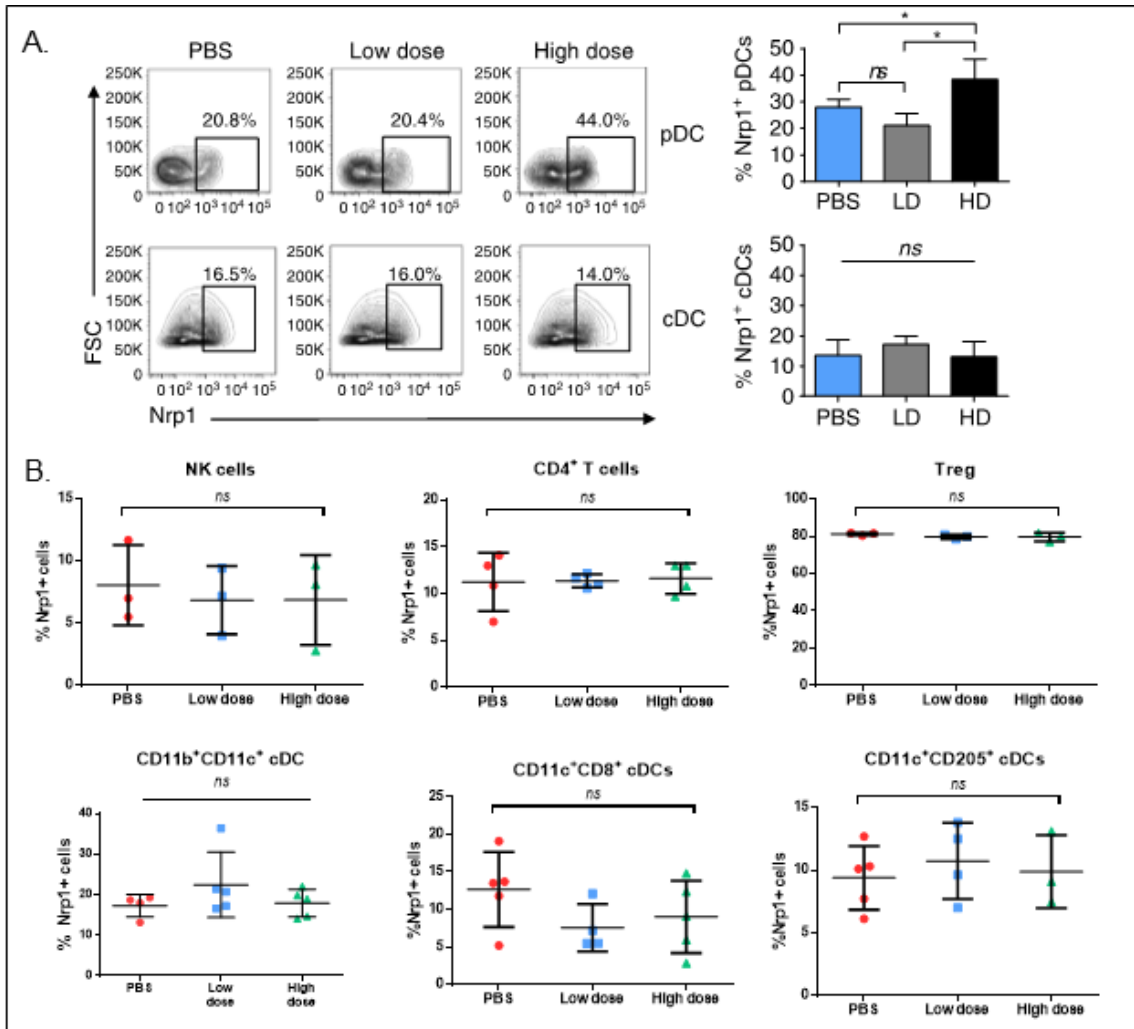


Figure 16. pDCs specifically increase expression of Nrp1 in response to HD gp96.

A. Mice were immunized with LD or HD gp96 and draining lymph nodes were harvested and stained with markers for pDC or cDC plus Nrp1. Cells were analyzed by flow cytometry for changes in percentage of Nrp1⁺ in respective pDC and cDC gates. One set of representative flow plots is shown. B. Lymph nodes were harvested after 18 hours and stained for NK cells (NK1.1), CD4⁺ T cells (CD3, CD4), Treg (CD3, CD4, Foxp3), and DC subsets (CD11b, CD11c, CD8, CD205). n=5, data are from 1 representative experiment of 3 independent experiments. Bar graphs on the right are the average percentages from multiple experiments

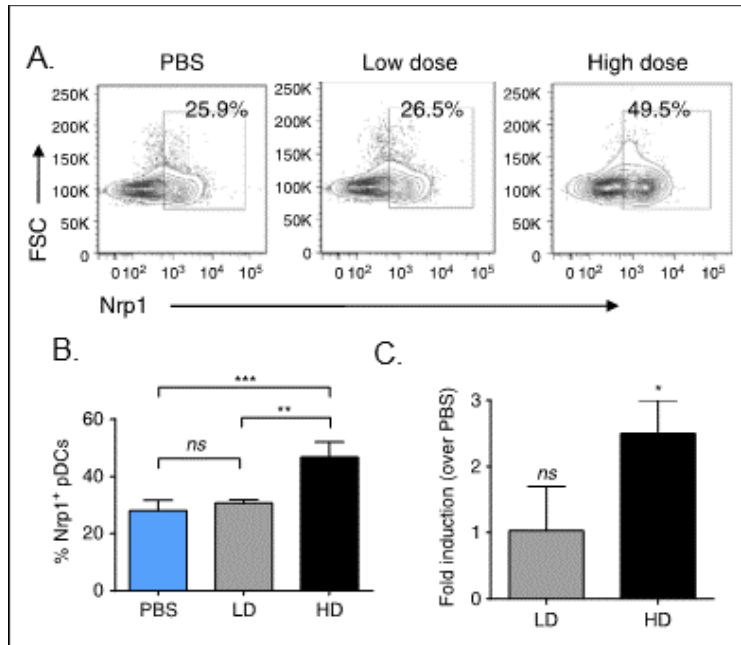


Figure 17. pDCs recapitulate in vivo HD phenotype in an in vitro culture system. A,B. Splenic pDCs were isolated, treated with LD or HD gp96 *ex vivo*, and Nrp1 expression was measured by flow cytometry. C. Splenic pDCs were isolated, treated with LD or HD gp96 *ex vivo*, and Nrp1 expression was measured by qPCR. In B and C, data are pooled from 3 independent experiments.

4.2.5 Gp96-mediated Nrp1 gene methylation regulates Nrp1 gene product expression in pDCs, but not cDCs

We established an *in vitro* system to examine the specific effect(s) of gp96 on pDCs observed in HD immunized mice. We chose our *in vitro* based on: 1) estimates of internal volume following i.d. injection, 2) number of cells exposed to injected gp96 at the injection site and draining lymph node, 3) historic data using gp96-treated DCs *in vitro*, 4) the amount of gp96 per tumor cell resulting in release of gp96 *in vivo* and 4) a dose titration which copied the phenotypes we observe with *in vivo* immunization. We used 200 $\mu\text{g/ml}$ and 10 $\mu\text{g/ml}$ gp96 in culture to represent HD and LD gp96 *in vivo* respectively. Nrp1 expression on the surface of pDCs was examined by flow cytometry following treatment of cells in culture with HD or LD. The percent of Nrp1⁺ pDCs is enhanced when cells were treated with HD gp96 but not LD gp96 or PBS, recapitulating the effects

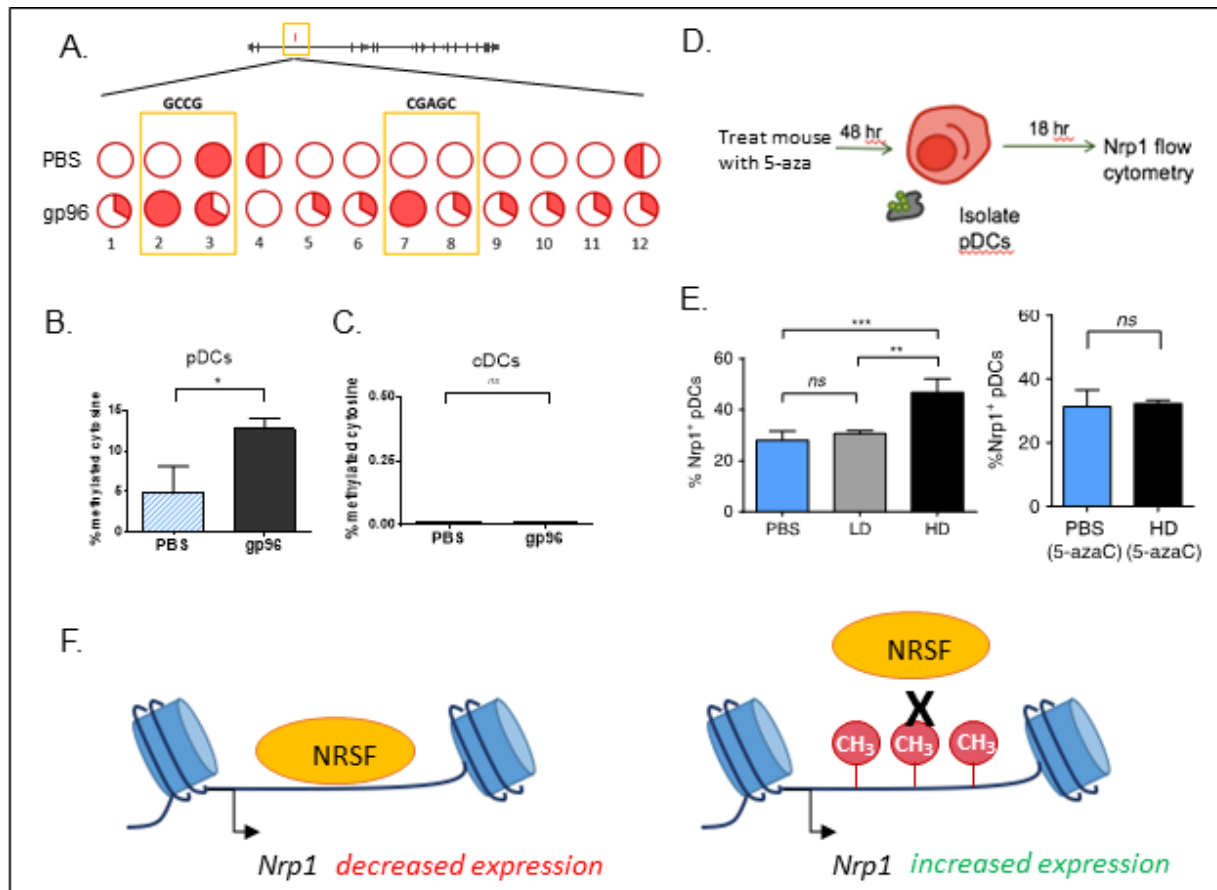


Figure 18. Intronic methylation of *Nrp1* enhances expression.

A. Schematic of methylation within *Nrp1* at intron 2 from whole genome methyl seq data. Splenic pDCs were isolated from naïve mice and stimulated with HD gp96. Purified DNA was analyzed by clonal bisulfite sequencing. Each line of bisulfite seq data represents one treatment group. Filled portions pie-charts signify methylated samples; open slices signify unmethylated samples. Only differentially methylated cytosines are shown; both CpG and non-CpG are included. B-C. Percent of methylated cytosines of total cytosines as measured by clonal bisulfite sequences is shown for pDCs (B) and BMDCs (C). Data are from 1 representative experiment of 2 independent experiments D. Schema of experiment. Mice were treated with 5 mg/kg 5-aza and 48 hr later pDCs were isolated for gp96 treatment. E. Splenic pDCs were stimulated with HD gp96 *ex vivo* for 18 hr. Cells were stained for pDC markers and Nrp1, and analyzed by flow cytometry. Percent of Nrp1⁺ pDCs of total pDCs is shown F. Proposed model of methylation of NRSF binding site in *Nrp1* gene body.

seen *in vivo* (Figure 17A,B). *Nrp1* mRNA levels were also measured in pDCs treated with LD or HD gp96 by qPCR (Figure 17C). In agreement with protein expression, *Nrp1* mRNA increased significantly when cells were treated with HD gp96 but not LD gp96. Following the consistent *Nrp1* protein expression patterns in pDCs *in vivo* and *in vitro* we next confirmed the methyl-seq data in pDCs stimulated with HD gp96 *in vitro*. pDCs were cultured in the presence of HD gp96, and analyzed at a single base resolution of the *Nrp1* intronic DMR by clonal bisulfite sequencing

(Figure 18A). Bisulfite-treated DNA was PCR amplified with specific primers. PCR amplicons were cloned and sequenced and are indicated as circles which represent individual cytosines differentially methylated in either sample (Figure 18A). Consistent with the methyl-seq dataset (Figure 15B), the percentage of total methylated cytosines within intron 2 of *Nrp1* was significantly increased in gp96-treated pDCs versus untreated pDCs (Figure 18B). cDCs (represented by BMDCs) did not exhibit this change in methylation of *Nrp1* (Figure 18C). These data are also consistent with previous observations, in that methylation within such non-promoter regions was associated with enhanced protein expression (198-200). The effect of DNA methylation initiated at the *Nrp1* locus on protein expression is reflected in the increase in protein expression (Figure 16A, 17). We next verified that DNA methylation was responsible for increased Nrp1 expression by inhibiting DNA methylation. Mice were administered 5-azaC, a potent inhibitor of DNMTs, 72 hr prior to isolation of pDCs. pDCs from 5-azaC treated or untreated mice were incubated *in vitro* with HD gp96 and analyzed for Nrp1 expression by flow cytometry (Figure 18D). 5-azaC completely blocked the upregulation of Nrp1 in pDCs treated with gp96 *in vitro* (Figure 18E).

To understand the disparity in methylation patterns at the *Nrp1* locus and Nrp1 expression in pDCs and cDCs, we examined chromatin accessibility in naïve cells (Figure 19). Chromatin was extracted from cDCs or pDCs and digested with nuclease. The *Nrp1* locus was then amplified and quantified with specific primers by qPCR. In this chromatin accessibility assay, when the DNA is in a heterochromatin (closed) state, it is inaccessible to nuclease digestion and will result in insignificant CT shifts between digested and undigested samples (Figure 19A). DNA in a euchromatin (open) state will be susceptible to nuclease digestion and result in large CT shifts upon amplification. We observed that at a basal state, *Nrp1* in pDCs is in an open confirmation

and thus more accessible, as revealed by the large fold enrichment score (Figure 19B). In contrast, *Nrp1* was in a closed chromatin state in cDCs. These data indicate that pDCs are more poised for regulation of *Nrp1* at a genetic level (Figure 19C).

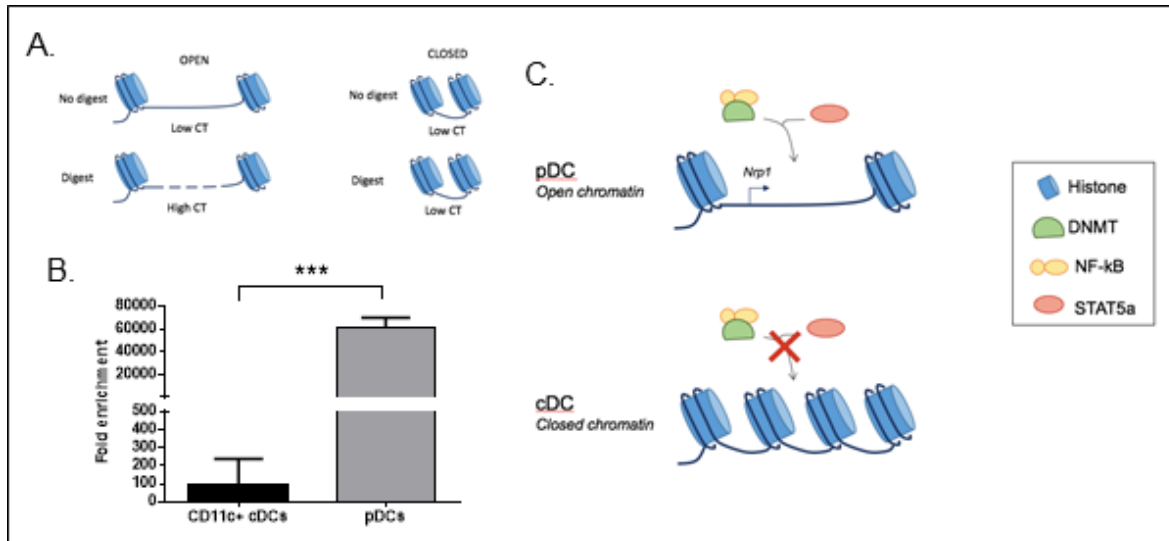


Figure 19. *Nrp1* is in an euchromatin conformation, and thus poised for regulation, in naïve pDCs but not cDCs.

A. Schematic of chromatin accessibility experiment. B. Chromatin was purified splenic pDCs or cDCs isolated from naïve mice and digested. Chromatin accessibility at the *Nrp1* region of interest was assessed by qPCR. Fold enrichment was calculated using the formula: $FE = 2^{(NseCT - noNseCT)} \times 100\%$. $n=3/\text{group}$, data are pooled from 3 independent experiments. C. *Nrp1* in pDCs is open and thus more accessible for regulatory factors including DNMT, NF-κB, and STAT5a.

4.2.6 Gp96-stimulated pDCs stabilize and prolong interactions with Treg in a *Nrp1*-dependent manner

Nrp1 expression by pDCs facilitates long-term homotypic *Nrp1*-*Nrp1* or heterotypic *Nrp1*-Sema4a interaction with Treg cells (195, 197). Having established that both HD gp96 immunization and *in vitro* gp96 stimulation result increased *Nrp1*⁺ pDCs, we investigated whether *in vitro* gp96-stimulated pDCs prolonged interaction with Tregs as measured by time-lapse live cell microscopy. pDCs and Tregs were isolated from spleens. pDCs were cultured for 18 hr with HD gp96, and for the last 2 hr in the presence or absence of *Nrp1* blocking or isotype control antibody. CellTracker

Red-labeled CD4⁺CD25⁺ Tregs were added to the culture and imaged for 2 hr, with frames taken at 5 min intervals. Figure 20A shows representative pDC-Treg interactions over time. HD gp96 significantly increased interaction time between pDCs and Tregs and this interaction could be blocked by α -Nrp1 antibodies but not by an isotype control antibody (Figure 20A,B,C). Interactions were considered “long” if the pDC-Treg interaction lasted >10 min. Any interaction that lasted <10min was deemed transient, and placed in the “little/no interaction” category. In all samples, some baseline level of long interaction was observed, which is in agreement with Tregs scanning for antigen and/or recognition of self-antigen to maintain the Treg lineage. However, Nrp1 antibody did not have an overall inhibitory effect on baseline long interactions. Over the course of the experiment the gp96-treated pDCs did not undergo maturation and maintained an immature phenotype (Figure 8B), further supporting previous findings that Nrp1-expressing immature DCs efficiently interact with Treg (195).

Furthermore, we tested whether this phenomenon is Treg-specific, or if gp96-stimulated pDCs increase interaction with conventional T cells (Tconv), identified as CD4⁺CD25⁻ isolates from the spleen. Tconv were co-cultured with pDCs treated in the same way as for the Treg in Figure 20B. There was no change in pDC-Tconv interaction regardless of gp96 or antibody treatment (Figure 20D,E), suggesting that this is a Treg-specific event and further supports the dependence of Nrp1 since Tconv do not express high levels of Nrp1.

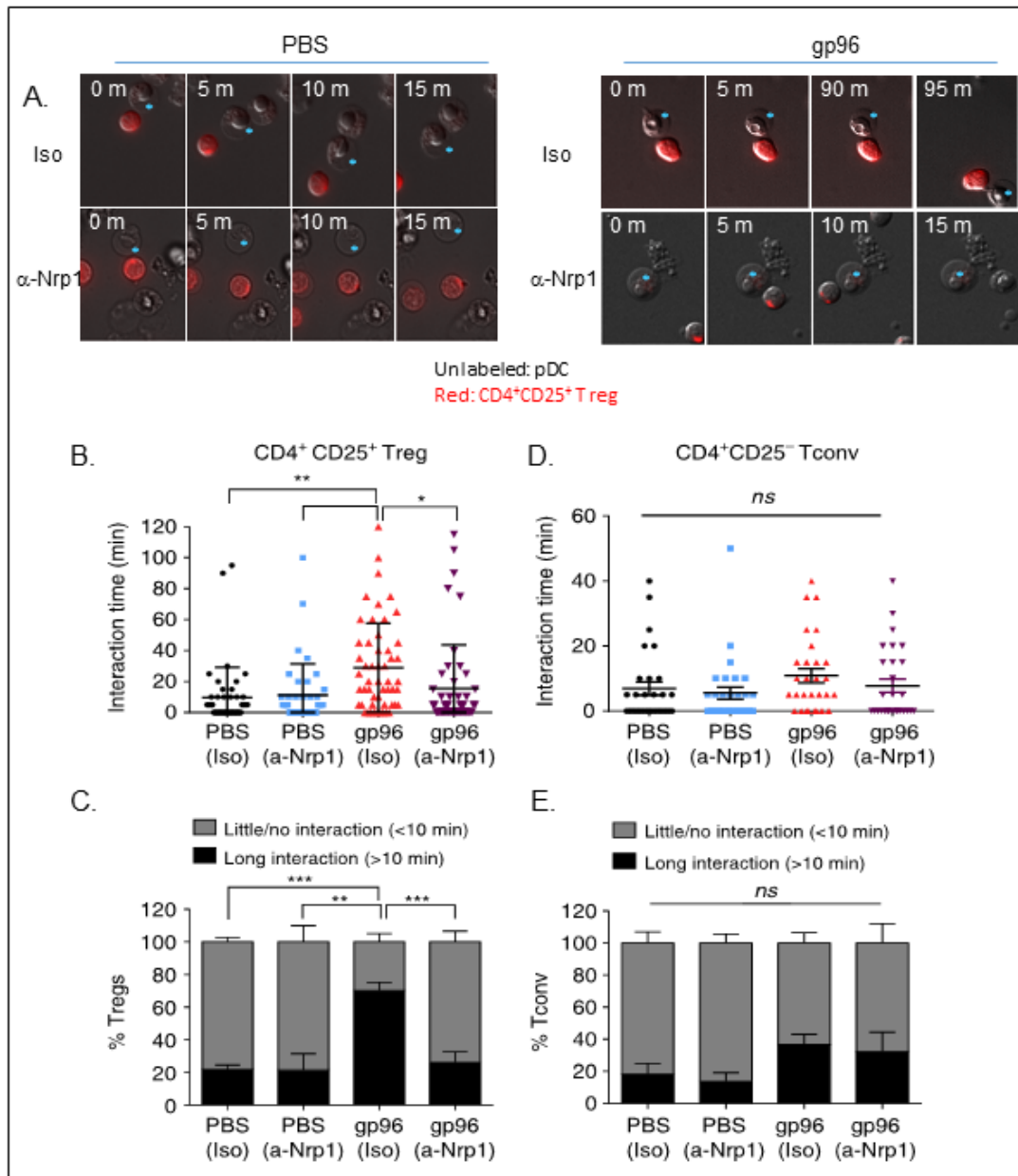


Figure 20. gp96-stimulated pDCs increase interaction with Treg in a Nrp1-dependent manner.

A-E. Splenic pDCs were plated on coverslips with or without HD gp96, and in the presence or absence of Nrp1 blocking antibody (α -Nrp1) or isotype control antibody (Iso). Prior to imaging, Treg (CD4⁺CD25⁺) or Tconv (CD4⁺CD25⁻) were labeled with Cell Tracker Red dye and added to the pDC culture dishes at a 2:1 DC:T cell ratio. Images were acquired at 5 min intervals for a total of 2 hr. Interaction and motility were analyzed. B. Treg were tracked using NIS Elements tracking software. Representative Treg-pDC interactions are shown for each treatment group for the indicated times. The interaction times of Tregs with pDCs from multiple images are quantified. All Tregs (including those that failed to interact with pDC) are included. C. The average percentage of Tregs which undergo long (>10 min) or short to no (0-10 min) interactions with pDCs were calculated for each group. D,E. Tconv were analyzed similarly to Treg. Total interaction time (D) and percentage of long interaction (E) are shown. All data are from 1 representative experiment of 2-3 independent experiments.

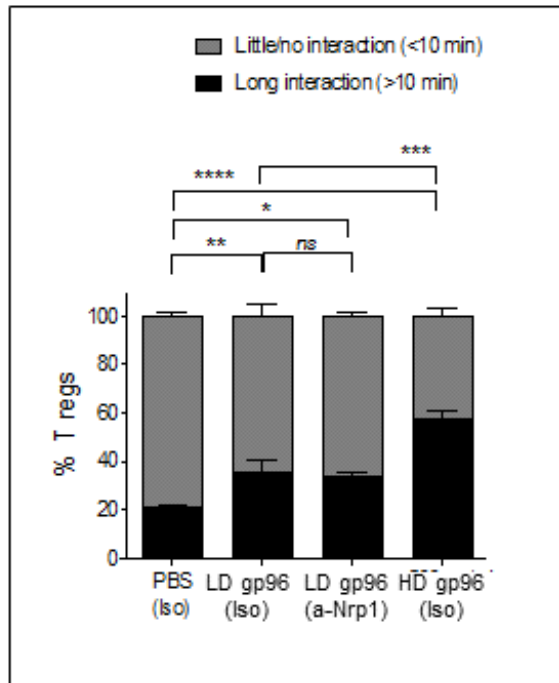


Figure 21. Duration of pDC-Treg interaction increases with increasing treatment dose of gp96.

pDCs were treated with LD or HD gp96 for 18 hr. As described in Methods, pDCs were also treated with α -Nrp1 blocking antibody or isotype control and co-cultured with labeled Treg. The percentage of cells which had undergone long term interactions in each group was calculated and is shown.

Although LD treatment of pDCs resulted in a marginal increase in pDC-Treg stabilization, it was significantly lower than stabilization achieved with HD (Figure 21). Stimulation of pDCs with gp96 therefore prepares these pDCs for longer interaction with Treg by increasing expression of Nrp1.

4.2.7 pDCs are required for gp96-mediated immune suppression by Tregs

We have implicated CD91⁺CD11c⁺ cells in HD gp96-mediated suppression of tumor immunity (Figure 3) and shown that gp96-conditioned pDCs have the capacity to engage and form stable interactions with Tregs via Nrp1 (Figure 20). We next established a gp96-mediated suppression

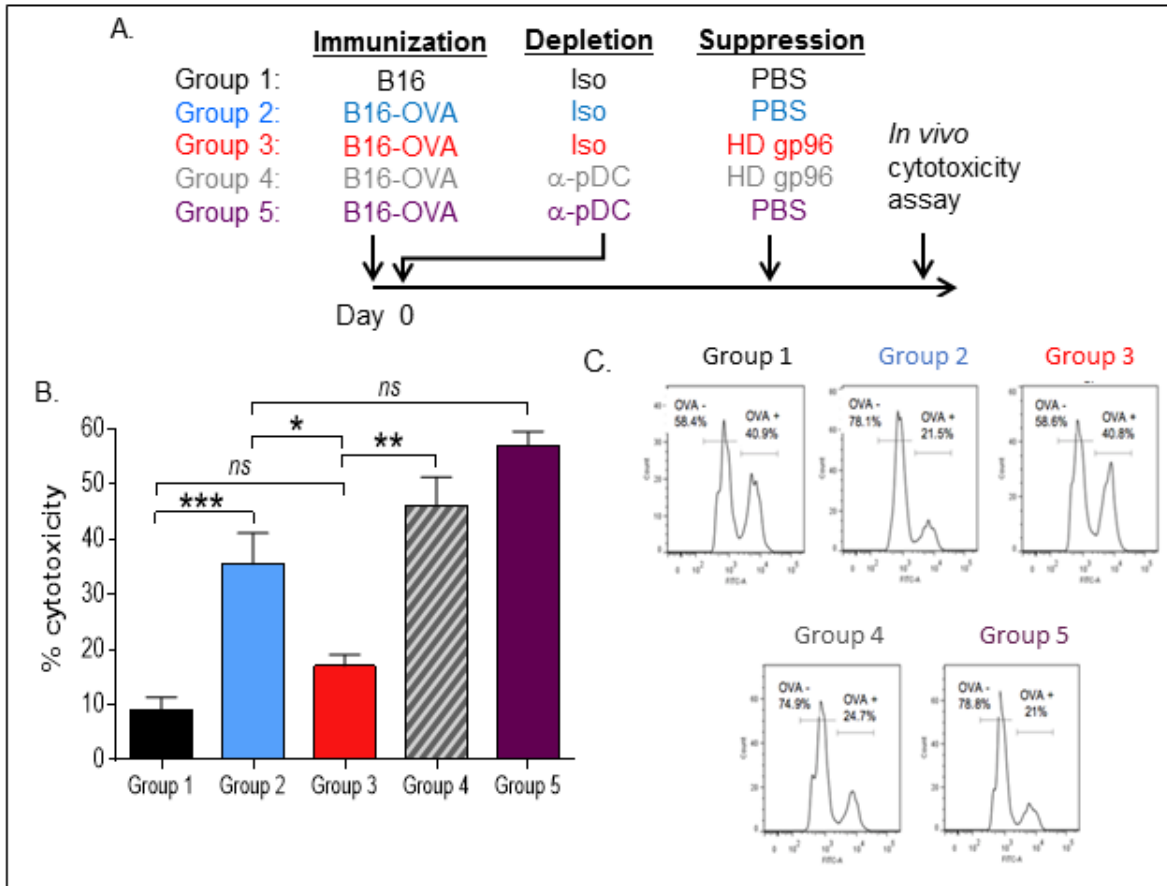


Figure 22. pDCs are required for efficient suppression of CTL-mediated cytotoxicity by HD gp96.

A. Schema for experiment. Mice were immunized intraperitoneally (i.p.) with irradiated OVA-expressing cells to generate an anti-OVA response. On the same day, mice were depleted of pDCs via intraperitoneal injection of α -PDCA depleting antibody. Mice were given a HD of gp96 24 hr later. *In vivo* cytotoxicity was measured 6 days later by flow cytometry. B. Percent cytotoxicity was calculated as described in Methods and is shown for each group. C. Shown are representative flow plots for CFSE-labeled SIINFEKL-pulsed target splenocytes (CFSE-high) and unpulsed non-target splenocytes (CFSE-low) for each treatment group. Data are pooled from 2 independent experiments.

assay to test the role of pDCs *in vivo* (Figure 22A). Mice were immunized with irradiated, antigen (OVA)-expressing or non-expressing B16 tumor cells (Group 1 and 2 respectively). OVA-specific

CTL activity was measured *in vivo* by intravenous injection of OVA peptide (SIINFEKL)-pulsed or unpulsed, differentially labeled target cells into mice. In this *in vivo* assay, CTL efficiently lysed SIINFEKL-pulsed target cells in mice immunized with B16-OVA (Group 2) but not with B16 (Group 1) (Figure 22B,C). When mice were immunized with B16-OVA and treated with HD gp96 one day later (Group 3), CTL activity was significantly abrogated (Figure 22B). This data is consistent with earlier observations of Treg generation by gp96 treatment. pDCs were depleted with specific antibody or control IgG in this assay as described in Methods. When pDCs were depleted (Group 4), HD gp96 treatment failed to abrogate CTL mediated lysis of target cells (Figure 22B). Control mice immunized with B16- OVA and depleted of pDCs in the absence of gp96 treatment (Group 5) still elicited CTL activity comparable to Group 2.

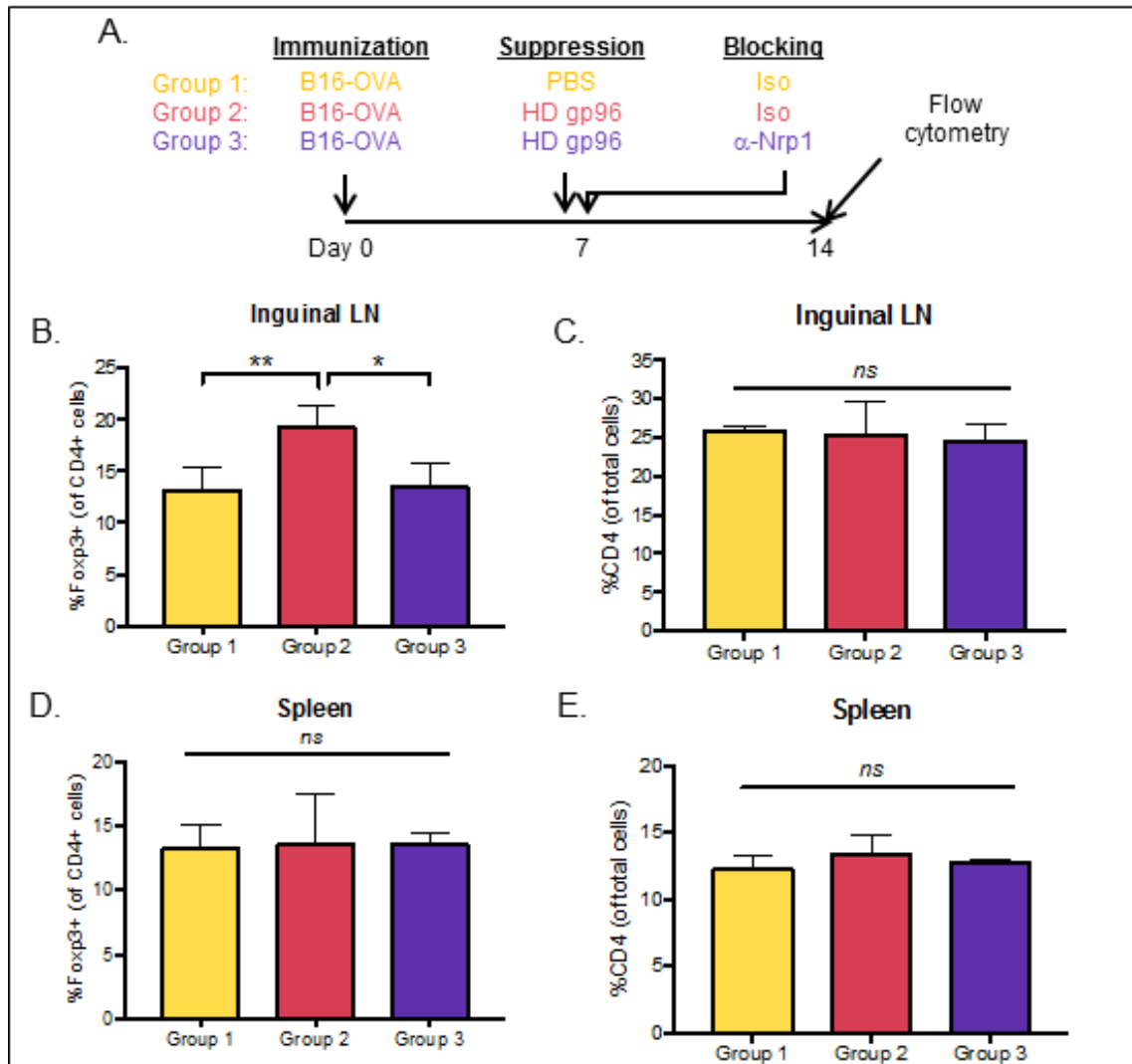


Figure 23. HD gp96-mediated Treg induction is Nrp1-dependent.

A. Schema to determine Nrp1 requirement for HD gp96-mediated suppression. Mice were immunized i.p. with irradiated tumor cells. On day 7, mice were given HD gp96 (i.d.) and one intraperitoneal dose of α -Nrp1 neutralizing antibody. On day 14, mice were sacrificed for analysis. Draining inguinal LNs (B,C) spleen (D,E) were harvested for flow cytometry analysis of CD4⁺Foxp3⁺ Treg and total CD4 cells. Data are pooled from 2 independent experiments.

4.2.8 Nrp1 is essential for gp96-mediated Treg generation

Using the HD gp96 assay previously established, we measured the increase in Treg populations as a function of HD gp96 administration (Figure 23A). Mice were immunized with irradiated B16-OVA followed by treatment with HD gp96. Nrp-1 blocking antibody or isotype control antibody

was co-administered with HD gp96. The increase in Treg percentages in draining lymph nodes achieved with HD gp96 was absent when Nrp1 antibody was co-administered (Figure 23B). The total percentage of CD4 T cells however did not change (Figure 23C). This seems to be a local effect in the draining lymph node, since no change in Treg or CD4⁺ T cells was observed in the spleen with any treatment (Figure 23D,E). This is in agreement with previous findings in which gp96 is passively drained to the lymph nodes where T cell responses to gp96-bound peptides are likely generated (61). OVA-specific CTLs in the draining lymph nodes of immunized animals were measured to determine whether HD gp96 immunization can prevent CTL activation. We observed only a slight increase in tetramer-positive CTLs with B16-OVA immunization, and this number did not decrease with HD gp96 administration (Figure 24A,B), suggesting that the rise in Treg does not effect antigen-specific CTL generation in our system. It is possible that, although there is no difference in the number of tetramer positive CTLs that are induced, that these CTLs are less active compared to those induced in the absence of HD gp96 immunization. The ability of these CTLs to lyse OVA⁺ tumor cells should be assessed in the future to test this possibility. Together these data identify pDCs as a key APC controlling HD gp96-mediated suppression of protective immunity and that Nrp1 is instrumental in these observations, via increased methylation and expression. Further experimentation is needed in order to understand the outcome of Nrp1-Nrp1 ligation in terms of its effects on Treg, including survival and expression of suppressive mediators such as IL-10.

immunity has recently begun to emerge. In our study, we assessed methylome changes in CD91⁺ cells isolated from immunized mice. Although the vast majority of CD91⁺ cells are DCs and macrophages, this does not represent a pure population of target cells and must be taken into account in interpreting the results of our methyl-seq dataset. However, our present study was focused on Nrp1, and we have identified the specific DC subset involved and have validated these data using bisulfite sequencing and flow cytometry in these DCs. Additional target genes identified in our screen and expressed in these particular subsets or others will need to be further investigated for their possible contributions in modulating the magnitude and nature of gp96-mediated immune responses, keeping in mind that DC-Treg interactions are mediated by a myriad of adhesion molecules. Once we identify the full complement of adhesion molecules, we can address the issue of Nrp1 sufficiency in the pDC-Treg interaction.

4.3.1 Activation of DNMTs, transient methylation, and non-promoter methylation

We have focused on DNA methylation here because of its emerging role in immune regulation. It has recently been shown that NF- κ B can directly associate with DNMT1 in tumor cells, effectively guiding DNMT1 to certain target genes (121). The role of NF- κ B signaling in response to immunogenic HSPs has been well documented by our lab and others, and is a known potentiator of gp96 responses in both cDCs and pDCs (1, 62, 70). It is possible that NF- κ B signaling downstream of CD91 is the catalyst for the methylome remodeling that we have observed. Although DNMT1 is primarily responsible for maintenance methylation, it can also cooperate with DNMT3 to initiate *de novo* methylation (151). In peritoneal macrophages, we observed both DNMT1 and DNMT3b punctae in response to gp96 stimulation, suggesting that both may be specifically recruited to chromatin. The accessibility of DNMT target sites to the enzyme provides

physical constraints on whether genes and/or regulatory elements are methylated and therefore can determine changes in expression. We observed that a regulatory element within *Nrp1* is in a closed chromatin formation (thus inaccessible) in naive cDCs but open in naive pDCs (Figure 19). This offers an explanation for the observed methylation patterns when stimulated with gp96, despite the similar activation patterns of DNMT1 in both cell types. Other epigenetic machinery which may be activated in response to gp96 including histone modifying microRNAs and enzymes are currently being examined in our model systems.

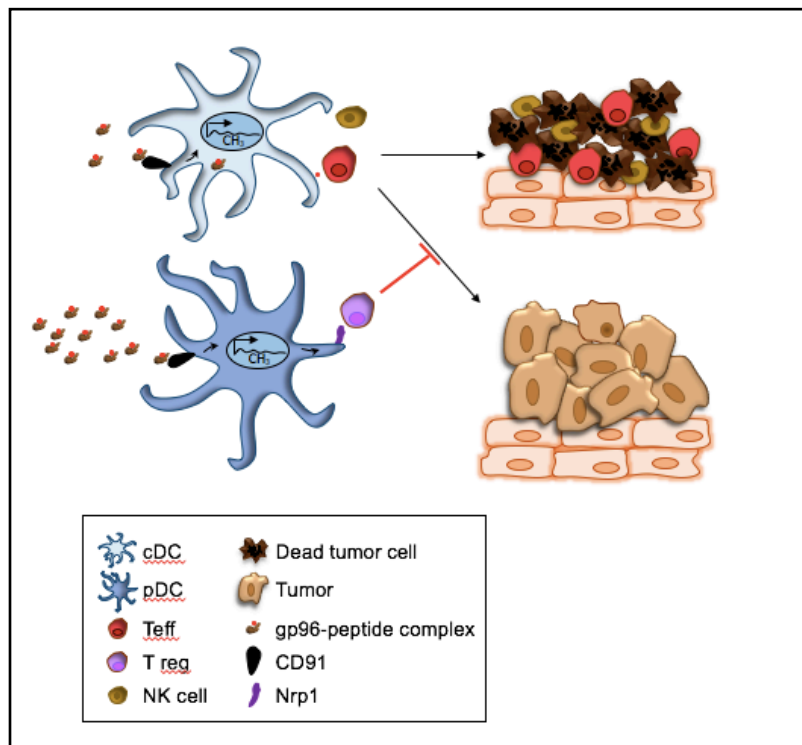


Figure 25. Chapter 2 summary.

At low doses, gp96 engages cDCs. Following epigenetic changes and cross-presentation of chaperoned peptides, cDCs elicits Th1 anti-tumor immunity, characterized by enhanced CTL and NK cell function. At high doses gp96 engages a significantly greater percentage of pDCs. Following epigenetic remodeling, distinct from that in cDCs, pDCs stabilize interactions with Tregs via Nrp1 that suppresses ongoing Th1 responses in tumors.

4.3.2 Methylation of cell-cell adhesion genes: lessons from neurobiology

The majority of the DMRs that we detected in this study are associated with genes involved in cell-cell contact and adhesion. Interestingly, DNA methylation is known to play a critical role in mediating cell-cell contact and synapse formation within the nervous system (201, 202). Transient DNA methylation in postmitotic neurons is catalyzed by both DNMT1 and DNMT3a (203, 204). There have been several reports that neuronal activity leads to modification of histones and the DNA methylome in adult brains (201, 202). Gene ontology (GO) analysis of differentially methylated genes showed enrichment of genes associated with synaptic function in mouse hippocampi treated by electroconvulsive stimulation. Yet little is known about how DNA methylation regulates contact between immune cell populations.

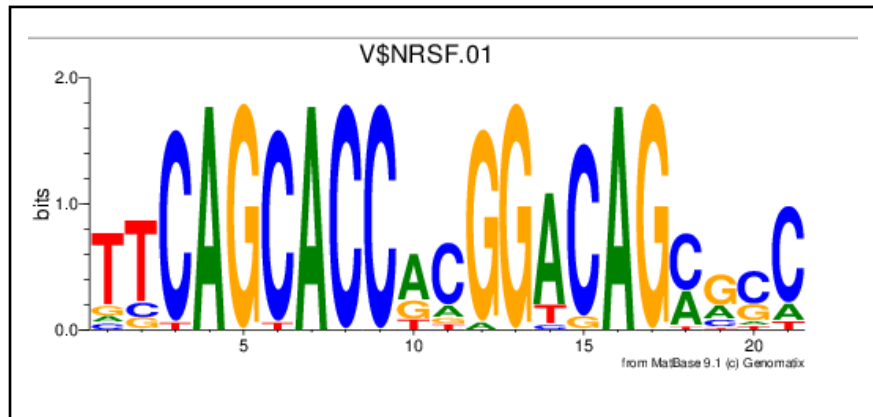


Figure 26. Potential NRSF binding motif identified in *Nrp1* locus by MatInspector/Genomatix.

Intragenic methylation of *Nrp1* has been observed in human monocytes, but the consequences of this alteration on protein expression and function were not evaluated (205). Contrary to promoter methylation, which is typically associated with decreased gene expression, methylation within the gene coding sequence (intragenic) is often a mark of active expression consistent with our observations for *Nrp1* in pDCs stimulated with gp96 (198). We performed

transcription factor binding analysis on the *Nrp1* DMR using Genomatix software and detected a possible binding site for NRSF/REST (Figure 26). This factor is a known repressor of *Nrp1* transcription in neurons and is highly expressed in non-neuronal cells including immune cells (206). It is possible that methylation at this site blocks the binding of the repressor and allows for increased *Nrp1* transcription, although this remains to be formally tested. It is interesting that the basal level of chromatin accessibility of *Nrp1* is different in naïve APC subsets. Whether gp96 treatment can alter accessibility at this region in pDCs and cDCs has not been tested, however we hypothesize that it would remain open in pDCs following binding of gp96 (particularly at HD), since transcription is increased in this situation. Gp96 treatment of cDCs would presumably have no effect on accessibility, as evidenced by the lack of *Nrp1* transcription in these cells.

In addition to *Nrp1*, other genes which regulate cell adhesion were differentially methylated in our dataset. Although *Nrp1* is most well-published in terms of APC-T cell interaction, it is entirely possible that other adhesion molecules are playing a role in the response to gp96. Several of the genes we identified are expressed by DCs and macrophages, including neuroligins, cadherins, and NCAM. Although the functional relevance of neuroligin on APCs is unknown, many molecules thought to be exclusively found on neurons have recently been appreciated in the context of immunity. For instance, targeting of neurokinin-1 receptor on DCs and Langherhans cells leads to increased cell survival, migration to lymph nodes, and IL-12 production (207-209). Cadherins can have diverse impacts on the activity of immune cells; for instance, homophilic E-cadherin interactions can result in prolonged APC-T cell engagement, whereas binding of E-cadherin on the APC to KLRG1 on T cells results in disruption of cellular interaction and release of anti-inflammatory cytokines by the APC (210). The significance of these additional adhesion molecules on the gp96 response is currently under investigation.

4.3.3 Regulation of pDC-Treg interaction

pDCs can elicit regulatory immune responses using a variety of mechanisms, including increased expression of IDO or upregulation of molecules associated with Treg stabilization and activation such as CTLA-4 and Nrp1 (195, 211). Nrp1 expression by immature DCs and pDCs facilitates long-term interaction with Treg via homotypic Nrp1-Nrp1 interaction (195, 196). The role of the Nrp1-Sema4a signaling axis in maintaining Treg populations via expression of Bcl-2 and other survival factors within the tumor microenvironment has been documented (197). Whether intercellular Nrp1-Nrp1 interactions trigger similar signaling in Treg is not known but is under active investigation. In agreement with previous reports, we did not observe any increase in maturation in gp96-stimulated pDCs (Figure 8B). These DC do, however, maintain moderate-high levels of MHC II expression, which is critical for effective Nrp1-Nrp1 interaction with CD4⁺ Treg. It is interesting that we observe Nrp1 dependence with HD gp96 immunization, given that pDCs are more likely to prime natural Treg (nTreg) in the lymph nodes of mice (212). In the context of solid organ transplant, this phenomenon is associated with increased graft survival due to Treg expansion. nTreg are distinguished from induced Treg (iTreg) in that they are educated in the thymus rather than at peripheral sites, show more stable expression of Foxp3 through complete demethylation of the Foxp3 promoter, and high expression of Nrp1 (213). Whether the preference of pDCs for nTreg is due to Nrp1 expression on both cell types was not tested. Additionally, it has been shown that immunization with a fragment of hsp70, called B29, results in increased expression of Nrp1 on Treg (214). Nrp1 expression is not upregulated on Treg following immunization with fully intact HSP in this study or ours. It is possible that administration of specific fragments of immunogenic HSPs can improve regulatory immunity by enhancing Nrp1 on both pDCs and Treg.

Although the circumstances in which antigen presentation occurs on pDCs is contested, it has been reported that the triggering of various endocytic receptors on pDCs results in the increased capacity of these cells to present antigen (215). Endocytosis of gp96-CD91 complexes on pDCs could allow for presentation of self antigen(s) chaperoned by gp96. We observed that HD gp96-mediated suppression is dependent on pDCs, since their depletion results in maintenance of CTL lysis of target cells (Figure 22). It is possible that higher doses of gp96 are required to diffuse to pDCs, which normally reside within the T cell zone or pDCs are less sensitive to gp96 and require a higher dose for activation. In addition to Treg activation, gp96 stimulated pDCs may also play a role in limiting cDC activation (1). Previous work from our lab has shown that, at least *in vitro*, gp96-stimulated pDCs abrogates the ability of cDCs to mediate pro-inflammatory responses. Considering that both DC types interact with gp96 after HD immunization, pDCs offer a two-pronged approach to inhibition of Th1 responses.

Our studies provide a better understanding of how dichotomous immune responses may be initiated and regulated based on the nature and dose of an administered immunogen. Following demonstrable efficacy in mouse models of cancer, LD gp96 is currently in clinical trials for the immunotherapy of cancer. HD gp96 therapy of autoimmune disease has only been documented in mice, but clinical trials are anticipated in the future. Although the specific amount of gp96 required for LD immunity in cancer trials has been calculated, it is unknown precisely how much gp96 is required to elicit the HD response in humans. Moreover, it is entirely possible that a successful dose in one patient will be unsuccessful in another, possibly due to the number of pDCs present in lymph nodes at the time of immunization and other immunosuppressive factors that are present within the tumor microenvironment. Although there are no known biomarkers to predict gp96 immunization success, results from this study suggest that a high number of Nrp1⁺ pDCs may be

detrimental for cancer immunotherapy, but beneficial in the context of autoimmunity. More studies are needed to test how we can increase pDC-mediated uptake of gp96 and how this may improve autoimmunity.

5.0 CHAPTER 3: STAT1 SIGNALING IN GP96-STIMULATED APCs

PREFACE

The data in this chapter has been generated for a manuscript co-authored with Abigail Sedlacek, a postdoctoral researcher in the lab. Some of the data presented has been generated by Dr. Sedlacek, and is included with her permission (indicated with ALS in the figure legend). Figures 34B and 36A,B are copyright (2016) Nature Publishing and is distributed under a Creative Commons CC-BY license (30). All other figures are unpublished work.

5.1 RATIONALE

In addition to acting as the endocytic receptor for HSP-peptide complexes, CD91 is also known to act as a signaling receptor. In response to all immunogenic HSPs that have been tested, it is known that: 1) the intracellular tail of CD91 contains two NPXY motifs that become phosphorylated upon ligand binding, 2) NF- κ B is activated and translocated to the nucleus, and 3) p38 MAPK is phosphorylated (62). NF- κ B is essential for the increased expression of maturation and costimulatory markers on the surface of APCs and is responsible for secretion of various cytokines. The role of p38 MAPK activation in gp96-treated APCs has not, to our knowledge, been fully tested. It can be inferred that MAPK may play a role in skewing of Th1 responses, as it is a known regulator of IL-12 production in APCs (216). As discussed in the Background section of this thesis, activation of p38 is associated with increased pSTAT1 levels, particularly on the serine site S727. It is therefore possible that HSP-CD91 binding can activate STAT1 through a p38-dependent

pathway (Figure 27). In addition to binding consensus sequences in target promoters, STAT1 can also enhance NF- κ B signaling under certain contexts (97). Many STAT1-regulated cytokines including those of the CXCL family can enhance NK cell activation and recruitment, and in some cases can enhance cross-talk between NK cells and APCs (217, 218). We and others have previously established a potential role for NK cells in the gp96-mediated response (30, 217-219). Whether CXCL chemokines direct this cross-talk event in the context of gp96 treatment remains unknown.

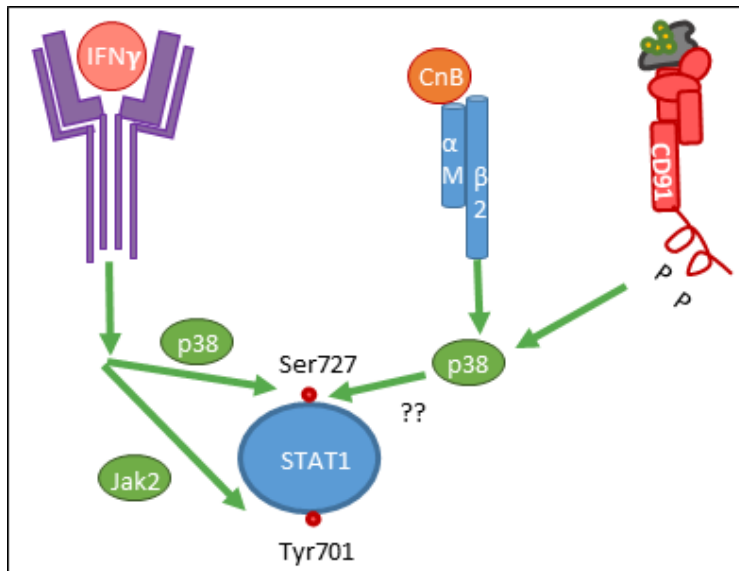


Figure 27. Activated p38 MAPK indirectly phosphorylates STAT1 at S727 site. p38 is known to direct STAT1 phosphorylation in response to IFN and integrin signaling. CD91 is known to activate p38 in response to HSPs. We propose that this event drives STAT1 signaling. IFN = interferon, Jak2 = Janus kinase 2, STAT1 = signal transducer and activator of transcription 1, CnB = calcineurin B subunit, α M β 2 = α M β 2 integrin.

NK cells play an important helper role in response to gp96 immunization, specifically in response to tumor-derived gp96 (30). Within this context, NK cells increase T cell-mediated lysis of tumor cells via IFN γ production. We also know that APCs are important facilitators of this activity and that they secrete cytokines known to enhance NK cell activation. Of the STAT1-

dependent cytokines that are released in response to gp96, we have become particularly interested in CXCL10 due to its involvement in NK cell activation (217). In this Chapter, I present data to show that STAT1 is phosphorylated at its S727 site in APCs treated with gp96. This event requires intact CD91 and p38 MAPK. Subsequently, STAT1 binds to a putative binding site on the *Cxcl10* promoter. This event may be methylation-dependent, but requires further experimentation. Lastly, we show that APC-NK cell cross-talk in response to gp96 occurs through a CXCR3 driven pathway. This work will provide additional prospective methods to strengthen HSP-mediated anti-tumor immunotherapy by targeting NK cells.

5.2 RESULTS

5.2.1 DNA methylation is enriched at transcription factor binding sites

Low dose			High dose		
Motif	TF	P-value	Motif	TF	P-value
	Tgif2	4.0e-260		MZF1	2.7e-029
	GATA1	1.3e-194		STAT1, NFATC2	5.0e-027
	Irf3	3.2e-176		ZEB1	2.3e-023
	Rxra	1.2e-061		Tcf7, Lef1	1.7e-020
	STAT1	3.5e-053		SPIB	2.9e-012
	NFATC2	2.0e-031		Rxra	8.9e-004
	GATA3	2.2e-003		Bcl6b	9.7e-003

Figure 28. DNA methylation is enriched at transcription factor binding sites.

Mice were treated as in Figure 14 and methylated DNA was sequenced. MEME-CHIP analysis of whole genome methyl-seq dataset is shown. The identified binding motifs and associated transcription factors are shown for the most significant motifs. Binding motifs containing methylated sequences in both low and high dose immunized mice are included. TF, transcription factor.

Methylated DNA from CD91⁺ cells isolated from LD or HD gp96 immunized mice was sequenced as described in Section 3.2.3 and Methods. This dataset was analyzed using MEME-CHIP software. MEME-CHIP performs comprehensive motif analysis to detect transcription factor binding sites (TFBS) in large sets of sequences. Using the parameters specified in Methods, we detected motifs associated with both LD and HD gp96 samples and have presented a select list including the detected motif, the predicted transcription factor, and p value (Figure 28). Predicted TFBS methylated only in LD included Tgif2 (repression of TGF- β target genes), GATA3 (Th2 responses), and Irf3 (IFN- γ response). Unique TFBS methylated in HD included Mzf1 (myeloid cell development), Zeb1 (inhibition of IL-2 expression), and Tcf7 (T cell survival). Intriguingly, STAT1, NFATC2 (T cell activation), and Rxra (retinoid receptor) binding sites were detected in both samples.

Whether methylation at binding sites contributes to actual binding of the transcription factor is controversial (220). If there is an effect at all, it is often thought that methylation at a binding site is detrimental to transcription factor binding by physically obscuring the site either through recruitment of MBD-containing factors or by the methyl group itself (221). This is highly dependent upon the local environment of the TFBS and may vary between transcription factors; in fact, methylation of TFBS can increase transcriptional activity of certain transcription factors (222). Given this, it is interesting that STAT1 was methylated in both LD and HD (Figure 28), since STAT1-dependent genes are upregulated following gp96 treatment. It is interesting to note that the STAT1 binding sites observed in LD vs HD are slightly different, and that the HD site may also be shared with NFATC2, a transcription factor which becomes activated after TCR stimulation.

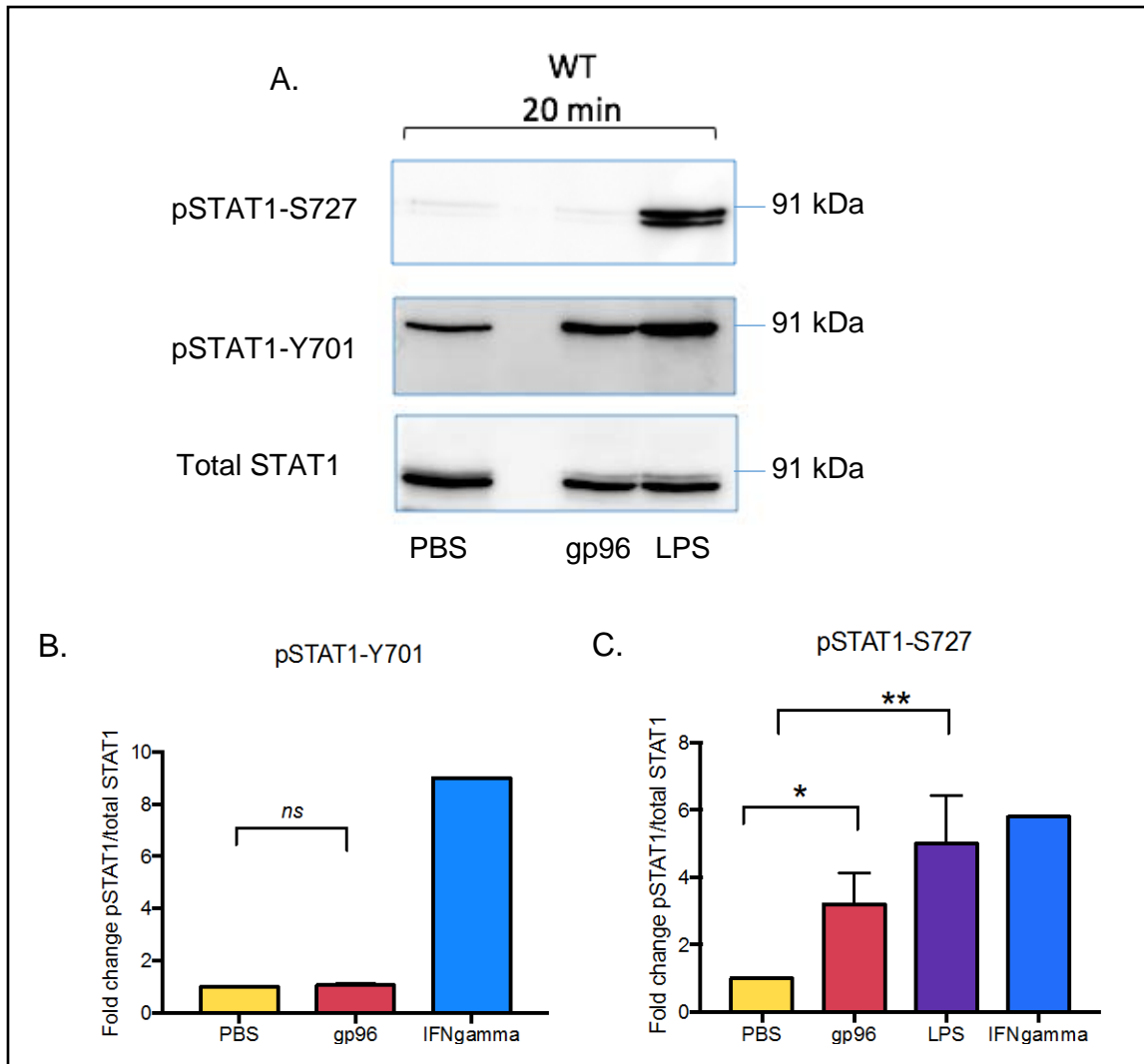


Figure 29. STAT1 is phosphorylated in response to 20 min gp96 stimulation.

A. Adherent PECs were treated with 200 μ g/ml gp96 for 20 min then lysed in NP-40 lysis buffer. IFN γ and LPS treated PECs were included as positive controls. Lysed cells were immunoblotted for pSTAT1-Y701, S727, or total STAT1. B-C. Densitometry analysis of PECs. Shown is the fold change in signal compared with PBS controls. pSTAT1 levels were normalized to total STAT1 in all experiments.

5.2.2 gp96 treatment preferentially targets pSTAT1-S727 in CD91⁺ APCs via a p38

MAPK-dependent pathway

To measure STAT1 activity, peritoneal macrophages (adherent PECs) were treated with gp96 for 20 min. The level of pSTAT1-Y701 and S727 was measured by western blot following treatment.

IFN γ and LPS treated cells were included as positive controls. IFN γ is known to induce both

pSTAT1-Y701 and S727, and indeed PECs showed increased signal for both motifs (Figure 29A,B,C). Gp96 stimulation had little effect on phosphorylation of Y701 at this time point (Figure 29A,B). However, densitometry analysis showed that the pSTAT1-S727 level in gp96-treated cells was ~3 fold higher than PBS treated cells as early as 20 min post treatment (Figure 29A,C). This increase was significant. In all samples, pSTAT1 signal was normalized to total STAT1. Total STAT1 levels did not change regardless of treatment. Treatment of PECs generated from CD91^{f/f}CD11c^{cre} mice with gp96 did not result in increased pSTAT1-S727 (Figure 30A,B), demonstrating the need for CD91. These cells were functional since STAT1 was phosphorylated upon treatment with LPS (Figure 30A,B). This shows not only that STAT1 phosphorylation in response to gp96 is CD91-dependent, but also rules out any contribution from potential LPS contamination in our gp96 preparations.

Given that STAT1 is an important mediator of IFN and other cytokine responses, it is possible that the STAT1 activation we have observed is simply an artifact of cytokines present in culture, including IL-6 and IL-1 β . To rule this out, WT PECs were treated with gp96 for 2 hr. Supernatants were then harvested from these cells and transferred onto CD91-deficient PECs. CD91-deficient PECs were cultured in these supernatants for 20 min then harvested for western blot analysis. If PECs make any factors that work in an autocrine pathway to enhance STAT1 activation, pSTAT1 should be detected in CD91-deficient PECs. However, pSTAT1 was not detectable (Figure 30C,D,E), therefore pSTAT1-S727 is directly due to gp96 stimulation and not due to cytokines or other stimuli that may be present in the culture.

In addition to RAW264.7 cells, PECs also phosphorylate p38 MAPK in response to gp96 after 20 min stimulation (Figure 31A). To test whether STAT1 phosphorylation was p38-dependent, PECs were pre-treated for 2 hrs with 10 μ M p38-specific inhibitor (SB203580), then

cultured with gp96 for 20 min. In the presence of this inhibitor, pSTAT1-S727 was no longer observed (Figure 31B). Taken together, these results suggest that the S727 residue is preferentially targeted downstream of CD91-gp96 interaction via a p38 MAPK-dependent pathway.

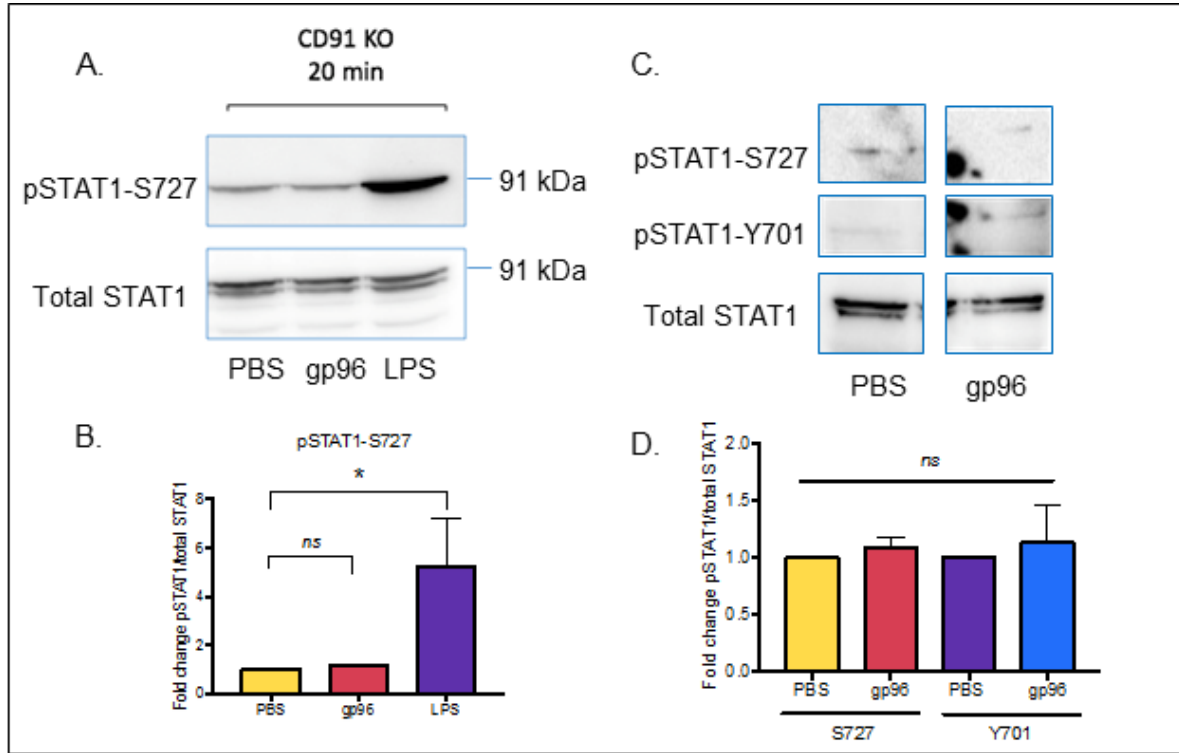


Figure 30. STAT1 phosphorylation is CD91 dependent and is not due to soluble factors produced by PECs.

A. Adherent CD91-deficient PECs were treated with 200 μ g/ml gp96 for 20 min then lysed in NP-40 lysis buffer. LPS treated PECs were included as positive controls. Lysed cells were immunoblotted for pSTAT1-S727 or total STAT1. B. Densitometry analysis of PECs. Shown is the fold change in signal compared with PBS controls. pSTAT1 levels were normalized to total STAT1 in all experiments. C. Wildtype PECs were treated with 200 μ g/ml gp96 for 2 hr. Supernatants were then transferred to CD91-deficient PECs. The cells were cultured in these supernatants for 20 min then immunoblotted for the indicated proteins. D. Densitometry of PECs.

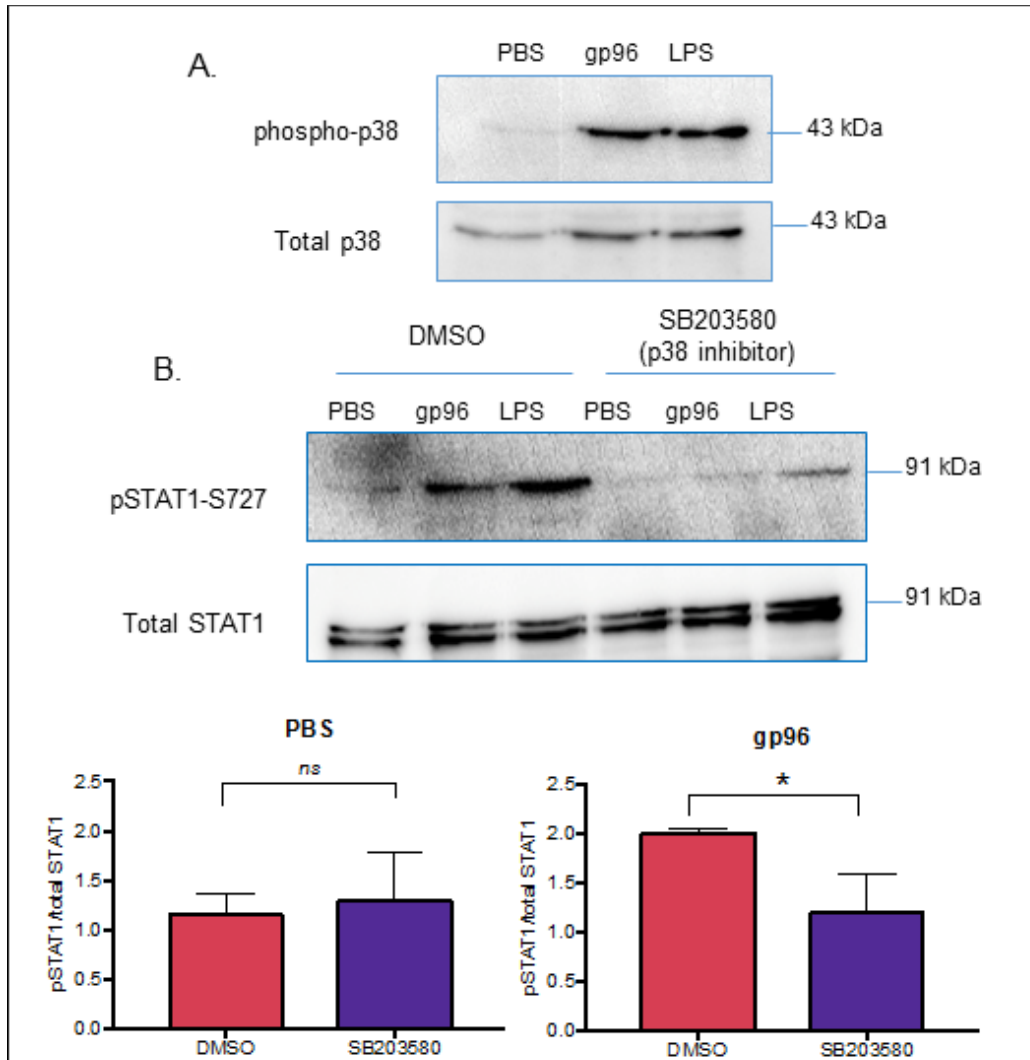


Figure 31. STAT1 phosphorylation is p38 MAPK-dependent.
 A. PECs were treated with 200 μ g/ml gp96 for 20 min, lysed, and immunoblotted for p38 MAPK.
 B. PECs were treated with 10 μ M SB203580 for 2 hr prior to gp96 treatment. Cells were then treated with 200 μ g/ml gp96 for 20 min, lysed, and immunoblotted for STAT1.

5.2.3 Gp96-stimulated APCs increase transcription and secretion of CXCL10 and promote STAT1 binding to the *Cxcl10* promoter

To confirm our previous findings that gp96-stimulated macrophages express CXCL10, peritoneal macrophages were isolated and treated with gp96 for 8 hrs. Cells and supernatants were harvested for qPCR and luminex, respectively. A dose-dependent increase in CXCL10 transcript was observed at this time point (Figure 32A). In agreement with this, secretion of CXCL10 was also increased in response to gp96 (Figure 32B)(30).

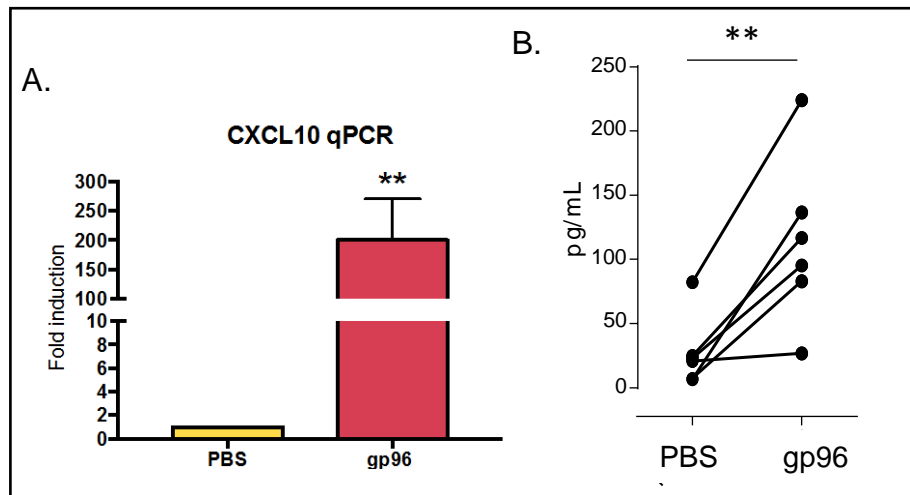


Figure 32. gp96 upregulates CXCL10 expression.

A-B. PECs were isolated from naïve mice and adherent cells were stimulated with indicated concentration of gp96 for 8 hr. Cell lysates and supernatants were harvested for qPCR (A) and luminex (B). Panel B in this Figure is from Sedlacek *et al.* (30), copyright (2016) Nature Publishing.

We next sought to understand how gp96 can regulate CXCL10 expression. STAT1 is known to bind the *Cxcl10* promoter to increase its expression. We identified a putative STAT1 binding site ~300 bp upstream of *Cxcl10* using the binding motif ATTTCCAG identified in Figure 28 by MEME-ChIP analysis (Figure 33A). PECs isolated from naïve or 5-azaC treated mice were pulsed with gp96 for 1 hr. DNA bound by STAT1 was isolated by ChIP. DNA was then amplified by conventional PCR and RT qPCR using primers against the putative binding site within the

Cxcl10 promoter (Figure 33B,C). STAT1 was enriched ~4-fold at this site following gp96 treatment compared with untreated cells (Figure 33C). PECs isolated from mice given 5-azaC exhibited less STAT1 binding regardless of gp96 treatment.

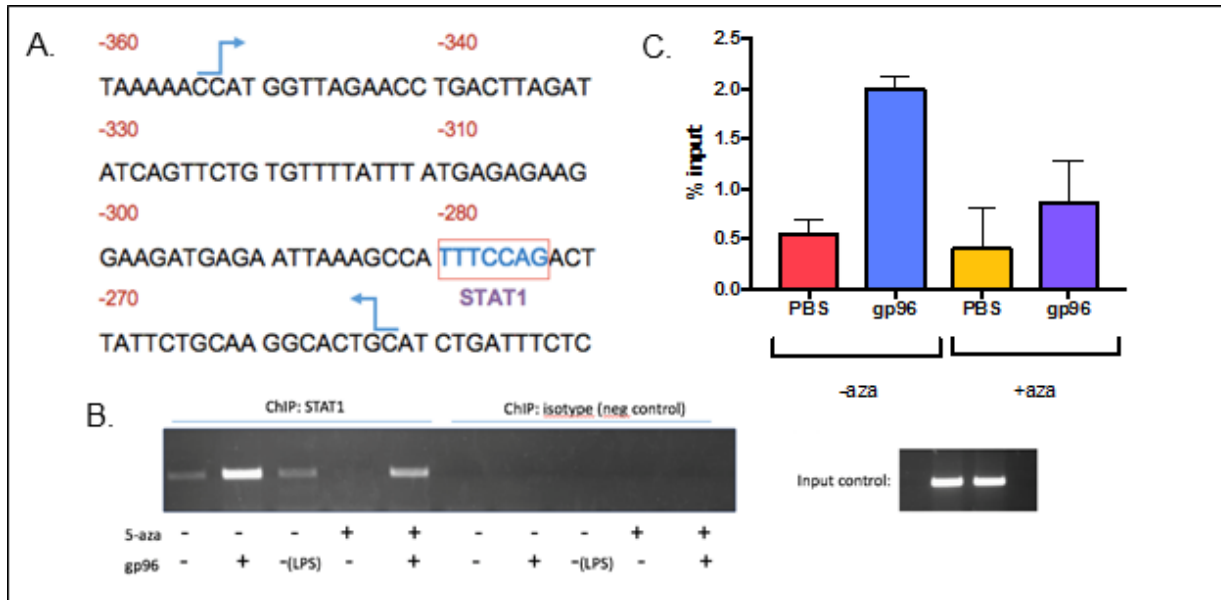


Figure 33. gp96 triggers STAT1 binding to the *Cxcl10* promoter.

A. Putative STAT1 binding site in *Cxcl10* promoter. Arrows indicate primer binding sites. B-C. PECs were harvested from naïve mice or mice treated with 5-aza for 48 hrs. Adherent cells were treated with gp96 for 1 hr then harvested and lysed. STAT1-bound DNA was isolated by ChIP. Isolated DNA was amplified by conventional PCR and run on an EtBr gel. (B) Isolated DNA was amplified by RT qPCR (C). % input was calculated (see Methods). Both methods were performed using the same primers.

5.2.4 NK cells require APCs and intact CXCR3 for maximal IFN γ production in response to gp96

CXCL10 is a known activator of NK cells and can promote their “helper” phenotype. Work from our lab has demonstrated that gp96 can enhance this NK cell helper role and is required for maximal activation of T cells (30). NK cells do not express CD91 and, when pulsed with gp96 *in vitro*, do not secrete IFN γ (Figure 34A)(30). Thus, NK cells are not directly activated by gp96. When these cells are co-cultured with gp96-activated PECs, however, IFN γ secretion increases significantly (Figure 34B). To determine whether CXCL10 plays a role in APC-NK cell cross-talk,

blocking antibodies to the CXCL10 receptor CXCR3 were added to wells in addition to NK cells. As shown in Figure 34C, gp96-dependent IFN γ secretion was diminished in the presence of CXCR3 antibody. This work demonstrates that a cross-talk mechanism exists between these two cell types to direct gp96-mediated immunity.

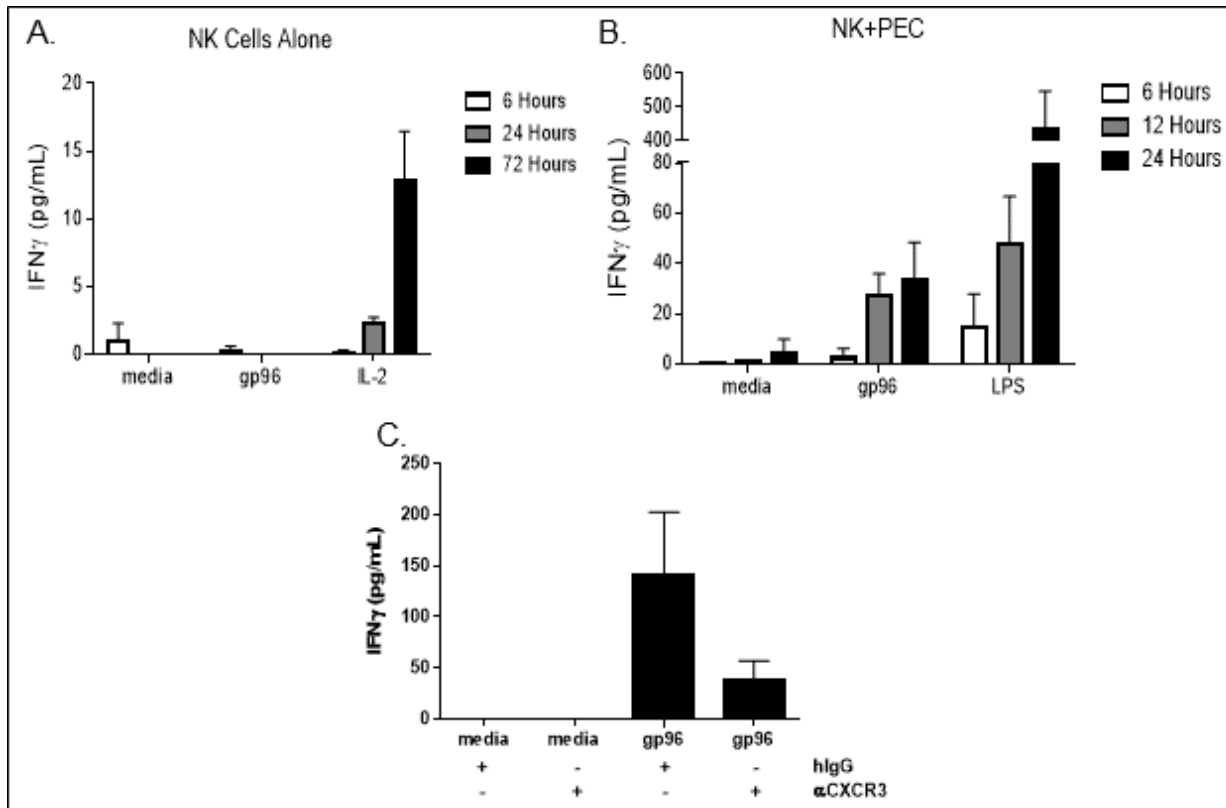


Figure 34. APC-NK cell cross-talk occurs in response to gp96 and is CXCR3-dependent.

All data in this figure generated by ALS. Panels A and B are from Sedlacek *et al* (30), copyright (2016) Nature Publishing. NK cells were isolated by negative selection and incubated with 200 μ g/ml gp96 (A) alone or (B) with adherent PECs for the indicated times. IFN γ was detected in the supernatants by ELISA to measure NK cell activation. C. NK cells were incubated with 200 μ g/ml gp96 with adherent PECs in the presence or absence of CXCR3 neutralizing antibody. IFN γ was measured by ELISA.

5.3 DISCUSSION

We have demonstrated for the first time a functional link between p38 MAPK activation by gp96 and anti-tumor immunity. In response to gp96, STAT1 is preferentially phosphorylated on S727

via a p38 MAPK pathway, distinct from IFN γ signaling. This activation is sufficient to initiate binding to the *Cxcl10* promoter and enhance expression. Our preliminary data suggests that CXCL10 is critical for APC-NK cell cross-talk and may play a role in promoting the NK cell helper role that is established by gp96 immunization.

5.3.1 Methylation of transcription factor binding sites

Classically, DNA methylation has been classified as a repressor mark. More recent data has suggested its role may be more complex than previously assumed. Using a systematic approach to look globally at transcription factor binding, Hu *et al.* performed protein microarrays to assess binding of 1300 transcription factors to methylated sequences. A group of transcription factors were unaffected by methylation of their binding sites. Methylation of the Kruppel-like factor-4 (KLF4) TFBS did not change KLF4 binding affinity, but did result in enhanced transcription of KLF4 target genes (222). It is possible that recruitment of co-factors and methyl-binding proteins alters the local environment and impacts gene expression.

We have observed that treatment of mice with 5-azaC results in an inability of macrophages to initiate binding of STAT1 to the *Cxcl10* promoter. However, our preliminary results also indicate that STAT1 activation is compromised in these cells (Figure 35). Reduced pSTAT1-Y701 was observed in PECs generated from 5-azaC treated mice (Figure 34A,B). Interestingly, whereas the α -isoform of pSTAT1-S727 is targeted in PECs from naïve mice, the β -isoform is phosphorylated in 5-azaC PECs. It is clear that 5-azaC treatment alters STAT1 signaling activity. How this may affect STAT1 binding to *Cxcl10* is unknown at this time, but we cannot rule out this as a possibility. 5-azaC treatment can have off-target effects such as cholesterol metabolism interference and aberrant enzyme activity (223, 224). There are several other DNMT inhibitors that are available

and potentially less detrimental to normal cell function, including zebularine and SGI-1027; however, these inhibitors may not be as effective as 5-azaC (225). In the future, we aim to use DNMT-deficient cells to specifically interrogate the effects of methylation on STAT1 binding.

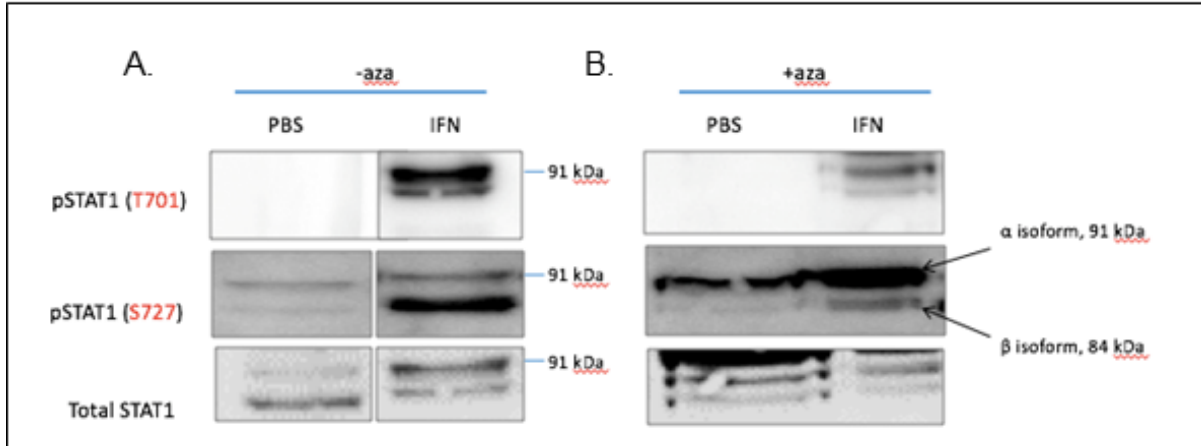


Figure 35. 5-aza treatment alters STAT1 activity.

A-B. Mice were treated with 5 mg/kg 5-aza and PECs were isolated 48 hr later. Adherent cells were treated with 200 μ g/ml gp96 for 20 min. Cell lysates were immunoblotted for STAT1 phosphorylation in PECs from naïve mice (A) or 5-aza treated mice (B).

5.3.2 Activation of STAT1 and its specific gene signatures

Consistent with what has been shown in other systems (97), we have observed p38-dependent phosphorylation of STAT1 in response to gp96. Others have used *in vitro* assays to test whether active ERK1, JNK1, p38 MAPK, MEK1, and MSK1 can result in STAT1 phosphorylation (226). JNK and p38 were both identified as indirect activators of STAT, although its direct activator was not identified.

The mechanisms governing STAT1 activation have largely been studied in the context of IFN responses. It has become clear that IFN-independent STAT1 activation may act differently in terms of how STAT1 is phosphorylated and which genes are targeted. S727 phosphorylation in response to microbial products, viral challenge, and IL-1 β treatment is sufficient for STAT1 nuclear translocation and target gene expression (93, 97, 227). The rapidity with which we observe

pSTAT1-S727 following gp96 treatment and its dependence on CD91 suggests that gp96 directly enhances STAT1 phosphorylation. It is possible that Y701 is phosphorylated at a later time point, either due to gp96 itself or indirectly through production of other cytokines (including IL-1 β and IL-6) known to activate pSTAT1-Y701. If this is indeed the case, then CD91 may utilize a STAT1 activation mechanism similar to TLRs (97). Regardless of the pathway being utilized, it is clear that stimulation with gp96 results in STAT1 binding to the *Cxcl10* promoter in macrophages. Further experimentation is required to understand the dynamics of pSTAT1 at both the S727 and Y701 sites.

The role of pSTAT-S727 in the absence of Y701 phosphorylation has been reported using several systems. Varinou *et al.* designed gene-targeted mutant mice which express an unphosphorylatable STAT1 S727 site (serine to alanine mutation)(228). These mice were less likely to succumb to septic shock induced by LPS treatment. While STAT1 binding to target genes was unaffected in these mice, recruitment of cofactors including histone acetyltransferases was diminished. Studies using macrophages have shown that stimulation of various TLRs results in rapid induction of pSTAT1-S727, and that pSTAT1-Y701 does not appear until later time points (60-180 min post-treatment). However, pSTAT1-S727 was sufficient for STAT1 translocation to the nucleus. Similarly, stimulation of pancreatic β cells with IL-1 β results in pSTAT1-S727 and binding of STAT1 to the promoters of *Cxcl1* and *Cxcl2* (227). It has been established that activation of STAT1 through this non-canonical pathway does not involve IFN. Finally, pSTAT1-S727 alone is required for expression of Fas/Fas ligand and certain caspases, suggesting that phosphorylation of S727 is sufficient for transcriptional activity of STAT1 (229, 230). It is also possible that pSTAT1-S727 can dimerize with other transcription factors in response to gp96, including STAT3 and IRF1.

In our system, it appears that PECs exhibit a low level of pSTAT1-S727 under basal conditions. Basal activity of STAT1 has been observed in a monocyte-like human cell line (231), RAW 264.7 macrophages (232), and mouse bone marrow-derived macrophages (233). Gp96 treatment elevates these levels similarly to LPS and IFN γ , albeit to a slightly lesser extent. The baseline STAT1 activity may contribute to the low levels of CXCL10 produced by untreated PECs in our study (Figure 29A, 32B). Because the *Cxcl10* promoter also contains an NF- κ B binding site, it is possible that there exists some cooperativity between transcription factors that are activated downstream of CD91. We are currently investigating how CXCL10 transcription can be altered by treatment of p38 inhibitor (SB203580), NF- κ B inhibitor (cardamonin), or a combination of the two. Our preliminary data also suggests that CXCL10 production by different APC types is not equal in response to gp96. More work is required to determine if this is due to a deficit in STAT1 signaling in different cell types. To this end, we are developing assays to further interrogate CD91 signaling on a molecular level using RAW264.7 macrophages that lack one or both of the NPXY signaling motifs on CD91. We are also investigating whether different cell types express increased basal levels of DUSP1, a phosphatase capable of targeting p38 MAPK.

5.3.3 APC-NK cell cross-talk and the role of NK cells in cancer

Although NK cells do not require antigen presentation by APCs to become activated, communication between these cells does exist, and under certain circumstances one cell type can enhance the activation of the other. Often this feedback primes NK cell helper phenotype; whereas NK cells are well known for their ability to kill tumor cells directly, various stimuli can result in a helper phenotype in which the NK cells produce factors to enhance maturation of APCs and tumoricidal activity of T cells. We have observed that NK cells co-cultured with APCs *in vitro* can

enhance APC maturation in response to gp96 (ALS, unpublished data). Treatment of NK cells with IL-18 can promote secretion of proinflammatory cytokines and chemokines which attract DCs and T cells to the tumor microenvironment (234). Fernandez *et al.* used a mouse tumor cell line (AK7) that expresses low to no MHC I and II, making it a strong target of NK cell lysis (235). Prior to AK7 tumor challenge, mice were treated with Flt3 ligand to expand DCs *in vivo*. Expansion of the DC population enhanced tumor killing compared with mice that were not given Flt3 ligand, demonstrating DC-NK cell cross-talk exists within a tumor setting. Co-culture studies with NK cells and DCs have shown that interaction between these cell types does occur and results in release of pro-inflammatory mediators IL-6, TNF, IL-8, GM-CSF, and IFN γ (236). Cell-cell contact is regulated through release of activin A, creating a negative feedback loop and terminating cytokine release. It is possible that, in our system, NK cell production of IFN γ may create a STAT1 feedback loop on the APCs, further driving CXCL10 secretion. We are currently testing whether this occurs.

Previous studies from our lab have shown that gp96-stimulated APCs enhance IFN γ production (28). We have expanded upon this and show here that CXCR3 is required for full activation of NK cells co-cultured with gp96-stimulated APCs. In addition to CXCL10, CXCR3 also binds CXCL9 and CXCL11. We have not ruled out the possibility that these other chemokines may be playing a role in activating NK cells in our model. We plan to follow up on these experiments using NK cells that are deficient in CXCR3 expression (CXCR3^{f/f}NK1.1^{cre}) and APCs that are deficient in CXCL10 expression (CXCL10^{f/f}CD11c^{cre}) to confirm our findings. Nevertheless, both CXCL9 and CXCL11 are STAT1 target genes, which still supports our hypothesis.

When present at elevated doses, CXCL10 activates naïve NK cells to become lytic and improve T cell proliferation (237). In this study, mice were challenged with either wildtype DA1-

3b tumor cells or DA1-3b that was engineered to overexpress CXCL10. Isolated CD8⁺ T cells and NK cells both exhibited greater lytic potential using an *in vitro* killing assay. The ability of T cells to lyse DA1-3b was significantly amplified when co-cultured with NK cells, suggesting that the CXCL10-conditioned NK cells facilitated T cell activation. Additionally, using labeled NK cells and tumor cells visualized by *in vivo* fluorescence imaging, Wennerberg *et al.* observed increased NK cell infiltration into tumors that express CXCL10 compared with tumors that did not express CXCL10 (238). It is possible that, in addition to skewing NK cell activation, CXCL10 production by gp96-stimulated APCs in the tumor microenvironment can lead to recruitment of NK cells.

It was shown several decades ago that prevention of tumor metastasis following gp96 immunization requires NK cells (32). Few studies have measured NK cell activity in humans treated with tumor-derived gp96, and the data that has been published has largely been correlative. One study found a higher frequency of NK cells in peripheral blood of patients treated with gp96 (34). Subsequent studies in mice suggest that co-administration of gp96 and IL-2 can significantly augment the NK cell population and prime them to become more protective in response to pathogen challenge (239). What has not been shown, however, is whether gp96 immunization can result in homing of NK cells to target tissues including tumor.

6.0 THESIS SUMMARY AND FUTURE DIRECTIONS

6.1 SUMMARY

Although HSPs are normally found within the cytosol and endoplasmic reticulum of their host cells, they may be released through cell death, expressed on the surface in response to cell stress, or introduced locally through vaccination. When this occurs, gp96 and other immunogenic HSPs may bind to APCs via their receptor CD91 to elicit specific immunity against the HSP-bound peptide. This phenomenon is precisely dose-dependent in that LD immunization results in Th1 and CTL-mediated responses, whereas higher doses are associated with Treg induction and immune suppression. The number of cells that are compromised and release HSP becomes important; small tumors prime anti-tumor immune responses whereas large tumors elicit immune hyporesponsiveness.

My data from Chapter 1 demonstrates that CD91-expressing APCs are required to elicit HD immunity. CD91 was found to be highly expressed by two major DC subsets: the CD11b⁺CD11c⁺ cDCs and CD11c^{low}B220⁺PDCA⁺ pDCs. Both subsets internalize gp96 at LD and HD; however, it seems that cDCs are saturated at HD and do not constitute a higher percentage of gp96⁺ cells as dose is increased. Yet following HD gp96 administration, there is a 5-fold increase in the percent of gp96⁺ pDCs in the draining lymph node, suggesting these cells are actively targeted at higher doses.

Chapter 2 establishes that DNMTs form punctae in the nuclei of various gp96-stimulated APCs. This change in DNMT architecture was correlated with genome-wide methylome

remodeling in CD91⁺ cells isolated from LD and HD gp96 immunized mice. The most robust differences in methylation were detected within gene families associated with cell-cell interaction/adhesion. Specifically, HD gp96 could induce increased expression and gene-body methylation of *Nrp1* in pDCs. Gp96-stimulated pDCs co-cultured with Treg established stable, *Nrp1*-dependent interactions. Intact pDCs and *Nrp1* was required to elicit HD immunity. Taken together, it is clear that gp96 may trigger unique genetic and epigenetic events depending on the type of APC. When gp96 favorably engages cDCs, such as during LD immunization, co-stimulatory molecule and cytokine secretion dictates the CTL response; following HD immunization, pDCs are preferentially bound and drive Treg responses via *Nrp1*.

Finally, Chapter 3 focuses on a newer area of research to establish a mechanism to explain the previously published phenomenon of APC-NK cell crosstalk in response to gp96. P38 MAPK is phosphorylated in gp96-treated PECs and this in turn activates pSTAT1-S727. STAT1 binds to a promoter sites upstream of *Cxcl10*, driving its expression. CXCL10 requires its receptor, CXCR3, to trigger NK cells. When CXCR3 is neutralized, APC-NK cell crosstalk is abolished and IFN γ production by NK cells is impaired. Future experimentation is required to fully understand this novel STAT1 pathway downstream of CD91. For example, time course experiments need to be performed in order to understand the dynamics of pSTAT1-S727 and whether pSTAT1-Y701 can be detected at later time points. We are also interested in how STAT1 activation can influence NK cell activation. Future experimentation will be performed using STAT1-deficient APCs co-cultured with NK cells.

6.2 FUTURE DIRECTIONS

6.2.1 Lymph node architecture and how gp96 engages pDCs versus cDCs

pDCs in the draining lymph node take up more gp96 at HD and drive the suppressive Treg response. What we have not shown is how this is possible. pDCs normally reside within the T cell zone of secondary lymphoid tissues including lymph nodes. Yet we have previously observed that gp96 is localized to the subcapsular sinus following immunization in the skin (61). We propose that, at HD, gp96 may either infiltrate deeper into the lymph node to reach pDCs, or pDCs migrate to the subcapsular sinus in response to factors produced by gp96⁺ macrophages and DCs. In response to viral infection, lymph node resident sinusoidal macrophages produce IFNs which drives relocalization of pDCs from the deep cortex to the subcapsular sinus and medulla (240). In the future, experiments will be performed using gp96_{A488} to visualize by microscopy whether higher doses can diffuse deeper within lymph nodes. pDC localization in response to immunization will also be observed.

6.2.2 Implications for clinical trials: Dosage and microneedle arrays

Given the data I have presented here, preventing gp96 uptake by pDCs in the context of cancer immunotherapy may improve the results of current clinical trials. Tip-loaded dissolvable microneedle arrays (TL-dMNAs) are a promising new technology that provide local delivery of therapeutics into the skin (241). The microneedles on TL-dMNAs can be loaded with precise amounts of therapeutic. When injected into skin, the microneedles are embedded and quickly dissolved within the dermis, allowing for local uptake of their contents. In collaboration with Louis

Falo, we will test whether gp96 injected with TL-dMNAs results in uptake by skin DC and preclusion of drainage into lymph nodes. We are currently testing if pDCs can take up TL-dMNA administered gp96 and whether this is a viable anti-cancer therapeutic *in vivo*. Our preliminary flow cytometry data suggests that HD gp96_{A488} is not taken up by pDCs if injected using these methods. If enhanced tumor protection is observed, TL-dMNAs may provide an exciting new route for clinical trials by circumventing uptake by suppressive DCs.

Additionally, we propose that HD gp96 can be used as a clinical therapy in autoimmunity and solid organ transplantation. To date, HD gp96 efficacy has not been measured in humans outside of *in vitro* studies. Increased soluble and cell-surface gp96 has been detected in the inflamed joints of RA patients (115-117). This is a macrophage-rich microenvironment, and uptake by these macrophages enhances inflammation (117). pDCs are also involved in the pathology of RA and other autoimmune diseases by producing large amounts of type I IFNs and exacerbating disease (242, 243). I have presented data in this thesis to suggest that gp96 can promote a suppressive phenotype in pDCs. We have not yet tested whether gp96 treatment is sufficient to switch the phenotype of IFN-producing pDCs in autoimmune patients. More experimentation is needed to understand the effect of gp96 on pDCs, and how gp96 uptake can be enhanced to treat autoimmune diseases such as RA.

6.2.3 CD91 in cholesterol storage and metabolism

Many questions remain open regarding CD91 signaling in the immune system. As it is part of the LDL receptor family, CD91 is closely tied to cell metabolism. Uptake, processing, and accumulation of cholesterol is controlled by CD91 in multiple cell types including vascular smooth

muscle cells and macrophages (76, 244). Canonical Wnt5a and p-GSK3 β pathways are activated downstream of CD91 and play a pivotal role in cholesterol storage (77). In this study, impairment of CD91 led to enhanced cholesterol storage and fatty acid synthesis via Wnt and GSK3 β , respectively. We have found that pDCs isolated from CD91^{f/f}CD11c^{cre} mice exhibit a defect in baseline p-GSK3 β levels compared with wildtype (Figure 36). It may be that metabolism in these cells is dysfunctional, although this remains to be formally tested.

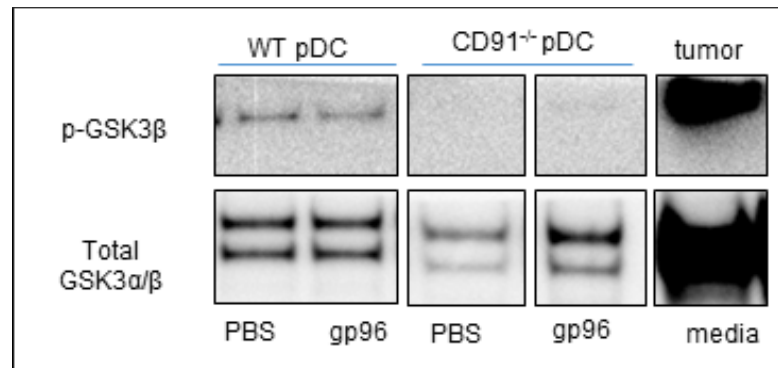


Figure 36. CD91-deficient pDCs have less p-GSK3 β at baseline compared with wildtype. pDCs were treated with 200 ug/ml gp96. After 15 min, cell lysates were harvested for western blot analysis and probed with the indicated antibodies.

We have interrogated CD91 expression on multiple APC types, with the data presented in this thesis and elsewhere. Expression and function of CD91 on non-APC immune cells such as T cells has not been extensively reported. Research into the metabolism of naïve, effector, and memory T cells has exploded in recent years. It is now apparent that naïve and memory T cells rely on fatty acid metabolism, whereas activated effector T cells require glycolysis to support the massive expansion during the effector phase of the immune response (245). CD4⁺ T cells can be differentially identified by flow cytometry using the following markers: CD44⁻CD62L^{+/-}CD25⁻ (naïve), CD44⁺CD62L⁻CD25⁺ (effector), CD44⁺CD62L⁻CD25⁻ (effector memory), and CD44⁺CD62L⁺CD25⁻ (central memory). Interestingly, our preliminary data shows transient, high CD91 expression exclusively on CD44⁺CD62L⁺CD25⁻ central memory T cells from mice

immunized with irradiated SVB6 tumor cells (Figure 37). Effector and effector memory T cells showed some intermediate expression compared with secondary only controls. Whether CD91 expression plays any role in fatty acid metabolism in these cells is an area of active interest in our lab.

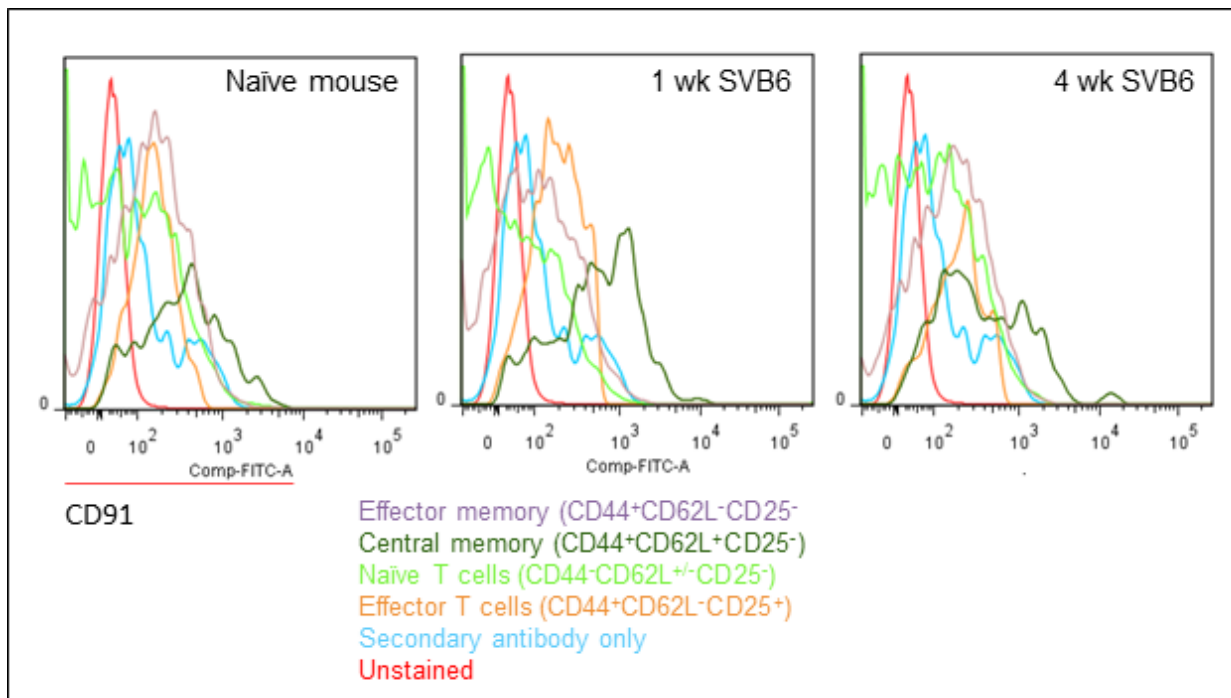


Figure 37. Central memory CD4⁺ T cells express CD91 following immunization.

Mice were immunized i.d. with irradiated SVB6 tumor cells. Draining lymph nodes were harvested 1 or 4 wk later and analyzed by flow cytometry. Cells were gated using the indicated markers and plotted for CD91 expression.

7.0 MATERIALS AND METHODS

7.1.1 WT mice

Female C57BL/6 mice were obtained from Jackson Laboratories (Bar Harbor, ME) and housed in DLAR at the University of Pittsburgh. All mice were 6-8 weeks old and all experimental procedures were approved by the Institutional Animal Care and Use Committee and performed in compliance with its guidelines.

7.1.2 Generation of CD91^{fl/fl}CD11c^{cre} mice

CD91^{fl/+} mice were purchased from Jackson Laboratory (Bar Harbor, ME) and mated to homozygosity (CD91^{fl/fl}). CD91^{fl/fl} mice were crossed with CD11c^{cre} to generate mice that were selectively deficient of CD91 on CD11c-expressing cells. These mice were previously characterized and have normal numbers of APCs and lymphocytes (26).

7.1.3 Cell lines

D122 and B16.F10 cells were cultured in DMEM containing 1% sodium pyruvate, 1% L-glutamine, 1% nonessential amino acids, 1% penicillin and streptomycin, 0.1% 2-mercaptoethanol, and 10% fetal bovine serum (FBS) (GIBCO). B16-OVA cells were cultured in complete DMEM supplemented with 5 mg/ml G418. Adherent cells were harvested using trypsin.

The mAb927 hybridoma was cultured in complete RPMI containing 10% FBS (GIBCO). Cells were serum starved for 3 days, supernatants were harvested, dialyzed, and run through a Melon Gel column (Thermo Fisher) for purification of the α -PDCA antibody. Antibody preparations were analyzed by SDS-PAGE.

7.1.4 Isolation of primary spleen cDCs, pDCs, NK cells, and T cells

All *ex vivo* isolated cells were cultured in RPMI containing 1% sodium pyruvate, 1% L-glutamine, 1% nonessential amino acids, 1% penicillin and streptomycin, 0.1% 2-mercaptoethanol, and 5% FBS (GIBCO). pDCs were isolated from mouse spleens using anti-PDCA1 microbeads according to the manufacturer's protocol (Miltenyi Biotec) and cultured in complete RPMI. For all pDC stimulation assays *ex vivo*, 5×10^5 cells were plated in round bottom plates with 10 μ g/ml or 200 μ g/ml gp96, or equivalent volume of PBS. For 5-azaC treated pDC generation, mice were administered 5 mg/kg 5-azaC in a total volume of 200 μ l i.p., and pDCs were isolated by magnetic-activated cell sorting (MACS) after 72 hr. NK cells were isolated using MACS kits with untouched protocols by negative selection using the NK cell isolation kit II. Isolation of Treg and Tconv were performed using the CD4⁺CD25⁺ regulatory T cell isolation kit. All non-T cells are first depleted from bulk splenocytes. T cells were separated from Treg using CD25 selection; the CD25⁺ population was used for Treg, the CD25⁻ population was used for Tconv. Isolations typically yielded at least 80% purity for all kits.

7.1.5 Generation of primary murine BMDCs and PECs

BMDCs; bone marrow cells were isolated from the femurs of female C57BL/6 and cultured in complete RPMI (10% FBS). Cells were cultured in RPMI supplemented with GM-CSF (Fisher Scientific). Media was supplemented after 3 days of culture and loosely adherent cells were harvested 6-7 days following initial plating. These cells were used as representative cDC populations for indicated *in vitro* experiments. BMDCs were plated at 5×10^5 cells/well with 200 $\mu\text{g/ml}$ gp96. PECs were isolated by peritoneal lavage of naïve or 5-azaC-treated mice with sterile PBS. Cells were plated for at least 6 hr, and non-adherent cells were removed.

7.1.6 Purification of HSPs

Purification of HSPs. In all experiments, gp96 was purified from mouse livers. Mouse livers were harvested and homogenized with a blender to a single cell suspension. Protein was stepwise precipitated out of an ultracentrifugation (100,000g) supernatant to 80% saturation stepwise. Protein was passed over immobilized Concanavalin A columns. Bound fraction was eluted with 10% mannose and buffer-exchanged with PD10 columns into 0.005M sodium phosphate solution containing 0.3M NaCl. This was applied to equilibrated DEAE columns. Bound fraction was eluted with 0.7M NaCl. Fraction 3-5 contained gp96 as assessed by SDS-PAGE and immunoblotting. We fully characterized all gp96 preparations; purity of gp96 preparations was assessed by SDS-PAGE gp96 and was determined to be a homogenous 96kDa protein (Figure 4A). The protein was recognized by a monoclonal gp96 antibody (clone 9G10, Enzo Life Sciences)(Figure 4B). Further, gp96 retained its enzymatic ATPase activity (Figure 4C). ATP hydrolysis was measured using the ATPase/GTPase Activity Assay kit (Sigma). Gp96 (10

mg/well) was incubated for indicated period of time with ATP at 37°C in a 96-well plate. Malachite green was added and absorbance was read at 600 nm. ATP hydrolysis was calculated using a standard curve. Gp96 was determined to be free from endotoxin contamination by LAL assay and western blot. Gp96 concentrations were determined by the Bradford assay. Preparations of gp96 were labeled with Alexafluor 488 (Invitrogen, Grand Island, NY) as recommended to obtain gp96_{A488}. Each molecule of gp96 was calculated to be labeled with four to nine molecules of A488. Protein was analyzed with standard SDS-PAGE and immunoblotting with anti-gp96 (Enzo Life Sciences Farmingdale, NY) and anti-A488 (Invitrogen, Grand Island, NY). All gp96 immunizations were delivered i.d. in a final volume of 100 µl PBS (LD = 1 µg; HD = 10 µg). For better resolution of gp96 *in vivo*, all gp96_{A488} immunizations were delivered s.c. in a final volume of 100 µl PBS (LD = 10 µg; HD = 100 µg). For all *in vitro* assays using cDCs or pDCs, cells were cultured with gp96 at the indicated concentration or an equivalent volume of PBS.

7.1.7 *In vivo* tumor growth assay

For active immunization, tumor cells were irradiated (6000 rad) and 1×10^6 cells were injected s.c. as indicated. One week later, mice were injected with PBS, LD gp96 (1 µg), HD gp96 (10 µg), or MSA. One week following treatment, mice were subsequently challenged i.d. with 5×10^4 tumor cells and monitored for tumor growth by measurement on two axes. For IL-12 experiments, mice were injected i.p. with 0.25 µg recombinant IL-12 on the same day as gp96 treatment and every day for 3 days following. Seven days after gp96 injection, mice were challenged with 5×10^4 tumor cells. IL-12 treatment was based on previously published experiments using similar systems (246). For all experiments, mice were sacrificed when tumors were 1.5 cm in any one diameter according to IACUC approved protocols. Group size was determined by power analyses in each experiment.

7.1.8 MBD methyl-sequencing and analysis

Mice were immunized i.d. with LD or HD gp96 or with PBS and sacrificed after 18 hr. Draining lymph nodes were harvested and CD91⁺ cells were isolated by FACS using a FACSAria instrument (BD Biosciences). DNA was purified, sonicated to an average size of 300 bp using a Bioruptor (Diagenode), and enriched for methylated sequences using MBD purification using the MethylMiner Enrichment Kit (Invitrogen). Precipitated DNA was analyzed for quality assurance prior to sequencing. Methylated fragments were sequenced using an Ion TorrentN sequencer (Life Technologies) at the Genomics and Proteomics Core (University of Pittsburgh, PA). The samples were sequenced to an average of 45 million reads. Raw sequencing reads (fastq format) were mapped to the mouse genome (mm9) using Bowtie 2, which can account for large gaps in sequencing reads. Only non-redundant and uniquely mapped reads were used for subsequent analysis. Methyl peaks were assigned using Model-based Analysis for ChIP-Seq software (247) with PBS treated mice used as a reference sample. Peaks were merged based on overlapping and book-end peaks, and coverage was calculated using BEDtools merge version 2.17.0. Peaks were annotated with the annotation provided by UCSC using a custom Perl wrapper and Tabix (248). Peaks within 2000 bp of a coding sequence were reported with annotation. Comparison of peaks and identification of DMRs was performed similar to previously reported studies by the University of Pittsburgh Bioinformatics Core using GEDA (Genome Expression Data Analyzer) software and Efficiency Analysis (249-251). DMRs were visualized using the UCSC Genome Browser and Genomatix software. Global distribution of intragenic DMRs (exon, intron, promoter) was performed using Genomatix Genome Analyzer (Genomatix Software GmbH). Distribution across TSS and CpG islands was determined using SeqMonk (Babraham Bioinformatics). Transcription factor binding analysis was performed using Genomatix software. Genetrail (252) was used to test

for gene ontology analysis using default parameters and Ensembl genes as background for enrichment. Results were corrected for multiple testing using Bonferroni adjustment.

7.1.9 Bisulfite sequencing

Mice were immunized as described for MBD methyl-seq experiments and CD91⁺ cells were isolated by FACS. For pDC experiments *in vitro*, splenic pDCs were isolated and pulsed with 200µg/ml gp96. Cells were harvested after 6 hr in Puregene cell lysis buffer (Qiagen) prior to DNA extraction. Genomic DNA was bisulfite converted with the EZ Lightning DNA Conversion Kit according to the manufacturer's protocol (Zymo Research). Methylated and unmethylated DNA controls were spiked into each sample to control for completeness of the bisulfite conversion. Bisulfite-converted DNA was amplified by PCR (F primer: TTGTATTGAGGTATATAAAGTTGGTA, R primer: AATTCAAAAACACAAATTTCTCTCC) and the amplicons were cloned using TOPO TA vectors (Invitrogen). Primers were designed using MethPrimer software (253). Colonies were isolated and minipreps were performed to isolate DNA. The DNA was then sequenced for Nrp1. Both CpG and non-CpG were considered in analyses.

7.1.10 Chromatin accessibility assay

Naive pDCs and total CD11c⁺ DCs were isolated from C57BL/6 spleens using anti-PDCA and anti-CD11c MACS isolation kits (Miltenyi Biotec) according to manufacturer protocols. Chromatin was immediately purified and digested from isolated DCs using the EpiQuik chromatin accessibility assay kit (Epigentek). Chromatin preps from each sample were split in two, and were

treated with nuclease (Nse) mix or left untreated. DNA was amplified using quantitative PCR using primers specific for the Nrpl region identified from the methyl-seq/bisulfite seq screen. Fold enrichment was calculated using the formula: $FE = 2^{(NseCT-noNseCT)} \times 100\%$. Samples were validated using positive and negative control primers provided by manufacturer.

7.1.11 Microscopy and analysis

Non-confluent cells (BMDCs, cDCs, pDCs, and PECs) were grown overnight on coverslips at 37°C then pulsed with PBS or gp96 for 6 hr. Cells were then washed, fixed in 2% paraformaldehyde for 15 min, permeabilized with triton X-100 for 15 min, blocked with 2% bovine serum albumin (BSA), and stained in 0.5% BSA with primary antibody anti-DNMT1 (clone 60B122.1, Epigentek) at a dilution of 1:100. Secondary antibodies were conjugated to Cy3, Cy5, or AF488. F-actin was stained with phalloidin-488 and nuclei were stained using Hoescht stain. All images were captured using an Olympus FV1000 confocal microscope. DNMT puncta were quantified using analyses developed by the Center for Biologic Imaging (University of Pittsburgh, PA) which calculates punctae intensity based on intensity threshold using NIS Elements (Nikon). The number of puncta per field of view were normalized to the total number of cells in that field of view. For cardamonin studies, PECs were treated with high dose gp96 in the presence of 10 mM cardamonin or equivalent amount of DMSO. Cells were stained for DNMT after 6 hr incubation at 37°C.

7.1.12 Western blotting

For DNMT western blotting, nuclear extracts were isolated using Epiquik Nuclear Extraction Kit (Epigentek). DNMT1 (clone 60B122.1; Epigentek) and Lamin B1(clone L-5; Invitrogen)

antibodies were used in immunoblots and were developed using X-ray film. Bands were quantified using ProteinSimple technology. For all other western blotting, cells were lysed in NP-40 lysis buffer supplemented with protease/phosphatase inhibitor cocktail. GSK α/β (clone D75D3, CST) phospho-GSK3 β Ser9 (clone 5B3, CST), STAT1 (clone D1K9Y, CST), phospho-STAT1 Ser727 (clone D3B7, CST), phospho-STAT1 Tyr701 (clone 58D6, CST), p38 (clone D13E1, CST), phospho-p38 Thr180/Tyr182 (clone 28B10, CST), and β -actin antibodies were used.

7.1.13 Live cell imaging and analysis

Live cell imaging and analysis. Splenic pDCs were plated at 5×10^5 cells/dish in 35-mm collagen-coated glass-bottom culture dishes (MatTek) in 10% FBS complete RPMI. Cells were pulsed with PBS or low dose or high dose gp96 for 18 hr. CD4⁺CD25⁺ Tregs or CD4⁺CD25⁻ Tconv were isolated from spleen using Treg isolation kit (Miltenyi) and labeled with CellTracker Red dye prior to addition to the culture and imaging. Nrp1 blocking monoclonal antibody (clone 761704; RnD Systems) or rat IgG2a isotype antibody (clone eBR2a; eBioscience) were added 2 hr prior to imaging at a final concentration of 10 mg/ml. Antibody clones and concentrations were based on previously established protocols (197). Cells were imaged on a Nikon A1 inverted microscope (Nikon) using a 40X objective. Images were captured every 5 min for a total of 1 or 2 hr. Videos were analyzed using NIS Elements (Nikon) and ImageJ (254) with Manual Tracking plugin. For interaction time analysis, total contact duration per Treg/Tconv detected from videos was calculated based on the number of frames in which a Treg/Tconv came in contact with a pDC.

7.1.14 Flow cytometry

Flow cytometry. Conjugated antibodies included: APC/Cy7 anti-CD11c (clone HL3, BD), PerCP-Cy5.5 anti-CD11b (clone M1/70, BD), APC anti-PDCA-1 (clone eBio927, eBioscience), BV421 anti-Nrp1 (clone 3E12, BioLegend), FITC anti-B220 (clone RA3-6B2, BD), anti-Lrp1 (clone 5A6, Abcam), PerCP-Cy5.5 anti-CD4 (clone RM4-5, BD), and APC anti-Foxp3 (clone FJK-16s, eBioscience). Surface marker staining was performed in staining buffer (0.5% BSA + 0.1% sodium azide in 1X PBS) at a 1:100 dilution for 20 min on ice followed by washing. Foxp3 staining was performed using overnight fixation and specific staining kit (eBioscience) after staining for surface markers. CD91 staining was performed at 4°C for 30 min following a 15 min fixation with BD fix/perm buffer. All experiments were performed using BD LSR II and BD LSRFortessa instruments and analyzed using FlowJo software.

7.1.15 *In vivo* T cell suppression assay

On day 1, C57BL/6 mice were immunized with 10^6 irradiated (6000 rad) B16 or B16-OVA cells i.p. in 200 μ l PBS. Mice were allowed to rest 4-6 hr then administered anti-PDCA (clone mab927) or control rat IgG2 in 200 μ l PBS for depletion of pDCs. Each mouse received 400 μ g i.p., consistent with previous studies using this antibody for *in vivo* depletion (255). pDC depletion was measured by the percent of pDCs present in the blood at the time of gp96 immunization (Figure 38), which confirmed at least ~90% depletion at this time point. One day later, mice were given HD gp96 i.d. On day 7, C57/BL6 mouse splenocytes were divided, pulsed with SIINFEKL peptide, and CFSE labeled. Unpulsed (CFSE-low) and SIINFEKL-pulsed (CFSE-high) were mixed at a 1:1 ratio and $1-2 \times 10^7$ cells were injected intravenously via tail vein. Recipient mice were sacrificed

5 hr later and analyzed by flow cytometry for lysis of the fluorescently-labeled target population. Percent cytotoxicity was calculated: $(1 - (\text{input ratio} / \text{sample ratio})) * 100$

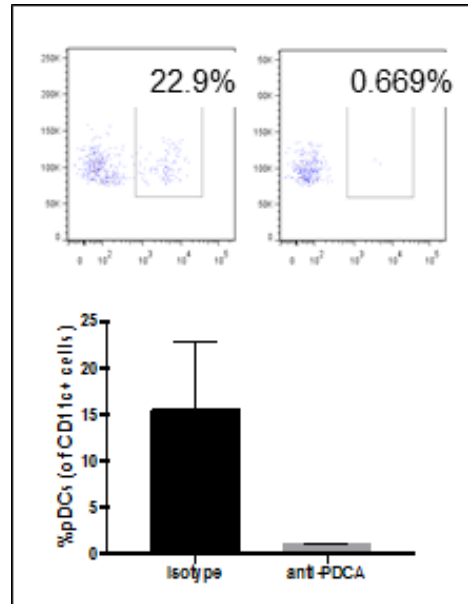


Figure 38. pDC depletion.

Mice were treated with 400 μ g anti-PDCA or isotype antibody i.p. 24 hr later, mice were bled via tail vein and pDC numbers were analyzed by flow cytometry.

7.1.16 *In vivo* Nrp1 neutralization assay

On day 1, C57BL/6 mice were immunized with 10⁶ irradiated (6000 rad) B16-OVA cells i.p. in 200 ml PBS. Seven days later, mice were given high dose gp96 i.d. in 100 ml PBS (or PBS only as control). On the same day, mice also received 100 mg Nrp1 blocking antibody (clone 761704, RnD Systems) or 100 mg rat IgG2a isotype antibody (clone eBR2a, eBioscience) via the i.p. route. Route and dose of Nrp1 antibody is based on previous reports using this antibody³⁸. One week later, all mice were sacrificed and draining lymph nodes were harvested for flow cytometry. The percent of Foxp3⁺ T cells was quantified.

7.1.17 Chromatin immunoprecipitation

3x10⁶ PECs were plated on a flat bottom 24 well plate in 1 ml RPMI and incubated 6 hr at 37° C. Non-adherent cells were removed by washing the wells with PBS. PECs were stimulated for 1 hr with 200 µg/ml gp96, an equimolar concentration of LPS, 10 ng/ml IFN γ , or equivalent volume PBS in a total volume of 0.35 ml. After 1 hr, supernatants were removed and 1.5 ml 1% formaldehyde solution (in serum-free RPMI) was added to each well to cross-link DNA. The plate was rocked at room temperature for 10 min. The formaldehyde solution was removed, 1.5 ml 1X glycine stop solution was added, and the plate was rocked at room temperature for 10 min. Cells were trypsinized, washed, and cell pellets were resuspended in lysis buffer. Lysates were sonicated using Bioruptor pico (Diagenode): 30s on, 30s off for 7 cycles. Lysates were run on a gel to confirm that the samples were fully sonicated to 100-300 bp. Using anti-STAT1 or isotype antibodies, DNA-protein complexes were precipitated, reverse cross-linked, and treated with proteinase K. STAT1, isotype, and input samples were analyzed by qPCR using the following primers designed against the CXCL10 promoter: (F primer: CCATGGTTAGAACCTGACTTAG; R primer: GCAGTGCCTTGCAGAATA). DNA was amplified with SYBER green using the following conditions: Taq activation for 10 min at 95 degrees, followed by 40 cycles of 15 s at 95° C and 1 min at 56° C. Quantification was performed by normalizing STAT1 precipitated samples to input. Percent input was calculated by: % input = 2^{deltaCT} x 100.

7.1.18 ELISA and Luminex

IFN γ ELISAs were performed with Mouse IFN γ Femto-HS Ready-Set-Go kit (eBioscience). Luminex (eBioscience) was used to detect secreted IP-10 protein. Samples were analyzed using a Bioplex II Luminex machine (Bio-Rad).

7.1.19 Statistical analyses

Statistical analyses were performed using 2-tailed t test for comparison between 2 variables or ANOVA with Tukey multiple corrections tests for comparison between 3 or more variables. For tumor growth studies, ANOVA of area under curve (AUC) analysis was used. Statistical significance was defined as $P < 0.05$. Graphs are presented as mean \pm standard error of mean (SEM) or standard deviation (SD) as noted. Statistical analyses were performed using Prism software (GraphPad, La Jolla, CA). ns, not significant; * $P < 0.05$, ** $P < 0.01$, *** $P < 0.001$

BIBLIOGRAPHY

1. De Filippo A, R.J. Binder, C. Camisaschi, V. Beretta, F. Arienti, A. Villa, P. Della Mina, G. Parmiani, L. Rivoltini, and C. Castelli. Human plasmacytoid dendritic cells interact with gp96 via CD91 and regulate inflammatory responses. *J Immunol.* 2008;181:6525-35
2. Chalmin F, S. Ladoire, G. Mignot, J. Vincent, M. Bruchard, J.P. Remy-Martin, W. Boireau, A. Rouleau, B. Simon, D. Lanneau, A. De Thonel, G. Multhoff, A. Hamman, F. Martin, B. Chauffert, E. Solary, L. Zitvogel, C. Garrido, B. Ryffel, C. Borg, L. Apetoh, C. Rébé, and F. Ghiringhelli Membrane-associated Hsp72 from tumor-derived exosomes mediates STAT3-dependent immunosuppressive function of mouse and human myeloid-derived suppressor cells. *J Clin Invest.* 2010;120:457-71.
3. Marvel D, and D.I. Gabrilovich. Myeloid-derived suppressor cells in the tumor microenvironment: expect the unexpected. *J Clin Invest.* 2015;125:3356-64.
4. Vermi W, M. Soncini, L. Melocchi, S. Sozzani, and F. Facchetti Plasmacytoid dendritic cells and cancer. *J Leukoc Biol.* 2011;90:681-90.
5. Harimoto H, M. Shimizu, Y. Nakagawa, K. Nakatsuka, A. Wakabayashi, C. Sakamoto, and H. Takahashi. Inactivation of tumor-specific CD8+ CTLs by tumor-infiltrating tolerogenic dendritic cells. *Immunology and Cell Biology.* 2013;91:545-55.
6. Zinkernagel RM, and P.C. Doherty. Restriction of in vitro T cell-mediated cytotoxicity in lymphocytic choriomeningitis within a syngeneic or semiallogeneic system. *Nature.* 1974;248:701-2.
7. Gross L. The importance of dosage in the intradermal immunization against transplantable neoplasms. *Cancer Res.* 1943;3:326-33.
8. Sharkey MS, G. Lizée, M.I. Gonzales, S. Patel, and S.L. Topalian. CD4(+) T-cell recognition of mutated B-RAF in melanoma patients harboring the V599E mutation. *Cancer Res.* 2004;64:1595-9.
9. Kawakami Y, N. Dang, X. Wang, J. Tupesis, P.F. Robbins, R. Fu Wang, J.R. Wunderlich, J.R. Yannelli, and S.A. Rosenberg. Recognition of shared melanoma antigens in association with major HLA-A alleles by tumor infiltrating T lymphocytes from 123 patients with melanoma. *J Immunother.* 2000;23:17-27.
10. Takenoyama M, J.F. Baurain, M. Yasuda, T. So, M. Sugaya, T. Hanagiri, K. Sugio, K. Yasumoto, T. Boon, and P.G. Coulie. A point mutation in the NFYC gene generates an antigenic peptide recognized by autologous cytolytic T lymphocytes on a human squamous cell lung carcinoma. *Int J Cancer.* 2006;118:1992-7.
11. Maher J, and E.T. Davies. Targeting cytotoxic T lymphocytes for cancer immunotherapy. *Br J Cancer.* 2004;91:817-21.
12. Schoenberger SP, R.E. Toes, E.I. van der Voort, R. Offringa, and C.J. Melief. T-cell help for cytotoxic T lymphocytes is mediated by CD40-CD40L interactions. *Nature.* 1998;393:480-3.
13. Flinsenberg TW, L. Spel, M. Jansen, D. Koning, C. de Haar, M. Plantinga, R. Scholman, M.M. van Loenen, S. Nierkens, L. Boon, D. van Baarle, M.H. Heemskerk, J.J. Boelens, and M. Boes. Cognate CD4 T-cell licensing of dendritic cells heralds anti-CMV CD8 T-cell immunity after human allogeneic umbilical cord blood transplantation. *J Virol.* 2015;89:1058-69.

14. Srivastava PK, A.B. DeLeo, and L.J. Old. Tumor rejection antigens of chemically induced sarcomas of inbred mice. *Proc Natl Acad Sci U S A*. 1986;83:3407-11.
15. Srivastava P. Roles of heat-shock proteins in innate and adaptive immunity. *Nat Rev Immunol*. 2002;2:185-94.
16. Kropp LE, M. Garg, and R.J. Binder. Ovalbumin-derived precursor peptides are transferred sequentially from gp96 and calreticulin to MHC I in the endoplasmic reticulum. *J Immunol*. 2010;184:5619-27.
17. Ménoret A, P. Peng, and P.K. Srivastava. Association of peptides with heat shock protein gp96 occurs in vivo and not after cell lysis. *Biochem Biophys Res Commun*. 1999;262:813-8.
18. Ishii T, H. Uono, T. Yamano, H. Ohta, A. Uenaka, T. Ono, A. Hizuta, N. Tanaka, P. K. Srivastava, and E. Nakayama. Isolation of MHC class I-restricted tumor antigen peptide and its precursors associated with heat shock proteins hsp70, hsp90, and gp96. *J Immunol*. 1999;162:1303-9.
19. Kunisawa J, and N. Shastri. Hsp90alpha chaperones large C-terminally extended proteolytic intermediates in the MHC class I antigen processing pathway. *Immunity*. 2006;24:523-34.
20. Callahan MK GM, Srivastava PK. Heat-shock protein 90 associates with N-terminal extended peptides and is required for direct and indirect antigen presentation. *Proc Natl Acad Sci U S A*. 2008;105:1662-7.
21. Berwin B, M.F. Rosser, K.G. Brinker, and C.V. Nicchitta. Transfer of GRP94(Gp96)-associated peptides onto endosomal MHC class I molecules. *Traffic*. 2002;3:358-66.
22. Wearsch PA, and P. Cresswell. The quality control of MHC class I peptide loading. *Curr Opin Cell Biol*. 2008;20:624-31.
23. Dong G, P. A. Wearsch, D. R. Peaper, P. Cresswell, and K. M. Reinisch. Insights into MHC class I peptide loading from the structure of the tapasin-ERp57 thiol oxidoreductase heterodimer. *Immunity*. 2009;30:21-32.
24. Li Z, and P.K. Srivastava. Tumor rejection antigen gp96/grp94 is an ATPase: implications for protein folding and antigen presentation. *EMBO J*. 1993;12:3143-51.
25. Arnold D, C. Wahl, S. Faath, H.G. Rammensee, and H. Schild. Influences of Transporter Associated with Antigen Processing (TAP) on the Repertoire of Peptides Associated with the Endoplasmic Reticulum-resident Stress Protein gp96. *J Exp Med*. 1997;186:461-6.
26. Zhou YJ, M.N. Messmer, and R.J. Binder. Establishment of tumor-associated immunity requires interaction of heat shock proteins with CD91. *Cancer Immunol Res*. 2014;2:217-28.
27. Uono H, and P.K. Srivastava. Heat shock protein 70-associated peptides elicit specific cancer immunity. *J Exp Med*. 1993;178:391-6.
28. Graner M, A. Raymond, E. Akporiaye, and E. Katsanis. Tumor-derived multiple chaperone enrichment by free-solution isoelectric focusing yields potent anti-tumor vaccines. *Cancer Immunol Immunother*. 2000;49:476-784.
29. Wang XY, L. Kazim, E.A. Repasky, and J.R. Subjeck. Characterization of heat shock protein 110 and glucose-regulated protein 170 as cancer vaccines and the effect of fever-range hyperthermia on vaccine activity. *J Immunol*. 2001;166:490-7.
30. Sedlacek AL, L.B. Kinner-Bibeau, and R.J. Binder. Phenotypically distinct helper NK cells are required for gp96-mediated anti-tumor immunity. *Sci Rep*. 2016;6:29889.
31. Kovalchin JT, A.S. Murthy, M.C. Horattas, D.P. Guyton, Y. Rajiv, and R.Y. Chandawarkar. Determinants of efficacy of immunotherapy with tumor-derived heat shock protein gp96. *Cancer Immunity*. 2001;1:7.

32. Tamura Y, P. Peng, L. Kang, M. Daou, and P.K. Srivastava. Immunotherapy of tumors with autologous tumor-derived heat shock protein preparations. *Science*. 1997;278:117–20.
33. Randazzo M, P. Terness, G. Opelz, and C. Kleist. Active-specific immunotherapy of human cancers with the heat shock protein Gp96-revisited. *Int J Cancer*. 2011;130:2219-31.
34. Janetzki S, D. Palla, V. Rosenhauer, H. Lochs, J.J. Lewis, and P.K. Srivastava. Immunization of cancer patients with autologous cancer-derived heat shock protein gp96 preparations: A pilot study. *Int J Cancer*. 2000;15:232-8.
35. Mazzaferro V, J. Coppa, M. G. Carrabba, L. Rivoltini, M. Schiavo, E. Regalia, L. Mariani, T. Camerini, A. Marchiano, S. Andreola, R. Camerini, M. Corsi, J. J. Lewis, P. K. Srivastava, and G. Parmiani. Vaccination with autologous tumor-derived heat-shock protein gp96 after liver resection for metastatic colorectal cancer. *Clin Cancer Res*. 2003;9:3235-45.
36. Belli F, A. Testori, L. Rivoltini, M. Maio, G. Andreola, M. R. Sertoli, G. Gallino, A. Piris, A. Cattelan, I. Lazzari, M. Carrabba, G. Scita, C. Santantonio, L. Pilla, G. Tragni, C. Lombardo, F. Arienti, A. Marchiano, P. Queirolo, F. Bertolini, A. Cova, E. Lamaj, L. Ascani, R. Camerini, M. Corsi, N. Cascinelli, J. J. Lewis, P. Srivastava, and G. Parmiani. Vaccination of metastatic melanoma patients with autologous tumor-derived heat shock protein gp96-peptide complexes: clinical and immunologic findings. *J Clin Oncol*. 2002;20:4169-80.
37. Pilla L, R. Patuzzo, L. Rivoltini, M. Maio, E. Pennacchioli, E. Lamaj, A. Maurichi, S. Massarut, A. Marchiano, C. Santantonio, D. Tosi, F. Arienti, A. Cova, G. Sovena, A. Piris, D. Nonaka, I. Bersani, A. Di Florio, M. Luigi, P. K. Srivastava, A. Hoos, M. Santinami, and G. Parmiani. A phase II trial of vaccination with autologous, tumor-derived heat-shock protein peptide complexes Gp96, in combination with GM-CSF and interferon-alpha in metastatic melanoma patients. *Cancer Immunol Immunother*. 2006;55(958-968).
38. Testori A, J. Richards, E. Whitman, G. B. Mann, J. Lutzky, L. Camacho, G. Parmiani, G. Tosti, J. M. Kirkwood, A. Hoos, L. Yuh, R. Gupta, and P. K. Srivastava. Phase III comparison of vitespen, an autologous tumor-derived heat shock protein gp96 peptide complex vaccine, with physician's choice of treatment for stage IV melanoma: the C-100- 21 Study Group. *J Clin Oncol*. 2008;26:955-62.
39. Eton O, M.I. Ross, M.J. East, P.F. Mansfield, N. Papadopoulos, J.A. Ellerhorst, A.Y. Bedikian, and J.E. Lee. Autologous tumor-derived heat-shock protein peptide complex-96 (HSPPC-96) in patients with metastatic melanoma. *J Transl Med*. 2010;8:9.
40. Younes A. A phase II study of heat shock protein-peptide complex-96 vaccine therapy in patients with indolent non-Hodgkin's lymphoma. *Clin Lymphoma*. 2003;4:183-5.
41. Oki Y, P. McLaughlin, L. E. Fayad, B. Pro, P. F. Mansfield, G. L. Clayman, L. J. Medeiros, L. W. Kwak, P. K. Srivastava, and A. Younes. Experience with heat shock protein-peptide complex 96 vaccine therapy in patients with indolent non-Hodgkin lymphoma. *Cancer* 2007;109:77-83.
42. Maki RG, P. O. Livingston, J. J. Lewis, S. Janetzki, D. Klimstra, D. Desantis, P. K. Srivastava, and M. F. Brennan. A phase I pilot study of autologous heat shock protein vaccine HSPPC-96 in patients with resected pancreatic adenocarcinoma. *Dig Dis Sci*. 2007;52:1964-72.
43. Jonasch E, C. Wood, P. Tamboli, L. C. Pagliaro, S. M. Tu, J. Kim, P. Srivastava, C. Perez, L. Isakov, and N. Tannir. Vaccination of metastatic renal cell carcinoma patients with autologous tumour-derived vitespen vaccine: clinical findings. *Br J Cancer*. 2008;98:1336-41.
44. Wood C, P. Srivastava, R. Bukowski, L. Lacombe, A. I. Gorelov, S. Gorelov, P. Mulders, H. Zielinski, A. Hoos, F. Teofilovici, L. Isakov, R. Flanigan, R. Figlin, R. Gupta, and B. Escudier. An adjuvant autologous therapeutic vaccine (HSPPC-96; vitespen) versus observation alone for

patients at high risk of recurrence after nephrectomy for renal cell carcinoma: a multicentre, open-label, randomised phase III trial *Lancet*. 2008;372:145-54.

45. Crane CA, S. J. Han, B. J. Ahn, J. Oehlke, V. Kivett, A. Fedoroff, N. Butowski, S. M. Chang, J. Clarke, M. S. Berger, M. W. McDermott, M. D. Prados, and A. T. Parsa. Individual patient-specific immunity against high-grade glioma after vaccination with autologous tumor derived peptides bound to the 96 KD chaperone protein. *Clin Cancer Res*. 2012;19:205-14.
46. Bloch O, and A.T. Parsa. Heat shock protein peptide complex-96 (HSPPC-96) vaccination for recurrent glioblastoma: a phase II, single arm trial. *Neuro Oncol*. 2014;16:758–9.
47. Bloch O, M. Lim, M.E. Sughrue, R.J. Komotar, J.M. Abrahams, D.M. O'Rourke, A. D'Ambrosio, J.N. Bruce, and A.T. Parsa. Autologous heat shock protein peptide vaccination for newly diagnosed glioblastoma: impact of peripheral PD-L1 expression on response to therapy. *Clin Cancer Res*. 2017.
48. Tobian AA, D.H. Canaday, W.H. Boom, and C.V. Harding. Bacterial heat shock proteins promote CD91-dependent class I MHC cross-presentation of chaperoned peptide to CD8+ T cells by cytosolic mechanisms in dendritic cells versus vacuolar mechanisms in macrophages. *J Immunol*. 2004;172:5277-86.
49. Binder RJ, and P.K. Srivastava. Peptides chaperoned by heat-shock proteins are a necessary and sufficient source of antigen in the cross-priming of CD8+ T cells. *Nat Immunol*. 2005;6:593-9.
50. Staib F, M. Distler, K. Bethke, U. Schmitt, P.R. Galle, and M. Heike. Cross-presentation of human melanoma peptide antigen MART-1 to CTLs from in vitro reconstituted gp96/MART-1 complexes. *Cancer Immun*. 2004;4:3.
51. Arnold D, S. Faath, H. Rammensee, and H. Schild. Cross-priming of minor histocompatibility antigen-specific cytotoxic T cells upon immunization with the heat shock protein gp96. *J Exp Med*. 1995;182:885-9.
52. Matsutake T, T. Sawamura, and P.K. Srivastava. High efficiency of CD91- and Lox-1-mediated re-presentation of gp96-chaperoned peptides by MHC II molecules. *Cancer Immun*. 2010;10:7.
53. Binder RJ, and P.K. Srivastava. Essential role of CD91 in re-presentation of gp96-chaperoned peptides. *Proc Natl Acad Sci U S A*. 2004;101:6128-33.
54. Tobian AAR, D.H. Canaday, and C.V. Harding. Bacterial Heat Shock Proteins enhance class II MHC antigen processing and presentation of chaperoned peptides to CD4+ T cells. *J Immunol*. 2004;173:5130-7.
55. Fischer N, M. Haug, W.W. Kwok, H. Kalbacher, D. Wernet, G.E. Dannecker, and U. Holzer. Involvement of CD91 and scavenger receptors in Hsp70-facilitated activation of human antigen-specific CD4+ memory T cells. *Eur J Immunol*. 2010;40:986-97.
56. Binder RJ, N.E. Blachere, and P.K. Srivastava. Heat Shock Protein-chaperoned peptides but not free peptides introduced into the cytosol are presented efficiently by Major Histocompatibility Complex I molecules. *J Biol Chem*. 2001;276:17163-71.
57. Blachere NE, Z. Li, R. Y. Chandawarkar, R. Suto, N. S. Jaikaria, S. Basu, H. Udono, and P. K. Srivastava. Heat shock protein-peptide complexes, reconstituted in vitro, elicit peptide-specific cytotoxic T lymphocyte response and tumor immunity. *J Exp Med*. 1997;186:1315.
58. Arnold-Schild D, D. Hanau, D. Spehner, C. Schmid, H.G. Rammensee, H. de la Salle, and H. Schild. Cutting edge: receptor-mediated endocytosis of heat shock proteins by professional antigen-presenting cells. *J Immunol*. 1999;162:3757-60.

59. Binder R.J. DKH, and P.K. Srivastava. CD91: a receptor for heat shock protein gp96. *Nat Immunol.* 2000;1:151-5.
60. Basu S, R.J. Binder, T. Ramalingam, and P.K. Srivastava. CD91 is a common receptor for heat shock proteins gp96, hsp90, hsp70, and calreticulin *Immunity.* 2001;14:303-13.
61. Messmer MN, J. Pasmowitz, L.E. Kropp, S.C. Watkins, and R.J. Binder. Identification of the cellular sentinels for native immunogenic heat shock proteins in vivo. *J Immunol.* 2013;191:4456-65.
62. Pawaria S, and R.J. Binder. CD91-dependent programming of T-helper cell responses following heat shock protein immunization. *Nat Commun.* 2011;2:521.
63. Delneste Y, G. Magistrelli, J. Gauchat, J. Haeuw, J. Aubry, K. Nakamura, N. Kawakami-Honda, L. Goetsch, T. Sawamura, J. Bonnefoy, and P. Jeannin. Involvement of LOX-1 in dendritic cell-mediated antigen cross-presentation. *Immunity.* 2002;17:353-62.
64. Berwin B, J.P. Hart, S. Rice, C. Gass, S.V. Pizzo, S.R. Post, and C.V. Nicchitta. Scavenger receptor-A mediates gp96/GRP94 and calreticulin internalization by antigen-presenting cells. *EMBO J.* 2003;22:6127-36.
65. Berwin B, Y. Delneste, R.V. Lovingood, S.R. Post, and S.V. Pizzo. SREC-I, a type F scavenger receptor, is an endocytic receptor for calreticulin. *J Biol Chem.* 2004;279:51250-7.
66. Vabulas RM, P. Ahmad-Nejad, S. Ghose, C.J. Kirschning, R.D. Issels, and H. Wagner. HSP70 as endogenous stimulus of the Toll/interleukin-1 receptor signal pathway. *J Biol Chem.* 2002;277:15107-12.
67. Vabulas RM, S. Braedel, N. Hilf, H. Singh-Jasuja, S. Herter, P. Ahmad-Nejad, C.J. Kirschning, C. Da Costa, H.G. Rammensee, H. Wagner, and H. Schild. The endoplasmic reticulum-resident heat shock protein Gp96 activates dendritic cells via the Toll-like receptor 2/4 pathway. *J Biol Chem.* 2002;277:20847-53.
68. Herz J, and D.K. Strickland. LRP: a multifunctional scavenger and signaling receptor. *J Clin Invest.* 2001;108:779-84.
69. Lillis AP, L.B. Van Duyn, J.E. Murphy-Ullrich, and D.K. Strickland. LDL receptor-related protein 1: unique tissue-specific functions revealed by selective gene knockout studies. *Physiol Rev.* 2008;88:887-918.
70. Basu S, R.J. Binder, R. Suto, K.M. Anderson, and P.K. Srivastava. Necrotic but not apoptotic cell death releases heat shock proteins, which deliver a partial maturation signal to dendritic cells and activate the NF-kappa B pathway. *Int Immunol.* 2000;12:1539-46.
71. Muratoglu SC, I. Mikhailenko, C. Newton, M. Migliorini, and D.K. Strickland. Low Density Lipoprotein Receptor-related Protein 1 (LRP1) forms a signaling complex with Platelet-derived Growth Factor Receptor- β in endosomes and regulates activation of the MAPK pathway. *J Biol Chem.* 2010;285:14308-17.
72. May P, A. Rohlmann, H.H. Bock, K. Zurhove, J.D. Marth, E.D. Schomburg, J.L. Noebels, U. Beffert, J.D. Sweatt, E.J. Weeber, and J. Herz. Neuronal LRP1 functionally associates with postsynaptic proteins and is required for normal motor function in mice. *Mol Cell Biol.* 2004;24:8872-83.
73. Ashcom JD, S.E. Tiller, K. Dickerson, J.L. Cravens, W.S. Argraves, and D.K. Strickland. The human α 2-macroglobulin receptor: identification of a 420-kD cell surface glycoprotein specific for the activated conformation of α 2-macroglobulin. *J Cell Biol.* 1990;110:1041-8.
74. Masson O, C. Chavey, C. Dray, A. Meulle, D. Daviaud, D. Quilliot, C. Muller, P. Valet, and E. Liaudet-Coopman. LRP1 receptor controls adipogenesis and is up-regulated in human and mouse obese adipose tissue. *PLoS One.* 2009;4:e7422.

75. Yoon C, E.A. Van Niekerk, K. Henry, T. Ishikawa, S. Orita, M.H. Tuszynski, and W.M. Campana. Low-density lipoprotein receptor-related protein 1 (LRP1)-dependent cell signaling promotes axonal regeneration. *J Biol Chem.* 2013;288:26557-68.
76. Lillis AP, S.C. Muratoglu, D.T. Au, M. Migliorini, M.J. Lee, S.K. Fried, I. Mikhailenko, and D.K. Strickland. LDL receptor-related protein-1 (LRP1) regulates cholesterol accumulation in macrophages. *PLoS One.* 2015;10:e012890.
77. Terrand J, V. Bruban, L. Zhou, W. Gong, Z. El Asmar, P. May, K. Zurhove, P. Haffner, C. Philippe, E. Woldt, R.L. Matz, C. Gracia, D. Metzger, J. Auwerx, J. Herz, and P. Boucher. LRP1 controls intracellular cholesterol storage and fatty acid synthesis through modulation of Wnt signaling. *J Biol Chem.* 2009;284:381-8.
78. Kinchen JM, and K.S. Ravichandran. Journey to the grave: signaling events regulating removal of apoptotic cells. *J Cell Sci.* 2007;120:2143-9.
79. Kinner-Bibeau LB, A.L. Sedlacek, M.N. Messmer, S.C. Watkins, and R.J. Binder. HSPs drive dichotomous T cell immune responses via DNA methylome remodeling in Antigen Presenting Cells. *Nat Commun.* 2017;8:15648.
80. Lipsker D, U. Ziylan, D. Spehner, F. Proamer, H. Bausinger, P. Jeannin, J. Salamero, A. Bohbot, J. P. Cazenave, R. Drillien, Y. Delneste, D. Hanau, and H. de la Salle. Heat shock proteins 70 and 60 share common receptors which are expressed on human monocyte-derived but not epidermal dendritic cells. *Eur J Immunol.* 2002;32:322-32.
81. Fischer N, M. Haug, W. W. Kwok, H. Kalbacher, D. Wernet, G. E. Dannecker, and U. Holzer. Involvement of CD91 and scavenger receptors in Hsp70-facilitated activation of human antigen-specific CD4(+) memory T cells. *Eur J Immunol.* 2010;40:986-97.
82. Boucher P, P. Liu, M. Gotthardt, T. Hiesberger, R.G. Anderson, and J. Herz. Platelet-derived growth factor mediates tyrosine phosphorylation of the cytoplasmic domain of the low Density lipoprotein receptor-related protein in caveolae. *J Biol Chem.* 2002;277:15507-13.
83. May P, E. Woldt, R.L. Matz, and P. Boucher. The LDL receptor-related protein (LRP) family: an old family of proteins with new physiological functions. *Ann Med.* 2007;39:219-28.
84. Arthur JS, and S.C. Ley. Mitogen-activated protein kinases in innate immunity. *Nat Rev Immunol.* 2016;13:679-92.
85. Kang YJ, J. Chen, M. Otsuka, J. Mols, S. Ren, Y. Wang, and J Han. Macrophage deletion of p38alpha partially impairs lipopolysaccharide-induced cellular activation. *J Immunol.* 2008;180:5075-82.
86. O'Keefe SJ, J.S. Mudgett, S. Cupo, J.N. Parsons, N.A. Chartrain, C. Fitzgerald, S.L. Chen, K. Lowitz, C. Rasa, D. Visco, S. Luell, E. Carballo-Jane, K. Owens, and D.M. Zaller. Chemical genetics define the roles of p38alpha and p38beta in acute and chronic inflammation. *J Biol Chem.* 2007;282:34663-71.
87. Jackson AM ML, Porte J, Franks HA, El Refaee M, Wang Q, Shah S, Zhu X, Patel PM. Role of mitogen-activated protein kinase and PI3K pathways in the regulation of IL-12-family cytokines in dendritic cells and the generation of T H-responses. *Eur Cytokine Netw.* 2010;21:319-28.
88. Cuadrado A, and A.R. Nebreda. Mechanisms and functions of p38 MAPK signalling. *Biochem J.* 2010;429:403-17.
89. Ramana CV, M. Chatterjee-Kishore, H. Nguyen and G.R. Stark. Complex roles of Stat1 in regulating gene expression. *Oncogene.* 2000;19:2619-27.
90. Kovarik P, D. Stoiber, P.A. Eyers, R. Menghini, A. Neininger, M. Gaestel, P. Cohen, and T. Decker. Stress-induced phosphorylation of STAT1 at Ser727 requires p38 mitogen-activated

protein kinase whereas IFN uses a different signaling pathway. *Proc Natl Acad Sci U S A*. 1999;96:13956–61.

91. Darnell JEJ, I.M. Kerr, and G.R. Stark. Jak-STAT pathways and transcriptional activation in response to IFNs and other extracellular signaling proteins. *Science*. 1994;264:1415-21.
92. Wen Z, Z. Zhong, and J.E. Darnell Jr. Maximal activation of transcription by Stat1 and Stat3 requires both tyrosine and serine phosphorylation. *Cell*. 1995;82:241-50.
93. Yu Y, R. Wang, Y. Nan, L. Zhang, and Y. Zhang. Induction of STAT1 phosphorylation at serine 727 and expression of proinflammatory cytokines by porcine reproductive and respiratory syndrome virus. *PLoS One*. 2013;8:e61967.
94. Kovarik P, D. Stoiber, M. Novy, and T. Decker. Stat1 combines signals derived from IFN-gamma and LPS receptors during macrophage activation. *EMBO J*. 1998;17:3660–8.
95. Decker T, and P. Kovarik. Serine phosphorylation of Stats *Oncogene*. 2000;19:2628–37.
96. Nguyen H, M. Chatterjee-Kishore, Z. Jiang, Y. Qing, C.V. Ramana, J. Bayes, M. Commane, X. Li, and G.R. Stark. IRAK-dependent phosphorylation of Stat1 on serine 727 in response to Interleukin-1 and effects on gene expression. *J Interferon Cytokine Res*. 2003;23:183-92.
97. Luu K, C.J. Greenhill, A. Majoros, T. Decker, B.J. Jenkins, and A. Mansell. STAT1 plays a role in TLR signal transduction and inflammatory responses. *Immunol Cell Biol*. 2014;92:761-9.
98. Chandawarkar RY, M.S. Wagh, and P.K. Srivastava. The dual nature of specific immunological activity of tumor-derived gp96 preparations. *J Exp Med*. 1999;189:1437-42.
99. Chandawarkar RY, M.S. Wagh, J.T. Kovalchin, and P. Srivastava. Immune modulation with high-dose heat-shock protein gp96: therapy of murine autoimmune diabetes and encephalomyelitis. *Int Immunol*. 2004;16:615-24.
100. Leiter EH. The NOD mouse: a model for insulin-dependent diabetes mellitus. *Curr Protocols Immunol*. 1997;24:15.9.1.
101. Wieten L, S.E. Berlo, C.B.T. Brink, P.J. van Kooten, M. Singh, R. van der Zee, T.T. Glant, F. Broere, and W. van Eden. IL-10 is critically involved in Mycobacterial HSP70 induced suppression of proteoglycan-induced arthritis. *PLoS One*. 2009;4:e4186.
102. Kovalchin JT, C. Mendonca, M.S. Wagh, R. Wang, and R.Y. Chandawarkar. In vivo treatment of mice with heat shock protein, gp 96, improves survival of skin grafts with minor and major antigenic disparity. *Transpl Immunol*. 2006;15:179-85.
103. Slack LK, M. Muthana, K. Hopkinson, S.K. Suvarna, E. Espigares, S. Mirza, B. Fairburn, and A.G. Pockley. Administration of the stress protein gp96 prolongs rat cardiac allograft survival, modifies rejection-associated inflammatory events, and induces a state of peripheral T-cell hyporesponsiveness. *Cell Stress Chaperones*. 2007;12:71-82.
104. Li X, Z. Liu, X. Yan, X. Zhang, Y. Li, B. Zhao, S. Wang, X. Zhou, G.F. Gao, and S. Meng. Induction of regulatory T cells by high-dose gp96 suppresses murine liver immune hyperactivation. *PLoS One*. 2013;8:e68997.
105. Liu Z, X. Li, L. Qiu, X. Zhang, L. Chen, S. Cao, F. Wang, and S. Meng. Treg suppress CTL responses upon immunization with HSP gp96 *Eur J Immunol*. 2009;39:3110-20.
106. Kimura Y, K. Yamada, T. Sakai, K. Mishima, H. Nishimura, Y. Matsumoto, M. Singh, and Y. Yoshikai. The regulatory role of heat shock protein 70-reactive CD4+ T cells during rat listeriosis. *Int Immunol*. 1998;10:117-30.
107. Schmidt A, N. Oberle, and P.H. Krammer. Molecular mechanisms of Treg-mediated T cell suppression. *Front Immunol*. 2012;3:51.

108. Thornton AM, and E.M. Shevach. CD4+CD25+ immunoregulatory T cells suppress polyclonal T cell activation in vitro by inhibiting interleukin 2 production. *J Exp Med.* 1998;188:287-96.
109. Takahashi T, Y. Kuniyasu, M. Toda, N. Sakaguchi, M. Itoh, M. Iwata, J. Shimizu, and S. Sakaguchi. Immunologic self-tolerance maintained by CD25+CD4+ naturally anergic and suppressive T cells: induction of autoimmune disease by breaking their anergic/suppressive state. *Int Immunol.* 1998;10:1969-80.
110. Szymczak-Workman AL, C.J. Workman, and D.A. Vignali. Cutting edge: regulatory T cells do not require stimulation through their TCR to suppress. *J Immunol.* 2009;182:5188-92.
111. Yan X, X. Zhang, Y. Wang, X. Li, S. Wang, B. Zhao, Y. Li, Y. Ju, L. Chen, W. Liu, and S. Meng. Regulatory T-cell depletion synergizes with gp96-mediated cellular responses and antitumor activity. *Cancer Immunol Immunother.* 2011;60:1763-74.
112. Reizis B, A. Bunin, H.S. Ghosh, K.L. Lewis, and V. Sisirak. Plasmacytoid dendritic cells: recent progress and open questions. *Annu Rev Immunol.* 2011;29:163-83.
113. Swiecki M, and M. Colonna. The multifaceted biology of plasmacytoid dendritic cells. *Nat Rev Immunol.* 2015;15:471-85
114. Gabrilovich D.I. aSN. Myeloid-derived suppressor cells as regulators of the immune system. *Nat Rev Immunol.* 2009;9:162-74.
115. Martin CA, S.E. Carsons, R. Kowalewski, D. Bernstein, M. Valentino, and F. Santiago-Schwarz. Aberrant extracellular and dendritic cell (DC) surface expression of heat shock protein (hsp)70 in the rheumatoid joint: possible mechanisms of hsp/DC-mediated cross-priming. *J Immunol.* 2003;171:5736-42.
116. Sedlackova L, T.T.H. Nguyen, D. Zlacka, A. Sosna, and I. Hromadnikova. Cell surface and relative mRNA expression of heat shock protein 70 in human synovial cells. *Autoimmunity.* 2009;42:17-24.
117. Huang Q, R. Sobkoviak, A. Jockheck-Clark, B. Shi, A.M. Mandelin II, P.P. Tak, G.K. Haines, C.V. Nicchitta, and R.M. Pope. Heat Shock Protein 96 is elevated in rheumatoid arthritis and activates macrophages primarily via TLR2 signaling. *J Immunol.* 2009;182:4965.
118. Gross C, W. Koelch, A. DeMaio, N. Arispe, and G. Multhoff. Cell surface-bound heat shock protein 70 (Hsp70) mediates perforin-independent apoptosis by specific binding and uptake of granzyme B. *J Biol Chem.* 2003;278:41173-81.
119. van Eden W, J.E. Thole, R. van der Zee, A. Noordzij, J.D. van Embden, E.J. Hensen, and I.R. Cohen. Cloning of the mycobacterial epitope recognized by T lymphocytes in adjuvant arthritis. *Nature.* 1988;331:171-3.
120. Borges TJ, L. Wieten, M.J. van Herwijnen, F. Broere, R. van der Zee, C. Bonorino, and W. van Eden. The anti-inflammatory mechanisms of Hsp70. *Front Immunol.* 2012;3:95.
121. Liu Y, M.W. Mayo, A.S. Nagji, P.W. Smith, C.S. Ramsey, D. Li, and D.R. Jones. Phosphorylation of RelA/p65 promotes DNMT-1 recruitment to chromatin and represses transcription of the tumor metastasis suppressor gene BRMS1. *Oncogene.* 2012;31:1143-54.
122. White GP, P.M. Watt, B.J. Holt, and P.G. Holt. Differential patterns of methylation of the IFN-gamma promoter at CpG and non-CpG sites underlie differences in IFN-gamma gene expression between human neonatal and adult CD45RO+ T cells. *J Immunol.* 2003;168:235-40.
123. Lister R, M. Pelizzola, R.H. Dowen, R.D. Hawkins, G. Hon, J. Tonti-Filippini, J.R. Nery, L. Lee, Z. Ye, Q.M. Ngo, L. Edsall, J. Antosiewicz-Bourget, R. Stewart, V. Ruotti, A.H. Millar, J.A. Thomson, B. Ren, and J.R. Ecker. Human DNA methylomes at base resolution show widespread epigenomic differences. *Nature.* 2009;462:315-22.

124. Guo JU, Y. Su, J.H. Shin, J. Shin, H. Li, B. Xie, C. Zhong, S. Hu, T. Le, G. Fan, H. Zhu, Q. Chang, Y. Gao, G.L. Ming, and H. Song. Distribution, recognition and regulation of non-CpG methylation in the adult mammalian brain. *Nat Neurosci.* 2014;17:215-22.
125. Sharma G, D.T. Sowpati, P. Singh, M.Z. Khan, R. Ganji, S. Upadhyay, S. Banerjee, V.K. Nandicoori, and S. Khosla. Genome-wide non-CpG methylation of the host genome during M. tuberculosis infection. *Sci Rep.* 2016;6:25006.
126. Handy DE, R. Castro, and J. Loscalzo. Epigenetic modifications: basic mechanisms and role in cardiovascular disease. *Circulation.* 2014;4:169-74.
127. Goll MG, and T.H. Bestor. Eukaryotic cytosine methyltransferases. *Annu Rev Biochem.* 2005;74:481-514.
128. Meaney MJ, and M. Szyf. Environmental programming of stress responses through DNA methylation, life at the interface between a dynamic environment and a fixed genome. *Dialogues Clin Neurosci.* 2005;7:103-23.
129. Arzate-Mejía RG, D. Valle-García, and F. Recillas-Targa. Signaling epigenetics: novel insights on cell signaling and epigenetic regulation. *IUBMB Life.* 2011;63:881-95.
130. Guo QY, M. Yuan, J. Peng, X.M. Cui, G. Song, X. Sui, and S.B. Lu. Antitumor activity of mixed heat shock protein/peptide vaccine and cyclophosphamide plus interleukin-12 in mice sarcoma. *J Exp Clin Cancer Res.* 2011;30:24.
131. Watt F, and P.L. Molloy. Cytosine methylation prevents binding to DNA of a HeLa cell transcription factor required for optimal expression of the adenovirus major late promoter *Genes Dev.* 1988;2:1136-43.
132. Bird AP, and A.P. Wolffe. Methylation-induced repression--belts, braces, and chromatin. *Cell.* 1999;99:451-4.
133. Jones PL, G.J. Veenstra, P.A. Wade, D. Vermaak, S.U. Kass, N. Landsberger, J. Strouboulis, and A.P. Wolffe. Methylated DNA and MeCP2 recruit histone deacetylase to repress transcription. *Nat Genet.* 1998;19:187-91.
134. Nan X, H.H. Ng, C.A. Johnson, C.D. Laherty, B.M. Turner, R.N. Eisenman, and A. Bird. Transcriptional repression by the methyl-CpG-binding protein MeCP2 involves a histone deacetylase complex. *Nature.* 1998;393:386-9.
135. Pradhan S, A. Bacolla, R.D. Wells, and R.J. Roberts. Recombinant human DNA (cytosine-5) methyltransferase I expression, purification, and comparison of de novo and maintenance methylation. *J Biol Chem.* 1999;274:33002-10.
136. Kondo Y. Epigenetic cross-talk between DNA methylation and histone modifications in human cancers. *Yonsei Med J.* 2009;50:455-63.
137. Hendrich B, and A. Bird. Identification and characterization of a family of mammalian methyl-CpG binding proteins. *Mol Cell Biol.* 1998;18:6538-47.
138. Wade PA, A. Geggion, P.L. Jones, E. Ballestar, F. Aubry, and A.P. Wolffe. Mi-2 complex couples DNA methylation to chromatin remodelling and histone deacetylation. *Nat Genet.* 1999;23:62-6.
139. Tamaru H, X. Zhang, D. McMillen, P.B. Singh, J. Nakayama, S.I. Grewal, C.D. Allis, X. Cheng, and E.U. Selker. Trimethylated lysine 9 of histone H3 is a mark for DNA methylation in *Neurospora crassa*. *Nat Genet.* 2003;34:75-9.
140. Li H, T. Rauch, Z.X. Chen, P.E. Szabo, A.D. Riggs, and G.P. Pfeifer. The histone methyltransferase SETDB1 and the DNA methyltransferase DNMT3A interact directly and localize to promoters silenced in cancer cells. *J Biol Chem.* 2006;281:19489-500.

141. Lehnertz B, Y. Ueda, A.A. Derijck, U. Braunschweig, L. Perez-Burgos, S. Kubicek, T. Chen, E. Li, T Jenuwein, and A.H. Peters. Suv39h-mediated histone H3 lysine 9 methylation directs DNA methylation to major satellite repeats at pericentric heterochromatin. *Curr Biol.* 2003;13:1192-200.
142. Cao R, L. Wang, H. Wang, L. Xia, H. Erdjument-Bromage, P. Tempst, R.S. Jones, and Y. Zhang. Role of histone H3 lysine 27 methylation in Polycomb-group silencing. *Science.* 2002;298:1039-43.
143. Viré E, C. Brenner, R. Deplus, L. Blanchon, M. Fraga, C. Didelot, L. Morey, A. Van Eynde, D. Bernard, J.M. Vanderwinden, M. Bollen, M. Esteller, L. Di Croce, Y. de Launoit, and F. Fuks. The Polycomb group protein EZH2 directly controls DNA methylation. *Nature.* 2005;439:871-4.
144. Schlesinger Y, R. Straussman, I. Keshet, S. Farkash, M. Hecht, J. Zimmerman, E. Eden, Z. Yakhini, E. Ben-Shushan, B.E. Reubinoff, Y. Bergman, I. Simon, and H. Cedar. Polycomb-mediated methylation on Lys27 of histone H3 pre-marks genes for de novo methylation in cancer. *Nat Genet.* 2006;39:232-6.
145. Davis CDAEOU. Dietary folate and selenium affect dimethylhydrazine-induced aberrant crypt formation, global DNA methylation and one-carbon metabolism in rats. *J Nutr.* 2003;133:2907-14.
146. Devlin AM, E. Arning, T. Bottiglieri, F.M. Faraci, R. Rozen, and S.R. Lentz. Effect of Mthfr genotype on diet-induced hyperhomocysteinemia and vascular function in mice. *Blood.* 2004;103:2624-9.
147. Mehrmohamadi M, L.K. Mentch, A.G. Clark, and J.W. Locasale. Integrative modelling of tumour DNA methylation quantifies the contribution of metabolism. *Nat Commun.* 2016;7:13666.
148. Robertson KD, E. Uzvolgyi, G. Liang, C. Talmadge, J. Sumegi, F.A. Gonzales, and P.A. Jones. The human DNA methyltransferases (DNMTs) 1, 3a and 3b: coordinate mRNA expression in normal tissues and overexpression in tumors. *Nucleic Acids Res.* 1999;27:2291-8.
149. Okano M, S. Xie, and E. Li. Cloning and characterization of a family of novel mammalian DNA (cytosine-5) methyltransferases. *Nat Genet.* 1998;19:219-20.
150. Gowher H, K. Liebert, A. Hermann, G. Xu, and A. Jeltsch. Mechanism of stimulation of catalytic activity of Dnmt3A and Dnmt3B DNA-(cytosine-C5)-methyltransferases by Dnmt3L. *J Biol Chem.* 2005;280:13341-8.
151. Fatemi M, A. Hermann, H. Gowher, and A. Jeltsch. Dnmt3a and Dnmt1 functionally cooperate during de novo methylation of DNA. *Eur J Biochem.* 2002;269:4981-4
152. Liang G, M.F. Chan, Y. Tomigahara, Y.C. Tsai, F.A. Gonzales, E. Li, P.W. Laird, and P.A. Jones. Cooperativity between DNA methyltransferases in the maintenance methylation of repetitive elements. *Mol Cell Biol.* 2002;22:480-91.
153. Pacis A, L. Tailleux, A.M. Morin, J. Lambourne, J.L. MacIsaac, V. Yotova, A. Dumaine, A. Danckaert, F. Luca, J.C. Grenier, K.D. Hansen, B. Gicquel, M. Yu, A. Pai, C. He, J. Tung, T. Pastinen, M.S. Kobor, R. Pique-Regi, Y. Gilad, and L.B. Barreiro. Bacterial infection remodels the DNA methylation landscape of human dendritic cells. *Genome Res.* 2015;25:1801-11
154. Laurson J, S. Khan, R. Chung, K. Cross, and K. Raj. Epigenetic repression of E-cadherin by human papillomavirus 16 E7 protein. *Carcinogenesis.* 2010;31:918-26.
155. Marr AK, J.L. MacIsaac, R. Jiang, A.M. Airo, M.S. Kobor, and W.R. McMaster. *Leishmania donovani* infection causes distinct epigenetic DNA methylation changes in host macrophages. *PLoS Pathog.* 2014;10:e1004419

156. Fitzpatrick DR, K.M. Shirley, L.E. McDonald, H. Bielefeldt-Ohmann, G.F. Kay, and A. Kelso. Distinct methylation of the Interferon γ (IFN- γ) and Interleukin 3 (IL-3) genes in newly activated primary CD8⁺ T lymphocytes: Regional IFN- γ promoter demethylation and mRNA expression Are heritable in CD44^{high}CD8⁺ T cells. *J Exp Med*. 1998;188:103–17.
157. Fitzpatrick DR, K.M. Shirley, and A. Kelso. Cutting Edge: Stable epigenetic inheritance of regional IFN- γ promoter demethylation in CD44^{high}CD8⁺ T lymphocytes. *J Immunol*. 1999;162:5053-7.
158. Scharer CD, B.G. Barwick, B.A. Youngblood, R. Ahmed, and J.M. Boss. Global DNA methylation remodeling accompanies CD8 T cell effector function. *J Immunol*. 2013;191:3419-29.
159. Komori HK, T. Hart, S.A. LaMere, P.V. Chew, and D.R. Salomon. Defining CD4 T cell memory by the epigenetic landscape of CpG DNA methylation. *J Immunol*. 2015;194:1565-79.
160. Bruniquel D, and R.H. Schwartz. Selective, stable demethylation of the interleukin-2 gene enhances transcription by an active process. *Nat Immunol*. 2003;4:235-40.
161. Bird A. I λ 2 transcription unleashed by active DNA demethylation. *Nat Immunol*. 2003;4:208-9
162. Li C, P.J. Ebert, and Q. Li. T Cell Receptor (TCR) and Transforming Growth Factor β (TGF- β) signaling converge on DNA (cytosine-5)-methyltransferase to control forkhead box protein 3 (foxp3) locus methylation and inducible regulatory T cell differentiation. *J Biol Chem*. 2013;288:19127-39.
163. Barwick BG, C.D. Scharer, A.P. Bally, and J.M. Boss. Plasma cell differentiation is coupled to division-dependent DNA hypomethylation and gene regulation. *Nat Immunol*. 2016;17:1216-25.
164. Shaknovich R, L. Cerchietti, L. Tsikitas, M. Kormaksson, S. De, M.E. Figueroa, G. Ballon, S.N. Yang, N. Weinhold, M. Reimers, T. Clozel, K. Luttrup, T.J. Ekstrom, J. Frank, A. Vasanthakumar, L.A. Godley, F. Michor, O. Elemento, and A. Melnick. DNA methyltransferase 1 and DNA methylation patterning contribute to germinal center B-cell differentiation. *Blood*. 2011;118:3559-69.
165. Kobayashi M, L. Fitz, M. Ryan, R.M. Hewick, S.C. Clark, S. Chan, R. Loudon, F. Shennan, B. Perussia, and G. Trinchieri. Identification and purification of natural killer cell stimulatory factor (NKSF), a cytokine with multiple biologic effects on human lymphocytes. *J Exp Med*. 1989;70:827-46.
166. Trinchieri G. Interleukin-12: a proinflammatory cytokine with immuno-regulatory functions that bridge innate resistance and antigen-specific adaptive immunity. *Annu Rev Immunol*. 1995;13:251.
167. Athie-Morales V, H.H. Smits, D.A. Cantrell, and C.M.U. Hilkens. Sustained IL-12 signaling is required for Th1 development. *J Immunol*. 2004;172:61-9.
168. Xu M, I. Mizoguchi, N. Morishima, Y. Chiba, J. Mizuguchi, and T. Yoshimoto. Regulation of antitumor immune responses by the IL-12 family cytokines, IL-12, IL-23, and IL-27. *Clin Dev Immunol*. 2010;2010:832454.
169. Zitvogel L, B. Couderc, J.I. Mayordomo, P.D. Robbins, M.T. Lotze, and W.J. Storkus. IL-12-engineered dendritic cells serve as effective tumor vaccine adjuvants in vivo. *Ann N Y Acad Sci*. 1996;795:284-93.
170. Pockley AG, J. Shepherd, and J.M. Corton. Detection of heat shock protein 70 (Hsp70) and anti-Hsp70 antibodies in the serum of normal individuals. *Immunol Invest*. 1998;27:367-77.

171. Pastor MD, A. Nogal, S. Molina-Pinelo, R. Melendez, A. Salinas, M. Gonzalez De la Pena, J. Martin-Juan, J. Corral, R. Garcia-Carbonero, A. Carnero, and L. Paz-Ares. Identification of proteomic signatures associated with lung cancer and COPD. *J Proteomics*. 2013;89:227-37.
172. Kern J, G. Untergasser, C. Zenzmaier, B. Sarg, G. Gastl, E. Gunsilius, and M. Steurer. GRP-78 secreted by tumor cells blocks the antiangiogenic activity of bortezomib. *Blood*. 2009;114:3960-7.
173. Zhu J, Y. Zhang, A. Zhang, K. He, P. Liu, and L.X. Xu. Cryo-thermal therapy elicits potent anti-tumor immunity by inducing extracellular Hsp70-dependent MDSC differentiation. *Sci Rep*. 2016;6:27136.
174. Kottke T, L. Sanchez-Perez, R.M. Diaz, J. Thompson, H. Chong, K. Harrington, S.K. Calderwood, J. Pulido, N. Georgopoulos, P. Selby, A. Melcher, and R. Vile. Induction of hsp70-mediated Th17 autoimmunity can be exploited as immunotherapy for metastatic prostate cancer. *Cancer Res*. 2007;67:11970-1979.
175. Jayaprakash P, H. Dong, M. Zou, A. Bhatia, K. O'Brien, M. Chen, D.T. Woodley, and W. Li. Hsp90 α and Hsp90 β together operate a hypoxia and nutrient paucity stress-response mechanism during wound healing. *J Cell Sci*. 2015;128:1475-80.
176. Mkaddem SB, C. Werts, J.M. Goujon, M. Bens, E. Pedruzzi, E. Ogier-Denis, and A. Vandewalle. Heat shock protein gp96 interacts with protein phosphatase 5 and controls toll-like receptor 2 (TLR2)-mediated activation of extracellular signal-regulated kinase (ERK) 1/2 in post-hypoxic kidney cells. *J Biol Chem*. 2009;284:12541-9.
177. Cheng CF, J. Fan, M. Fedesco, S. Guan, Y. Li, B. Bandyopadhyay, A.M. Bright, D. Yerushalmi, M. Liang, M. Chen, Y.P. Han, D.T. Woodley, and W. Li. Transforming growth factor alpha (TGF α)-stimulated secretion of HSP90 α : using the receptor LRP-1/CD91 to promote human skin cell migration against a TGF β -rich environment during wound healing. *Mol Cell Biol*. 2008;28:3344-58.
178. Gulic T, G. Laskarin, A. Redzovic, S. Eminović, H. Haller, and D. Rukavina. The significance of heat-shock protein gp96 and its receptors' CD91 and Toll-like receptor 4 expression at the maternal foetal interface. *Am J Reprod Immunol*. 2013;70:10-23.
179. Siegal FP, N. Kadowaki, M. Shodell, P.A. Fitzgerald-Bocarsly, K. Shah, S. Ho, S. Antonenko, and Y.J. Liu. The nature of the principal type 1 interferon-producing cells in human blood. *Science*. 1999;284:1835-7.
180. Dzionek A, Y. Sohma, J. Nagafune, M. Cella, M. Colonna, F. Facchetti, G. Günther, I. Johnston, A. Lanzavecchia, T. Nagasaka, T. Okada, W. Vermi, G. Winkels, T. Yamamoto, M. Zysk, Y. Yamaguchi, and J. Schmitz. BDCA-2, a novel plasmacytoid dendritic cell-specific type II C-type lectin, mediates antigen capture and is a potent inhibitor of interferon alpha/beta induction. *J Exp Med*. 2001;194:1823-34.
181. Blasius A, W. Vermi, A. Krug, F. Facchetti, M. Cella, and M. Colonna. A cell-surface molecule selectively expressed on murine natural interferon-producing cells that blocks secretion of interferon-alpha. *Blood*. 2004;103:4201-6.
182. Meyer-Wentrup F, D. Benitez-Ribas, P.J. Tacken, C.J. Punt, C.G. Figdor, I.J. de Vries, and G.J. Adema. Targeting DCIR on human plasmacytoid dendritic cells results in antigen presentation and inhibits IFN-alpha production. *Blood*. 2008;111:4245-53.
183. Ochando JC, C. Homma, Y. Yang, A. Hidalgo, A. Garin, F. Tacke, V. Angeli, Y. Li, P. Boros, Y. Ding, R. Jessberger, G. Trinchieri, S.A. Lira, G.J. Randolph, and J.S. Bromberg. Alloantigen-presenting plasmacytoid dendritic cells mediate tolerance to vascularized grafts. *Nat Immunol*. 2006;7:652-62.

184. Hadeiba H, T. Sato, A. Habtezion, C. Oderup, J. Pan, and E.C. Butcher. CCR9 expression defines tolerogenic plasmacytoid dendritic cells able to suppress acute graft-versus-host disease. *Nat Immunol.* 2008;9:1253-60.
185. Kavousanaki M, A. Makrigiannakis, D. Boumpas, and P. Verginis. Novel role of plasmacytoid dendritic cells in humans: induction of interleukin-10-producing Treg cells by plasmacytoid dendritic cells in patients with rheumatoid arthritis responding to therapy. *Arthritis Rheum.* 2010;62:53-63.
186. Vermi W, R. Bonecchi, F. Facchetti, D. Bianchi, S. Sozzani, S. Festa, A. Berenzi, M. Cella, and M. Colonna. Recruitment of immature plasmacytoid dendritic cells (plasmacytoid monocytes) and myeloid dendritic cells in primary cutaneous melanomas. *J Pathol.* 2003;200:255-68.
187. Munn DH, M.D. Sharma, D. Hou, B. Baban, J.R. Lee, S.J. Antonia, J.L. Messina, P. Chandler, P.A. Koni, and A.L. Mellor. Expression of indoleamine 2,3-dioxygenase by plasmacytoid dendritic cells in tumor-draining lymph nodes. *J Clin Invest.* 2004;114:280-90.
188. Sharma MD, B. Baban, P. Chandler, D.Y. Hou, N. Singh, H. Yagita, M. Azuma, B.R. Blazar, A.L. Mellor, and D.H. Munn. Plasmacytoid dendritic cells from mouse tumor-draining lymph nodes directly activate mature Tregs via indoleamine 2,3-dioxygenase. *J Clin Invest.* 2007;117:2570-82.
189. Popovic PJ, R. DeMarco, M.T. Lotze, S.E. Winikoff, D.L. Bartlett, A.M. Krieg, Z.S. Guo, C.K. Brown, K.J. Tracey, H.J. Zeh 3rd. High mobility group B1 protein suppresses the human plasmacytoid dendritic cell response to TLR9 agonists. *J Immunol.* 2006;177:8701-7.
190. Nolan KD, O.E. Franco, M.W. Hance, S.W. Hayward, and J.S. Isaacs. Tumor-secreted Hsp90 subverts polycomb function to drive prostate tumor growth and invasion. *J Biol Chem.* 2015;290:8271-82.
191. Rhee I, K.E. Bachman, B. Ho Park, K. Jair, R. C. Yen, K.E. Schuebel, H. Cui, A.P. Feinberg, C. Lengauer, K.W. Kinzler, S.B. Baylin, and B. Vogelstein. DNMT1 and DNMT3b cooperate to silence genes in human cancer cells. *Med Mycol.* 2005;43:381-9.
192. Sun L, H. Zhao, Z. Xu, Q. Liu, Y. Liang, L. Wang, X. Cai, L. Zhang, L. Hu, G. Wang, and X. Zha. Phosphatidylinositol 3-kinase/protein kinase B pathway stabilizes DNA methyltransferase I protein and maintains DNA methylation. *Cell Signal.* 2007;19:2255-63.
193. Hayashi H, R.B. Campenot, D.E. Vance, and J.E. Vance. Protection of neurons from apoptosis by apolipoprotein E-containing lipoproteins does not require lipoprotein uptake and involves activation of phospholipase Cgamma1 and inhibition of calcineurin. *J Biol Chem.* 2009;284:29605-13.
194. Hayashi H, Y. Eguchi, Y. Fukuchi-Nakaishi, M. Takeya, N. Nakagata, K. Tanaka, J.E. Vance, and H. Tanihara. A potential neuroprotective role of apolipoprotein E-containing lipoproteins through low density lipoprotein receptor-related protein 1 in normal tension glaucoma. *J Biol Chem.* 2012;287:5395-406.
195. Sarris M, K.G. Andersen, F. Randow, L. Mayr, and A.G. Betz. . Neuropilin-1 expression on regulatory T cells enhances their interactions with dendritic cells during antigen recognition. *Immunity.* 2008;28:402-13
196. Tordjman R, Y. Lepelletier, V. Lemarchandel, M. Cambot, P. Gaulard, O. Hermine, and P.H. Roméo. . A neuronal receptor, neuropilin-1, is essential for the initiation of the primary immune response. *Nat Immunol.* 2002;3:477-82
197. Delgoffe GM, S.R. Woo, M.E. Turnis, D.M. Gravano, C. Guy, A.E. Overacre, M.L. Bettini, P. Vogel, D. Finkelstein, J. Bonnevier, C.J. Workman, and D.A. Vignali. Stability and

- function of regulatory T cells is maintained by a neuropilin-1-semaphorin-4a axis. *Nature*. 2013;501:252-6.
198. Yang X, H. Han, D.D. De Carvalho, F.D. Lay, P.A. Jones, and G. Liang. Gene body methylation can alter gene expression and is a therapeutic target in cancer. *Cancer Cell*. 2014;26:577-90.
199. Bender CM, M.L. Gonzalgo, F.A. Gonzales, C.T. Nguyen, K.D. Robertson, and P.A. Jones. Roles of cell division and gene transcription in the methylation of CpG islands. *Mol Cell Biol*. 1999;19:6690-8.
200. Salem CE, I.D. Markl, C.M. Bender, F.A. Gonzales, P.A. Jones, and G. Liang. PAX6 methylation and ectopic expression in human tumor cells. *Int J Cancer*. 2000;87:179-85.
201. Nelson ED, and L.M. Monteggia. Epigenetics in the mature mammalian brain: effects on behavior and synaptic transmission. *Neurobiol Learn Mem*. 2011;96:53-60.
202. Guo JU, D.K. Ma, H. Mo, M.P. Ball, M.H. Jang, M.A. Bonaguidi, J.A. Balazer, H.L. Eaves, B. Xie, E. Ford, K. Zhang, G.L. Ming, Y. Gao, and H. Song. Neuronal activity modifies the DNA methylation landscape in the adult brain. *Nat Neurosci*. 2011;14:1345-51.
203. Feng J, H. Chang, E. Li, and G. Fan. Dynamic expression of de novo DNA methyltransferases Dnmt3a and Dnmt3b in the central nervous system. *J Neurosci Res*. 2005;79:734-46.
204. Inano K, I. Suetake, T. Ueda, Y. Miyake, M. Nakamura, M. Okada, and S. Tajima. Maintenance-type DNA methyltransferase is highly expressed in post-mitotic neurons and localized in the cytoplasmic compartment. *J Biochem*. 2000;128:315-21.
205. Tserel L, M. Limbach, M. Saare, K. Kisand, A. Metspalu, L. Milani, and P. Peterson. CpG sites associated with NRP1, NRXN2 and miR-29b-2 are hypomethylated in monocytes during ageing. *Immun Ageing*. 2014;11:1.
206. Kurschat P, D. Bielenberg, M. Rossignol-Tallandier, A. Stahl, and M. Klagsbrun. Neuron restrictive silencer factor NRSF/REST is a transcriptional repressor of neuropilin-1 and diminishes the ability of semaphorin 3A to inhibit keratinocyte migration. *J Biol Chem*. 2006;281:2721-9.
207. Mathers AR, O.A. Tkacheva, B.M. Janelsins, W.J. Shufesky, A.E. Morelli, and A.T. Larregina. In vivo signaling through the neurokinin 1 receptor favors transgene expression by Langerhans cells and promotes the generation of Th1- and Tc1-biased immune responses. *J Immunol*. 2007;178:7006-17.
208. Janelsins BM, A.R. Mathers, O.A. Tkacheva, G. Erdos, W.J. Shufesky, A.E. Morelli, and A.T. Larregina Proinflammatory tachykinins that signal through the neurokinin 1 receptor promote survival of dendritic cells and potent cellular immunity. *Blood*. 2009;113:3017-26.
209. Janelsins BM, T.L. Sumpter, O.A. Tkacheva, D.M. Rojas-Canales, G. Erdos, A.R. Mathers, W.J. Shufesky, W.J. Storkus, L.D. Falo Jr, A.E. Morelli, and A.T. Larregina. Neurokinin-1 receptor agonists bias therapeutic dendritic cells to induce type 1 immunity by licensing host dendritic cells to produce IL-12. *Blood*. 2013;121:2923-33.
210. Banh C, C. Fugère, and L. Brossay. Immunoregulatory functions of KLRG1 cadherin interactions are dependent on forward and reverse signaling. *Blood*. 2009;114:5299-306.
211. Krummel MF, and J.P. Allison CTLA-4 engagement inhibits IL-2 accumulation and cell cycle progression upon activation of resting T cells. *J Exp Med*. 1996;183:2533-40
212. Irla M, N. Küpfer, T. Suter, R. Lissilaa, M. Benkhoucha, J. Skupsky, P.H. Lalive, A. Fontana, W. Reith, and S. Hugues. MHC class II-restricted antigen presentation by plasmacytoid dendritic cells inhibits T cell-mediated autoimmunity. *J Exp Med*. 2010;207:1891-905.

213. Yadav M, C. Louvet, D. Davini, J.M. Gardner, M. Martinez-Llordella, S. Bailey-Bucktrout, B.A. Anthony, F.M. Sverdrup, R. Head, D.J. Kuster, P. Ruminski, D. Weiss, D. Von Schack, and J.A. Bluestone. Neuropilin-1 distinguishes natural and inducible regulatory T cells among regulatory T cell subsets in vivo. *J Exp Med.* 2012;209:1713-22.
214. van Herwijnen MJ, L. Wieten, R. van der Zee, P.J. van Kooten, J.P. Wagenaar-Hilbers, A. Hoek, I. den Braber, S.M. Anderton, M. Singh, H.D. Meiring, C.A. van Els, W. van Eden, and F. Broere. Regulatory T cells that recognize a ubiquitous stress-inducible self-antigen are long-lived suppressors of autoimmune arthritis. *Proc Natl Acad Sci U S A.* 2012;109:14134-9.
215. Zhang J, A. Raper, N. Sugita, R. Hingorani, M. Salio, M.J. Palmowski, V. Cerundolo, and P.R. Crocker. Characterization of Siglec-H as a novel endocytic receptor expressed on murine plasmacytoid dendritic cell precursors. *Blood.* 2006;107:3600-8
216. Jackson AM, L.A. Mulcahy, J. Porte, H.A. Franks, M. El Refaee, Q. Wang, S. Shah, X. Zhu, and P.M. Patel. Role of mitogen-activated protein kinase and PI3K pathways in the regulation of IL-12-family cytokines in dendritic cells and the generation of Th-responses. *Eur Cytokine Netw.* 2010;21:319-28.
217. Saudemont A, N. Jouy, D. Hetuin, and B. Quesnel NK cells that are activated by CXCL10 can kill dormant tumor cells that resist CTL-mediated lysis and can express B7-H1 that stimulates T cells. *Blood.* 2005;105:2428-35.
218. Thapa M, R.S. Welner, R. Pelayo, and D.J.J. Carr. CXCL9 and CXCL10 expression are critical for control of genital herpes simplex virus type 2 infection through mobilization of HSV-specific CTL and NK cells to the nervous system. *J Immunol.* 2008;180:1098–106.
219. Zeng Y, X. Chen, N. Larmonier, C. Larmonier, G. Li, M. Sepassi, M. Marron, S. Andreansk, and E. Katsanis. Natural killer cells play a key role in the antitumor immunity generated by chaperone-rich cell lysate vaccination *Int J Cancer.* 2006;119:2624-31.
220. Maurano MT, H. Wang, S. John, A. Shafer, T. Canfield, K. Lee, and J.A. Stamatoyannopoulos. Role of DNA methylation in modulating transcription factor occupancy. *Cell Rep.* 2015;12:1184-95.
221. Domcke S, A.F. Bardet, P. Adrian Ginno, D. Hartl, L. Burger, and D. Schübeler. Competition between DNA methylation and transcription factors determines binding of NRF1. *Nature.* 2015;528:575-9.
222. Hu S, J. Wan, Y. Su, Q. Song, Y. Zeng, H.N. Nguyen, J. Shin, E. Cox, H.S. Rho, C. Woodard, S. Xia, S. Liu, H. Lyu, G.L. Ming, H. Wade, H. Song, J. Qian, and H. Zhu. DNA methylation presents distinct binding sites for human transcription factors. *Elife.* 2013;2:e00726.
223. Poirier S, S. Samami, M. Mamarbachi, A. Demers, T.Y. Chang, D.E. Vance, G.M. Hatch, and G. Mayer. The epigenetic drug 5-azacytidine interferes with cholesterol and lipid metabolism. *J Biol Chem.* 2014;289:18736-51.
224. Cihák A. Biological effects of 5-azacytidine in eukaryotes. *Oncology.* 1974;30:405-22.
225. Gnyszka A, Z. Jastrzebski, and S. Flis. DNA methyltransferase inhibitors and their emerging role in epigenetic therapy of cancer. *Anticancer Res.* 2013;33:2989-96.
226. Zhang Y, Y. Cho, B.L. Petersen, F. Zhu, and Z. Dong. Evidence of STAT1 phosphorylation modulated by MAPKs, MEK1 and MSK1. *Carcinogenesis.* 2004;25:1165-75.
227. Burke SJ, D. Lu, T.E. Sparer, T. Masi, M.R. Goff, M.D. Karlstad, and J.J. Collier. NF- κ B and STAT1 control CXCL1 and CXCL2 gene transcription. *Am J Physiol Endocrinol Metab.* 2014;306:E131-E49.

228. Varinou L, K. Ramsauer, M. Karaghiosoff, T. Kolbe, K. Pfeffer, M. Müller, and T. Decker. Phosphorylation of the Stat1 transactivation domain is required for full-fledged IFN-gamma-dependent innate immunity. *Immunity*. 2003;19:793-802.
229. Stephanou A, T.M. Scarabelli, B.K. Brar, Y. Nakanishi, M. Matsumura, R.A. Knight, and D.S. Latchman. Induction of apoptosis and Fas receptor/Fas ligand expression by ischemia/reperfusion in cardiac myocytes requires serine 727 of the STAT-1 transcription factor but not tyrosine 701. *J Biol Chem*. 2001;276:28340-7.
230. Ramsauer K, I. Sadzak, A. Porras, A. Pilz, A.R. Nebreda, T. Decker, and P. Kovarik. p38 MAPK enhances STAT1-dependent transcription independently of Ser-727 phosphorylation. *Proc Natl Acad Sci U S A*. 2002;99:12859-64.
231. Agrawal S, M. Febbraio, E. Podrez, M.K. Cathcart, G.R. Stark, and G.M. Chisolm. Signal transducer and activator of transcription 1 is required for optimal foam cell formation and atherosclerotic lesion development. *Circulation*. 2007;115:2939-47.
232. Barnholt KE, R.S. Kota, H.H. Aung, and J.C. Rutledge. Adenosine blocks IFN- γ -induced phosphorylation of STAT1 on serine 727 to reduce macrophage activation. *J Immunol*. 2009;183:6767-77.
233. Sadzak I, M. Schiff, I. Gattermeier, R. Glinitzer, I. Sauer, A. Saalmüller, E. Yang, B. Schaljo, and P. Kovarik. Recruitment of Stat1 to chromatin is required for interferon-induced serine phosphorylation of Stat1 transactivation domain. *Proc Natl Acad Sci U S A*. 2008;105:8944-9.
234. Wong JL, E. Berk, R.P. Edwards, and P. Kalinski. IL-18-primed helper NK cells collaborate with dendritic cells to promote recruitment of effector CD8+ T cells to the tumor microenvironment. *Cancer Res*. 2013;73:4653-62.
235. Fernandez NC, A. Lozier, C. Flament, P. Ricciardi-Castagnoli, D. Bellet, M. Suter, M. Perricaudet, T. Tursz, E. Maraskovsky, and L. Zitvogel. Dendritic cells directly trigger NK cell functions: cross-talk relevant in innate anti-tumor immune responses in vivo. *Nat Med*. 1999;5:405-11.
236. Seeger P, D. Bosisio, S. Parolini, R. Badolato, A. Gismondi, A. Santoni, and S. Sozzani. Activin A as a mediator of NK-dendritic cell functional interactions. *J Immunol*. 2014;192:1241-8.
237. Saudemont A JN, Hetuin D, Quesnel B. NK cells that are activated by CXCL10 can kill dormant tumor cells that resist CTL-mediated lysis and can express B7-H1 that stimulates T cells. *Blood*. 2005;105:2428-35.
238. Wennerberg E, V. Kremer, R. Childs, and A. Lundqvist. CXCL10-induced migration of adoptively transferred human natural killer cells toward solid tumors causes regression of tumor growth in vivo. *Cancer Immunol Immunother*. 2015;64:225-35.
239. Newman RG, M.J. Dee, T.R. Malek, E.R. Podack, and R.B. Levy. Heat shock protein vaccination and directed IL-2 therapy amplify tumor immunity rapidly following bone marrow transplantation in mice. *Blood*. 2014;103:3045-55.
240. Iannacone M, E.A. Moseman, E. Tonti, L. Bosurgi, T. Junt, S.E. Henrickson, S.P. Whelan, L.G. Guidotti, and U.H. von Andrian. Subcapsular sinus macrophages prevent CNS invasion upon peripheral infection with a neurotropic virus. *Nature*. 2010;465:1079-83.
241. Korkmaz E, E.E. Friedrich, M.H. Ramadan, G. Erdos, A.R. Mathers, O.B. Ozdoganlar, N.R. Washburn, and L.D. Falo Jr. Tip-loaded dissolvable microneedle arrays effectively deliver polymer-conjugated antibody inhibitors of tumor-necrosis-factor-alpha into human skin. *J Pharm Sci*. 2016;105:3453-7.

242. Lande R, E. Giacomini, B. Serafini, B. Rosicarelli, G.D. Sebastiani, G. Minisola, U. Tarantino, V. Ricciari, G. Valesini, and E.M. Coccia. Characterization and recruitment of plasmacytoid dendritic cells in synovial fluid and tissue of patients with chronic inflammatory arthritis. *J Immunol.* 2004;173:2815-24.
243. Wenzel J, and T. Tüting. An IFN-associated cytotoxic cellular immune response against viral, self-, or tumor antigens is a common pathogenetic feature in "interface dermatitis". *J Invest Dermatol.* 2008;128:2392-402.
244. Llorente-Cortés V, T. Royo, O. Juan-Babot, and L. Badimon. Adipocyte differentiation-related protein is induced by LRP1-mediated aggregated LDL internalization in human vascular smooth muscle cells and macrophages. *J Lipid Res.* 2007;48:2133-40.
245. Buck MD, D. O'Sullivan, and E.L. Pearce. T cell metabolism drives immunity. *J Exp Med.* 2015;212:1345.
246. Yap G, M. Pesin, and A. Sher. Cutting Edge: IL-12 is required for the maintenance of IFN- γ production in T cells mediating chronic resistance to the intracellular pathogen, *Toxoplasma gondii*. *J Immunol.* 2000;165:628-31.
247. Zhang Y, T. Liu, C.A. Meyer, J. Eeckhoutte, D.S. Johnson, B.E. Bernstein, C. Nusbaum, R.M. Myers, M. Brown, W. Li, and X.S. Liu. . Model-based analysis of ChIP-Seq (MACS). *Genome Biol.* 2008;9:R137.
248. Li H. Tabix: fast retrieval of sequence features from generic TAB-delimited files. *Bioinformatics.* 2011;27:718-9.
249. Patel S, and J. Lyons-Weiler. A web application for the integrated analysis of global gene expression patterns in cancer *Applied Bioinformatics.* 2004;3:49-62.
250. Jordan R, S. Patel, H. Hu, and J. Lyons-Weiler. Efficiency Analysis of competing tests for finding differentially expressed genes in lung adenocarcinoma. *Cancer Inform.* 2008;6:389-421.
251. Dobrowolski SF, J. Lyons-Weiler, A. Biery, K. Spridik, G. Vockley, E. Kranik, K. Skvorak, and T. Sultana. Methylome repatterning in a mouse model of Maternal PKU Syndrome. *Mol Genet Metab.* 2014;113:194-9.
252. Backes C, A. Keller, J. Kuentzer, B. Kneissl, N. Comtesse, Y.A. Elnakady, R. Müller, E. Meese, and H.P. Lenhof. GeneTrail—advanced gene set enrichment analysis. *Nucleic Acids Res.* 2007;35:W186-W92.
253. Li LC, and R. Dahiya. MethPrimer: designing primers for methylation PCRs. *Bioinformatics.* 2002;18:1427-31.
254. Abramoff MD, P.J. Magalhaes, and S.J. Ram. Image Processing with ImageJ. *Biophotonics Int.* 2004;11:36-42.
255. Blasius AL, E. Giurisato, M. Cella, R.D. Schreiber, A.S. Shaw, and M. Colonna. Bone marrow stromal cell antigen 2 is a specific marker of type I IFN-producing cells in the naive mouse, but a promiscuous cell surface antigen following IFN stimulation. *J Immunol.* 2006;177:3260-5.

